T-4458

RAMAN STUDY OF TETRAHYDROFURAN CLATHRATE HYDRATE

by

Xiaoping Long

ProQuest LLC.
789 East Eisenhower Parkway
P.O. Box 1346
Ann Arbor, MI 48106 – 1346

T-4458

A thesis submitted to the Faculty and the Board of Trustees of the Colorado School of Mines in partial fulfillment of the requirements for the degree of Master of Science(Chemical and Petroleum-Refining Engineering).

Golden, Colorado
Date Nov. 12, 1993

Signed: Xiaoping Long
Xiaoping Long

Approved: E. Dendy Sloan, Jr.
E. Dendy Sloan, Jr., and
Robert C. Burruss
Thesis Advisors

Golden, Colorado
Date Nov. 12, 1993

Robert M. Baldwin
Professor and Head, Chemical
and Petroleum-Refining
Engineering Department

ABSTRACT

As the oil and gas industry becomes more and more concerned with problems, e.g. plugging pipeline, plugging turbo expander, etc., due to natural gas hydrate formation, there is an immediate need to understand the kinetics of hydrate formation processes. This understanding is the key to determination of the kinetic inhibition mechanism and the design of better inhibitors.

The following experiments were conducted during the course of this research. Tetrahydrofuran(THF) hydrate was used as a model hydrate in this research because of experimental simplicity. An experimental spectroscopic and computer analysis study was conducted on this system. The Raman spectra of THF+H_2O solutions at different THF concentrations and different temperatures and the Raman spectra of THF with different solvents (e.g., CH_3OH, $CHCl_3$, and CCl_4)were obtained. The degree of hydrogen bonding between THF and solvents is a strong function of THF concentration in the solutions. Isotopic substitutions of H_2O (i.e., D_2O and HDO) were also conducted in the study. Symmetrical hydrogen bonding between THF and water molecules was suggested to interpret the spectral observation. A study of polarized Raman spectra was also conducted on THF+H_2O liquid solution and the THF+H_2O

hydrate to gain more understanding of the interaction between THF and water. The first time-dependent Raman spectrum of the THF hydrate formation process was obtained. The hydrogen bonding between water and THF molecule decreases in intensity appreciably after hydrate formation.

Deconvolution techniques using Gaussian and Lorentz profiles were conducted on both THF C-O-C stretching region and OH stretching region for all the systems mentioned above, as well as pure liquid water. Rotational relaxation times were calculated for THF molecules in the solutions and in the hydrate. Depolarization ratios were also calculated for the THF C-O-C stretching band.

The Raman spectra of THF+H_2O+inhibitors with and without salt were obtained. The qualitative relationship between inhibitors and water structure was obtained based on the interpretation of the spectra. Inhibitors increase both the degree and strength of hydrogen bond of water. It may change the water structure in a way which is not favorable for hydrate formation.

TABLE OF CONTENTS

TABLE OF CONTENTS

(Continued)

TABLE OF CONTENTS

(Continued)

TABLE OF CONTENTS

(Continued)

LIST OF FIGURES

LIST OF FIGURES

(Continued)

LIST OF FIGURES

(Continued)

LIST OF FIGURES

(Continued)

LIST OF FIGURES

(Continued)

LIST OF FIGURES

(Continued)

LIST OF FIGURES

(Continued)

LIST OF FIGURES

(Continued)

LIST OF TABLES

TABLES **Page**

LIST OF TABLES

(Continued)

ACKNOWLEDGMENTS

The author would like to express his gratitude to Dr. E. Dendy Sloan, Jr., for his wonderful encouragement, intensive guidance, and great patience during the course of the research.

Dr. Robert C. Burruss, from the United States Geological Survey, Denver, Colorado, deserves special thanks for his timely help with the experiments, intensive discussions throughout the research, and great patience during the revision of this dissertation. Without his advice, this thesis would not stand in the position it is right now.

Thanks to the members of the graduate committee, Professors Robert M. Baldwin and James F. Ely, for their helpful suggestions to the final details of the thesis.

I would like to thank my brother, Jinping Long, and my wife, Qing Yang, for their love and support. It was Jinping's advice that led me to the chemical engineering area and interested me in this wonderful world. My wife, Qing Yang, deserves thanks for her support and love throughout my stay at Colorado School of Mines.

I would like to thank all the members of the hydrate group, namely, Ajay Mehta, Jim McCulloch, Jinping Long, Joe Lederhos, Kevin Wagner, Kristin Mollenhauer, Ron Pratt, Taras

Makogon, and Vibha Bansal, for the thoughts, ideas and discussions.

I would like to thank the following companies and agencies for their financial support:

Amoco, Arco, Chevron, Conoco, DoE, Exxon, Marathon, Mobil, Oryx, Petrobras, Phillips, Shell, Texaco.

DEDICATION

This dissertation is dedicated to

my mother, Liyun Yang;

my father, Shengxiang Long; and

my wife, Qing Yang

CHAPTER I

INTRODUCTION

Ever since the discovery of gas hydrates by Sir Humphrey Davy in 1811(Sloan, 1990), there has been considerable thermodynamic research conducted on gas hydrates. Natural gas hydrates are of substantial future concern due to their potential as an energy resource. At present natural gas hydrates are widely considered as hazards in the gas and oil industry because they plug pipe lines, turbo-expanders, Joule-Thompson valves, etc. and cause severe problems.

The classical way of inhibiting gas hydrate formation is by injecting methanol or ethylene glycol to shift the hydrate equilibrium line to a lower temperature and higher pressure(Sloan, 1990). This kind of inhibitor is called a thermodynamic inhibitor. Recently, a new kind of hydrate inhibition technique has been developed -- kinetic inhibition, which appears to delay nucleation or hinder growth of the gas hydrate crystal.

An important aspect of understanding the inhibition mechanism and identifying good kinetic inhibitors is knowledge of the kinetics of hydrate formation. Understanding hydrate kinetics is the objective of this research. The primary concern is how gas hydrate nuclei form and how these nuclei

grow to form bulk hydrates. There are two basic approaches to address this problem. One is a macroscopic viewpoint, measuring temperature, pressure and other macroscopic variables to probe phenomena at the microscopic level. The other approach is microscopic in nature, using spectroscopic techniques to study the problem. The second approach was used in this research. The technique used here is called Raman spectroscopy, which is able to probe energetic interactions between molecules in both liquid solutions and solid hydrates.

In this research, tetrahydrofuran(THF) hydrate was used as a model hydrate. THF is a structure II(sII) hydrate former and goes into the large cavity of sII. There are two significant points that cause THF hydrate to be different from other systems. First of all, THF is totally miscible with water. Secondly, THF hydrate has the exact composition of THF to water with a molar ratio of 1:17 so that it is possible to make a solution which has exactly the mole ratio of THF to water as that of THF hydrate.

There are five objectives of this research.

1. Study the interaction between water and THF molecules with the stable and metastable solution phase and within the clathrate lattice.
2. Gain an understanding of hydrate nucleation processes.
3. Study time-dependent changes of the system.
4. Get supportive microscopic evidence for inhibition

results.

5. Evaluate the feasibility of using vibrational spectroscopic observations to understand the hydrate formation processes.

While hydrate researchers have concentrated on studying the solid hydrate phase for some time due to the limitations and requirements of thermodynamic measurements, seldom has anyone paid attention to the subcooled solution prior to hydrate formation. However, understanding the behavior of the subcooled solution is very important since it may provide information about the interaction between solute and solvent molecules and may describe how the interaction changes from one phase to another.

The first time-dependent spectrum of the THF hydrate formation process was obtained in the work which follows. Classical nucleation theory shows that the time required to form nuclei is relatively long compared to the time of rapid growth(Dunning, 1969). However, the microscopic phenomena which occur during the nucleation period are unknown. Spectra of the C-O-C region were recorded as a function of time during crystallization from the subcooled solution to solid hydrate. This implies that the Raman technique is a valid analytical tool for determination of hydrate formation.

This research differs fundamentally from previous work in both approach and objectives(Johari and Chew, 1983; Johari and

Chew, 1984). The previous work mainly concentrated on the OH stretching region and the objectives of the previous work were to understand the hydrogen bonded lattice of water structure of hydrate sII, especially THF hydrate. The approach in this study is different in that vibrational spectra ranging from 25-4000 cm^{-1} were recorded for both subcooled liquid solutions and solid hydrates, and with particular emphasis on the THF C-O-C stretching region and OH stretching region in the subcooled liquid solutions.

CHAPTER II

LITERATURE REVIEW

2.1 Clathrate Hydrates

Clathrate hydrates are solid solutions containing small cavities of host water molecules surrounding at most one guest molecule per cavity. These compounds are formed only under certain favorable pressure and temperature conditions(Sloan, 1990). The water molecules in the hydrate are linked together by hydrogen bonding. Figure 2.1 shows the hydrogen bond linkage between the water molecules. The water molecule has a natural tendency to maximize the number of hydrogen bonding(Franks, 1973). There is no other chemical bonding other than van der Waals interactions between hydrate guest molecules and host molecules. However, the integrity of the hydrate structure requires the presence of the guest molecules to stabilize the structure of the surrounding water molecules.

The two common hydrate structures are Structure I (sI) and Structure II (sII) which are shown in Figure 2.2 and Figure 2.3 respectively. These two structures differ in the number and type of cavities. Any cavity can only hold at most one guest molecule, but it can also remain an empty cavity. The unit cell of sI hydrate is composed of 2 small cavities,

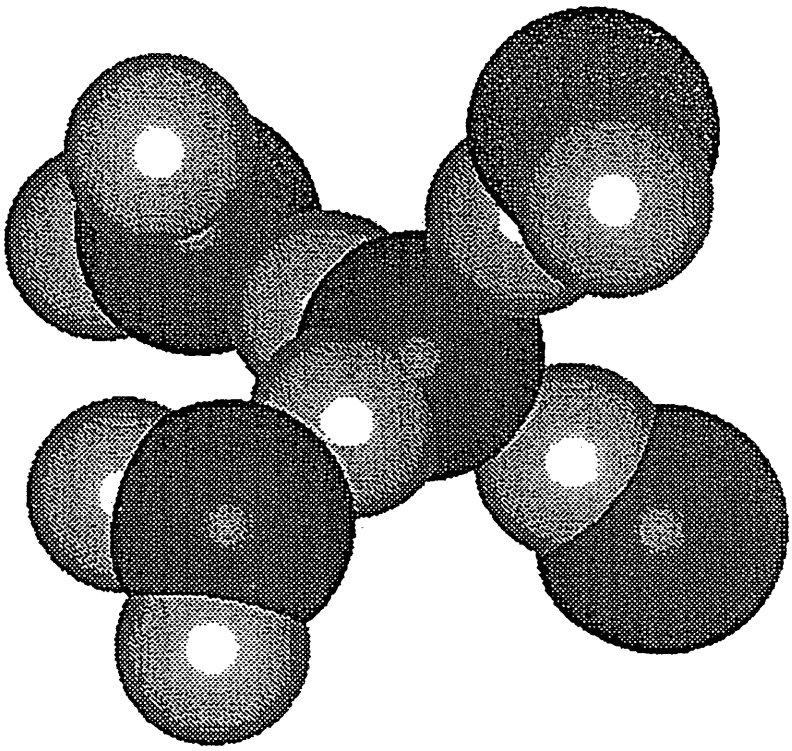

Figure 2.1 Hydrogen bonds linkage of water molecule

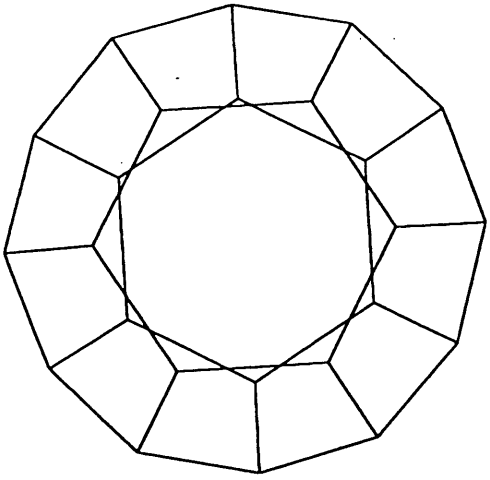

14-HEDRON
(TETRAKAIDECAHEDRON)

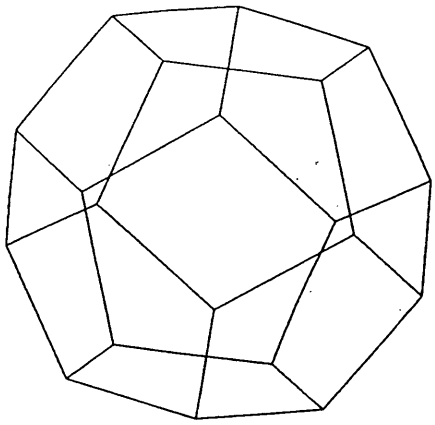

12-HEDRON
(DODECAHEDRON)

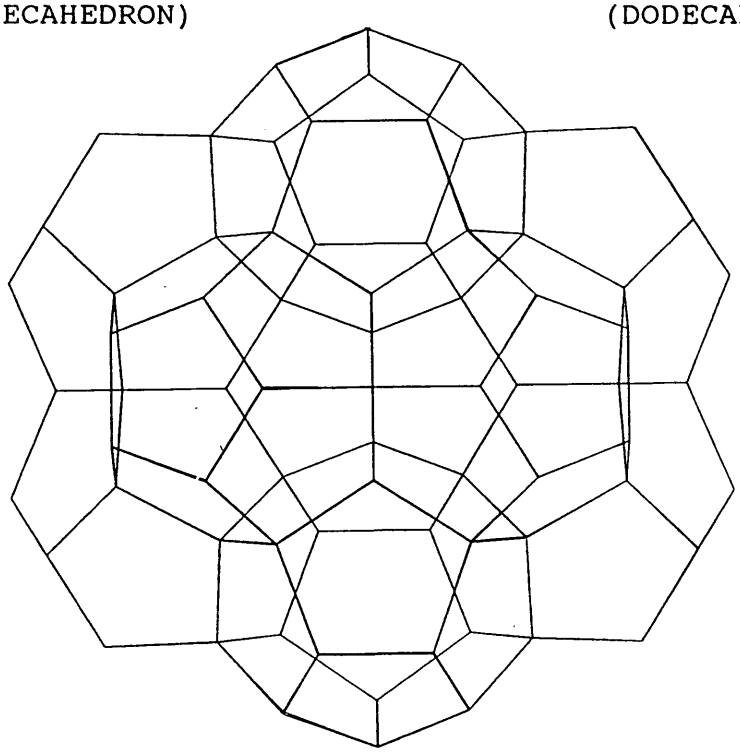

Figure 2.2 Unit Cell and Individual Cavities of sI Hydrate

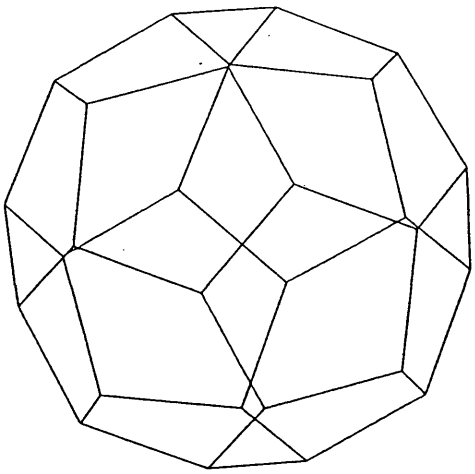

16-HEDRON
(HEXAKAIDECAHEDRON)

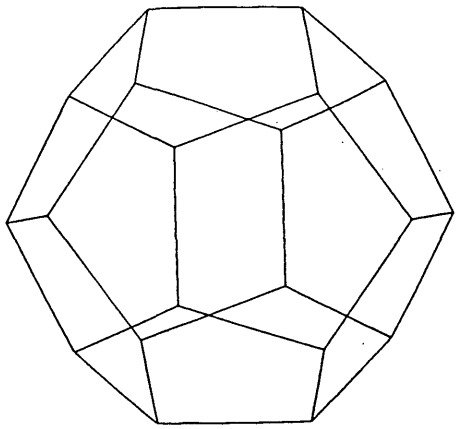

12-HEDRON
(DODECAHEDRON)

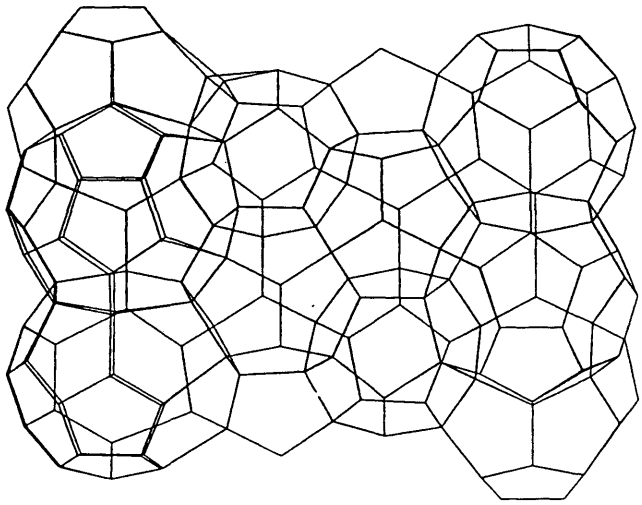

Figure 2.3 Unit Cell and Individual Cavities of sII Hydrate

referred to as pentagonal dodecahedra (or 5^{12}, having 12 pentagonal faces) and 6 large cavities, referred to as tetrakaidecahedra (or $5^{12}6^2$, having 12 pentagonal faces and 2 hexagonal faces). Structure II hydrate is composed of 16 small 5^{12} cavities and 8 large cavities,referred to as hexakaidecahedra (or $5^{12}6^4$, having 12 pentagonal faces and 4 hexagonal faces). The cavity that is the basic building block of the clathrate lattice is the small pentagonal dodecahedron, as shown in Figure 2.2 and Figure 2.3. The linkage of the different cavities between different hydrate structures is different. When 5^{12} cavities and $5^{12}6^2$ cavities are linked together through their vertices, they form structure I with a space group Pm3n. When 5^{12} cavities and $5^{12}6^4$ cavities are linked together by face sharing, they form structure II with a space group Fd3m. The formation of different cavities and thus structures is mostly determined by the size of guest molecules(Sloan, 1990). Excellent reviews on the history of discovering hydrates, notation of hydrate structure and other thermodynamic properties can be found in several monographs(Davidson, 1973; Makogon, 1981; Sloan, 1990).

There are many similarities between ice and hydrate. Most of the physical properties of the clathrate, like elasticity, mechanical deformation, Young's modulus, permitivity, thermal conductivity and the vibrational spectrum, are determined by the structure of the host lattice.

Thus, they are very similar to that of ice. The similarities are due to the fact that water molecules are hydrogen bonded to four other water molecules(Franks, 1973). However, the hydrate is a framework of close-packed polyhedra in a cage-like structure known as the host lattice. In order to stabilize the host structure, guest molecules must occupy most cages. A detailed discussion can be found in a recent monograph(Sloan, 1990).

2.2 Review of Water, Ice, and Pure THF Structure and Spectra

2.2.1 Structure and Spectra of Water and Ice

Many books and excellent reviews exist on the subject of the structure and spectra of water in its various states (Eisenberg and Kauzmann, 1969; Walrafen, 1973; Scherer, 1989). In terms of the actual structure and interpretation of the vibrational spectra, there is considerable controversy. Although there are several models of water structure in the literature(Eisenberg and Kauzmann, 1969), there are two distinct models of the structure of liquid water(Scherer, 1989) -- the mixture model and the continuum model. The mixture model of liquid water assumes the existence of a small number (nine or less) of species (e.g. dimers, trimers and pentamers) that differ in the number and the configurations of hydrogen bonds(Eisenberg and Kauzmann, 1969; Rahman and

Stillinger, 1973). The spectra of the liquid are usually separated into components which are attributed to different species. However, the number of species contributing to the vibrational spectra of water is still a unknown parameter which leads to controversial multi-peak band fitting. The continuum model assumes that all water molecules are four-coordinated as in ice, but the hydrogen bonds are irregular and distorted, giving rise to a continuous distribution of hydrogen bond strengths and a correspondingly broad OH stretching spectrum(Eisenberg and Kauzmann, 1969; Curnutte and Bandekar, 1972; Bryan and Curnutte, 1972).

The H_2O molecule has three normal vibrational modes as shown in Figure 2.4. These are H-O-H bending, asymmetric stretching(proton motions out of phase), and symmetric stretching(proton motions in phase). H-O-H bending occurs in the gas phase around 1595 cm^{-1}, with symmetric stretching at 3562 cm^{-1} and asymmetric stretching at 3756 cm^{-1}. These three vibrational frequencies are modified by intermolecular interactions. H-O-H bending in the liquid phase occurs near 1650 cm^{-1}, and the O-H stretching gives rise to a broad, structured band with a peak in the vicinity of 3400 cm^{-1} (Walrafen *et. al,* 1990).

The vibrational spectrum of liquid water contains intermolecular vibrations in addition to the H-O-H bending and O-H stretching vibrations. These intermolecular vibrations are

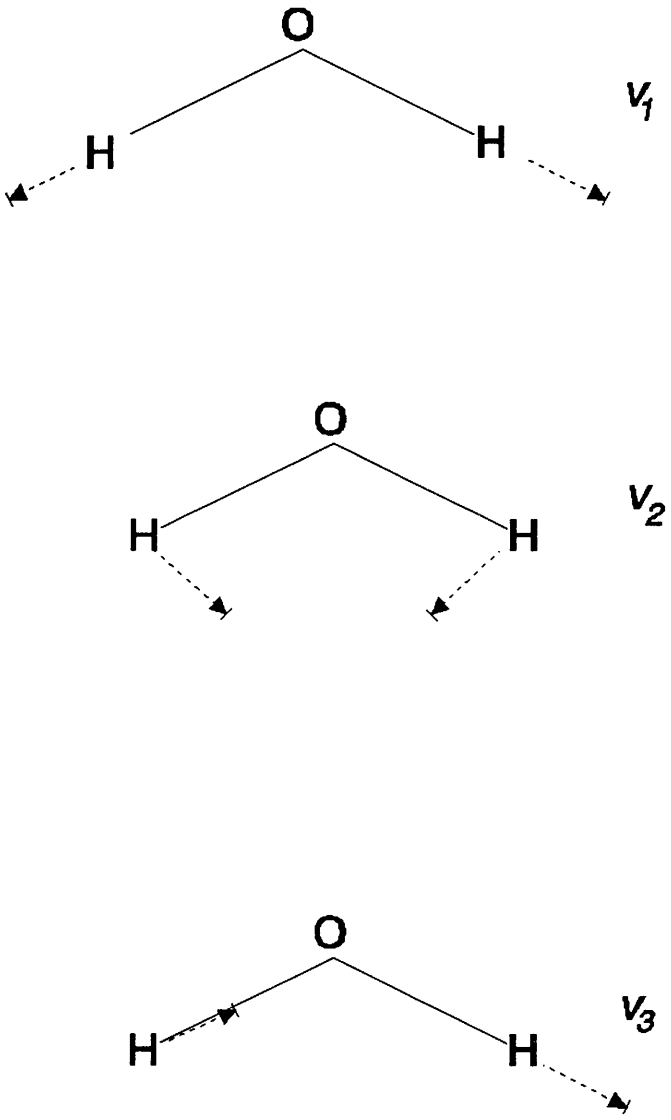

Figure 2.4 Three normal vibrational modes of water molecule

essentially the liquid counterparts of the gas-phase rotations and translations, namely, the free rotations about the three moments of inertia of the H_2O molecule, and the free translations of the H_2O molecule along the x, y, and z directions. However, the rotations are restricted by hydrogen bonds in the liquid and thus they are called librations or rotational vibrations. The translations are also restricted by the hydrogen bonds and they are called restricted translations.

For studying water, Raman spectroscopy has several advantages over infrared spectroscopy. Infrared spectra of liquid water and ice have fewer distinct features and are correspondingly more difficult to interpret(Walrafen, 1973). The OH stretching bands shift from 3600 cm^{-1} at higher temperatures. The OH stretching bandwidth is the greatest in the spectra of liquid near room temperature but the band structure is far more complex for ice at lower temperature(Walrafen, 1973).

A Raman spectrum of pure liquid water from 100 cm^{-1} to 4000 cm^{-1} is shown in Figure 2.5. The H-O-H bending and OH stretching frequencies are shown on the spectrum. The OH stretching band is broad but intense and the H-O-H bending band is weak.

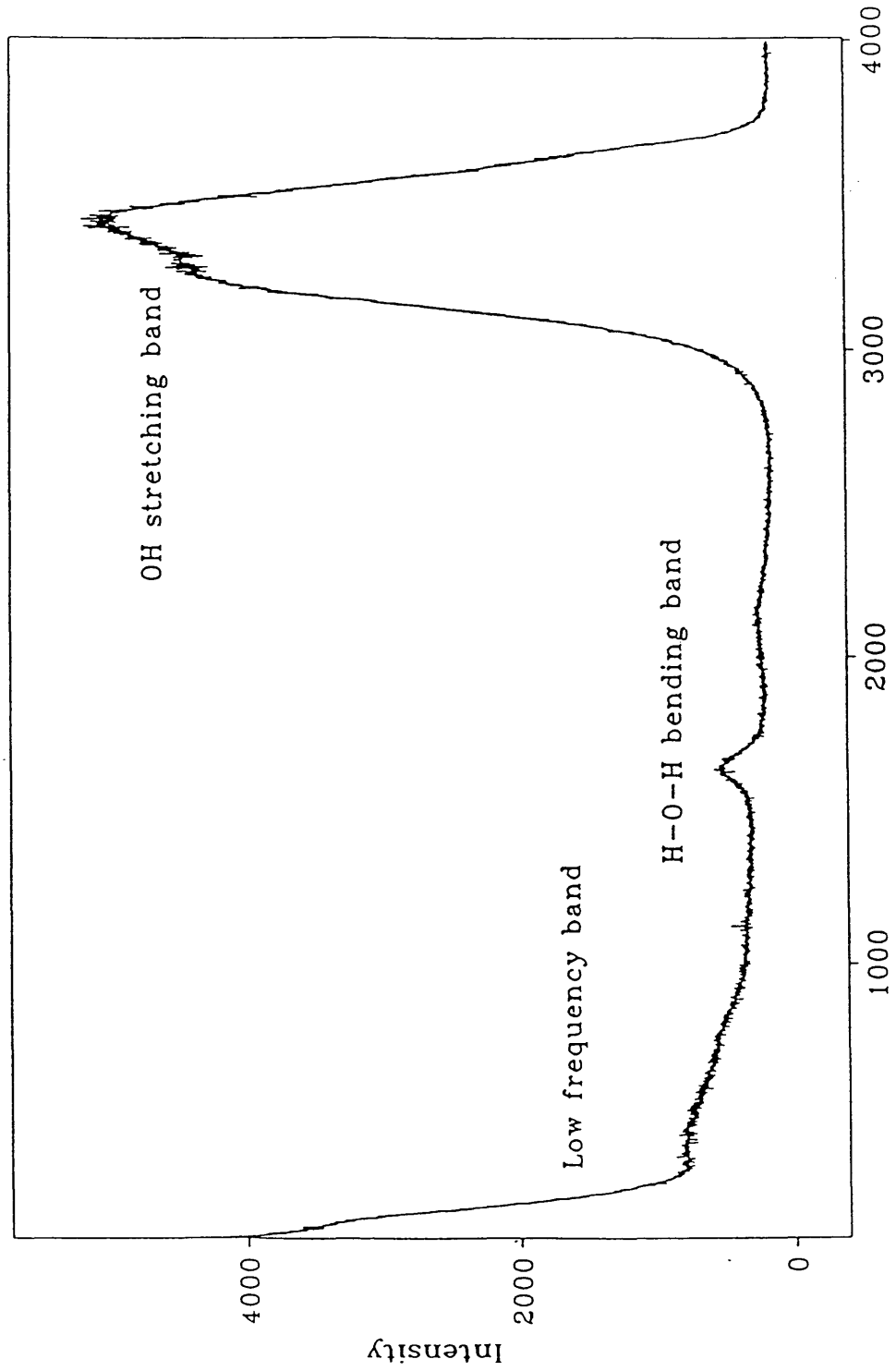

Figure 2.5 Pure liquid water spectrum at room temperature

2.2.2 Structure and Spectra of Pure Tetrahydrofuran (THF)

Tetrahydrofuran is a very common organic solvent. The tetrahydrofuran (THF) molecule has the formula C_4H_8O with the structure shown in Figure 2.6. The presence of the oxygen atom

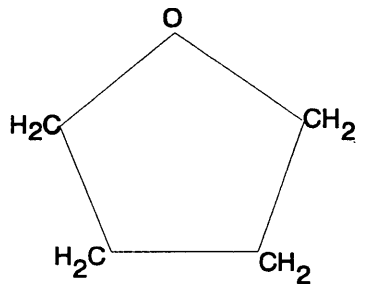

Figure 2.6 Molecular structure of THF molecule

in the carbon ring causes THF molecule to be a polar molecule so that it is totally miscible with water.

A series of infrared spectra for tetrahydrofuran and deuterated tetrahydrofuran were obtained in the gaseous, liquid and solid states in the region between 3200 cm^{-1} and 350 cm^{-1}(Palmer and Bissell, 1960). The observed adsorption bands were assigned to the normal modes of vibration by taking advantage of isotopic shifts and effects due to phase changes. The Raman spectra of THF and d_8-THF(the eight hydrogen atoms attached to the carbon atoms on the carbon ring are substituted by eight deuterium atoms) were measured and the

vibrational modes assigned in several studies(Kohlrausch and Reitz, 1940; Luther *et al.*, 1950; and Tschamler and Voetter, 1952). The assignments of the bands based on both infrared and Raman spectra are shown in Table 2.1.

2.3 Spectroscopic and Physical Properties of THF+H_2O System

2.3.1 THF+Water Solution

Hydrogen bonding of in THF-water solutions was studied by infrared spectroscopy(Bonner and Choi, 1974). The water bands were resolved by a computer analysis to three Gaussian components related to complexes at the 1:1 water-solvent and 1:2 water:solvent ratios. These ratios were verified by dilution of the complexes with CCl_4 and C_6H_6. The positions of the bands and their widths at half-intensity varied in a predictable manner with the degree of hydrogen bonding.

The hydrogen bonding ability of THF with solvents, like water, not only is being studied by spectroscopic methods, but also being used to explain some macroscopic phenomena.

Anomalies in the surface energy of water in the tetrahydrofuran-water system were ascribed to hydrogen bonding(Kunze, 1948). The same hydrogen bonding concept was also used to explain the solubility of tetrahydrofuran in water(Ferguson, 1955) and to explain a minimum boiling azeotrope and a viscosity maximum for THF+H_2O system

Table 2.1 Raman and Infrared Spectral Data and Probale Assignments for Liuiud THF

(Modified from Palmer, A. and Bissell, E.R, 1960)

Liquid		Probable Assignments
Raman+	Infrared Absorption bands	
THF	THF	
2975	2977 vs	CH stretch (a)
2938		CH stretch (a)
2865	2861 vs	CH stretch (a)
2717	2860 m	Σ
	1972 m	Σ
1486		CH_2 bend
1452	1461 s	CH_2 bend
	1364 m	CH_2 wag
	1333 m	CH_2 wag
	1289 m	CH_2 wag
1234	1234 m	CH_2 wag
1174	1177 s	ring stretch (a)
1104		CH_2 twist
1071	1067 vs	ring stretch (a)
964		CH_2 rock
913	908 vs	ring stretch (s)
651	654 s	CH_2 rock
596		ring i-p bend
276		ring o-p bend
215		ring o-p bend

(Montgomery *et al.*, 1949). The temperature for maximum density of the tetrahydrofuran-water system was measured but no anomalies similar to those shown by the analogous dioxane-water system were found for THF+H_2O system(Wada and Uneda, 1962).

The viscosity of THF+H_2O solutions changes in a step-wise fashion with variation in the THF concentrations. The maximum viscosity for THF+H_2O solution at room temperature occurs at a ratio of 1:8 THF molecule to water molecule(Pinder, 1965).

2.3.2 Macroscopic Measurements of THF Hydrate

The tetrahydrofuran hydrate is reported to have seventeen water molecules for each tetrahydrofuran molecule(von Stackelberg and Meuthen, 1958). The dissociation temperature for pure THF hydrate was reported to be 5.1 °C(Pinder, 1965).

Due to the complexity of kinetic measurements, most of the research has concentrated on the thermodynamic and physical properties of the tetrahydrofuran-water system. However, the rate of formation of THF hydrate was measured and it was found that the concentration changed in a stepwise manner, with breaks at concentrations which corresponded to water to THF mole ratio of 10:1, 8:1, 7:1, 5.5:1, 3.5:1. 3:1 and 2.5:1(Pinder, 1965). It was postulated that these results were due to hydrogen bonding in the solution, forming

complexes of finite molar ratios of water to THF corresponding to the breaks in the concentration versus time curves(Pinder, 1965). The rate of hydrate formation was interpreted to be controlled by diffusion of one complex to the other(Pinder 1965). The time dependent rheology of the THF-hydrogen sulfide hydrate slurry was also studied(Pinder, 1965).

In addition to viscosity measurements, there are experimental measurements of the phase behavior of tetrahydrofuran-water system(Hanley *et al.*, 1989; Dyadin *et al.*, 1973). The phase diagram is shown in Figure 2.7.

2.3.3 Review of Spectroscopic Measurements on Hydrate

The infrared spectrum of clathrate hydrates at 4.3K and 100K was measured and the features were assigned to the various modes of vibration of water molecules(Bertie and Jacobs, 1977; Bertie and Jacobs, 1982; Bertie and Jacobs, 1983). The results showed that the translational region of the vibrational spectrum is dominated by the motions of the disordered water lattice with guest species has little apparent influence. This leads to the suggestion that the strength of hydrogen bonds in hydrates is very similar to that in ice. From both the X-ray and NMR work, it is known that, the water molecules are orientationally disordered(Davidson *et al.*, 1977), and all the lattice vibrations are, in principle,

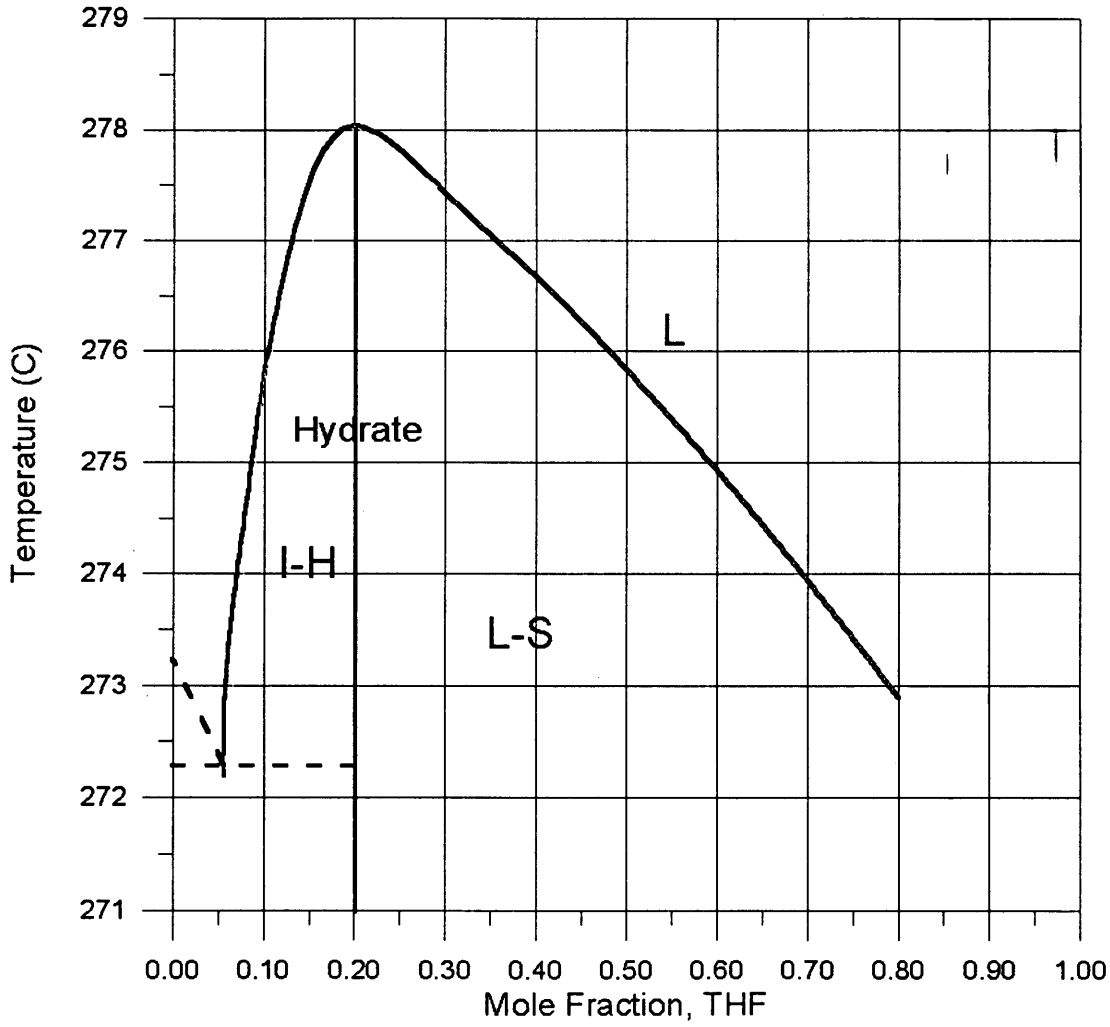

Figure 2.7 Phase diagram of THF+H_2O solutions

active in the infrared region.

Several other sI hydrates were investigated using infrared techniques. Far infrared spectra of CO_2 hydrate and N_2 were obtained(Devlin and Richardson, 1978). The spectrum features were attributed to the mobile defects of the lattices and the relaxation of guest molecule inside the cages.

NMR spectroscopy and dielectric constant measurements provide information about the motion of water molecules in the hydrate crystal structure(Davidson and Ripmeester, 1984). The rotational relaxation time obtained from both the NMR and dielectric measurements have given insights into the kinetics of molecule reorientation inside the hydrate cage. Other workers(Albayrak and Zeilder, 1987) also did similar NMR relaxation in THF clathrate hydrates. It was concluded from the comparison between guest molecules in the clathrate hydrate, in the corresponding aqueous mixtures and in the pure liquid that the fastest motion was present in the clathrate hydrate.

A comparison between the dielectric relaxation features of the guest molecules and of rigid molecular glass has lead to a qualitative understanding of the intrinsic mobility of THF in the glassy state of pure THF(Johari and Chew, 1983).

The effect of pressure on the vibrational spectrum of THF hydrates was studied by Raman spectroscopy(Johari and Chew, 1984). That study concentrated on three spectral regions: 100-

350, 2200-2800 and 2800-3500 cm^{-1}, in the temperature range of 250-275 K and a pressure range of 1-1500 bar. The results showed that there was no simple relationship between the OH stretching frequencies and the near-neighbor distance of water molecule. This study was the first Raman spectroscopic study of clathrate hydrates.

Natural O_2 and N_2 clathrates were also measured using Raman spectroscopy(Nakahara *et al.*, 1988). Temperature-dependent Raman spectra were obtained. The peak positions of the guest molecules shift to lower frequencies at lower temperature. This structure was considered to arise from over-damping of the rotation modes of the guest molecules.

CHAPTER III

EXPERIMENTS

3.1 Introduction to Raman Spectroscopy

The Raman effect was first discovered by C. V. Raman in early 1921 by conducting a series of experimental studies on the scattering of light from different transparent media. The Raman effect was an entirely new phenomenon which allowed recording of the characteristic molecular vibration frequencies more conveniently than infrared techniques uSing the scattering of light in the visible region. When a sample is irradiated with high energy radiation, e.g., laser, mercury arc, etc., a small amount (approximately 1%) of the radiation is scattered. Most of the scattered radiation is elastic scattering which is called Rayleigh scatter, but in addition, certain discrete frequencies above and below that of the incident beam are also inelastic scattered, called Raman scattering. The intensity of Raman scattering is approximately 10^{-8} that of the source and therefore is very weak.

The following is a very short and simple introduction to Raman spectroscopy. It is combined from several excellent review papers and books(Anderson, 1971; Szymanski, 1970; Gilson and Hendra, 1969; Long, 1977; Wilson *et al.*, 1955). A

more detailed and elaborate treatment of Raman effect can also be found in the above monographs.

3.1.1 The Origin of the Raman Effect

When a static electromagnetic radiation is applied to a molecule, the molecule has some charge distortion, with the positively charged nuclei attracted to the negative pole of the applied field, and the electrons attracted to the positive pole. An induced dipole moment is set up in the molecule, and the molecule is said to be polarized. The polarizability is defined to describe the degree of distortion of the charge distribution of the molecule in the field. The polarizability can be described by an ellipsoid referred to as polarizability ellipsoid.

By the application of classical mechanical theories to the Raman effect, the simple picture of the mechanism of the Raman effect is furnished by considering the interaction between a photon and a molecule as a inelastic collision, satisfying the law of conversation of energy. If the incident light photon suffers a loss of energy as a result of that collision, it appears in the spectrum as a radiation of increased wavelength, i.e., as Stokes line, $\vartheta-\vartheta_1$, while the molecule which absorbs the energy of the photon is transported

to a higher level of rotation or vibration. It is also possible to conceive of the collision in which the molecule, already in an excited state, gives up its energy to the incident photon and decays to a lower vibration or rotation level. The scattered light will then appear in the spectrum as a line of diminished wavelength or of increased frequency, i.e., as an anti-Stokes line, $\vartheta+\vartheta_1$. In both cases the frequency shifts of the scattered radiations from the incident line give a measure of the rotational or vibrational frequencies of the molecule.

The Raman scattering effect is very much less intense than Rayleigh scattering. The intensity of the lines depends on the magnitude of the change in the polarizability during the molecular vibration. If there is no change in the polarization of the bond during the vibration, no Stokes' and anti-Stokes' lines will be observed and that particular molecular vibration mode is called Raman inactive.

The classical treatment of Raman scattering explains the appearance of both the Stokes' and anti-Stokes' lines. However, the classical approach fails to predict the intensities of these lines. Equal intensity of these lines are predicted from the classical approach. In practice, for vibrational changes, because of the Boltzmann thermal distribution law, the Stokes' lines are much more intense than

the anti-Stokes' lines.

Quantum mechanics theory treats monochromatic radiation of frequency υ as a stream of photons having discrete energy $h\upsilon$, where h is Plank's constant. The schematic representation of the scattering process is shown in Figure 3.1. In Rayleigh scattering, the incident photon collides with a molecule and suffer no energy lose. In the Raman effect, the collision of the photon induces the molecule to undergo a transition in the vibrational states and the frequency of the scattered radiation is different than that of the incident photon. If, for a molecule undergoing a vibrational transition from the ground state (υ=0) to the first excited state (υ=1), the frequency of the radiation required to induce this transition is ϑ_1, the scattered photon will be diminished in energy by $h\vartheta_1$ i.e., the energy of the scattered photon will be $h(\vartheta-\vartheta_1)$. In contrast, if the molecule is already in an excited vibrational state when the incident photon collides with it, the transition υ=1 to υ=0 may be induced and the photon will be scattered with an enhanced energy $h(\vartheta+\vartheta_1)$. The photons with lower energy give rise to Stokes' lines whereas those with an enhanced energy give anti-Stokes' lines. By applying the Boltzmann thermal distribution law, it can be shown that at room temperature the population of molecule in the ground state is much higher than that in the first excited state or

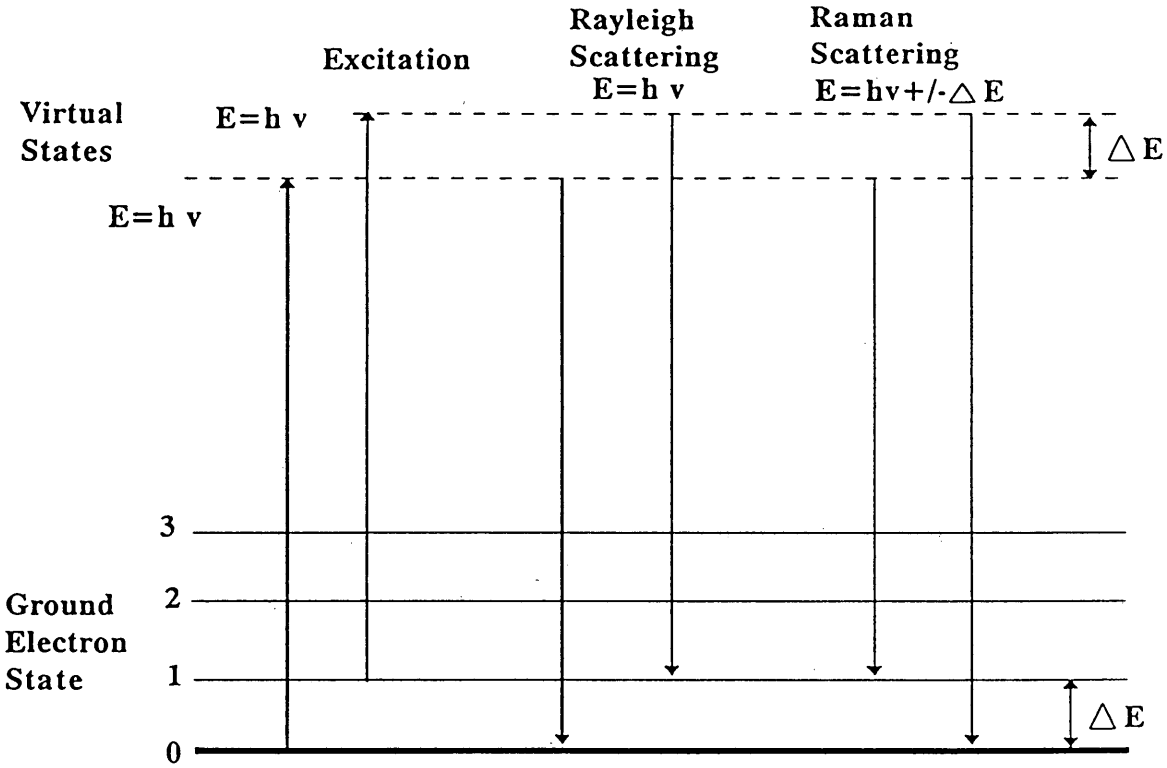

Figure 3.1 Diagram of Origin of Raman and Rayleigh Scattering

any other excited states and therefore the Stokes' lines will be more intense than anti-Stokes' lines. Thus the Stokes' lines are always observed in practice instead of the anti-Stokes lines.

3.1.2 Important Observations

The important observations obtained from Raman spectroscopy are the frequency shifts, the state of the polarization, the intensities of the Raman lines, and the width of the Raman lines. The frequency shifts are expressed in wavenumber (cm^{-1}) which is the reciprocal of wavelength, and are obtained as the differences of the wavenumber of the incident exciting line and the corresponding Raman lines. If these are multiplied by $3x10^{10}$ cm/sec (light velocity) one gets the actual frequencies in any Raman spectrum. The state of polarization which is called depolarization ratio, is expressed as the ratio of the intensities of the horizontally polarized component to the vertically polarized component of the Raman line. If this value is less than 0.1, the line is considered as polarized and if it is more than 0.5(Krishnan, 1971), it is considered as depolarized. In chapter 5, the depolarization ratio of THF C-O-C ring stretching mode is determined through polarized study.

3.1.3 Raman Spectra

The Raman effect is an inelastic light scattering process and therefore is not an absorption but an emission phenomenon. However, several other emission phenomena can also occur. Fluorescence is one of them and can have a broad emission which appears as a sharply varying and often intense background in a Raman spectrum, on which the Raman bands are superimposed. This can make the determination of Raman band positions and intensities difficult. Methods have to be used to eliminate this background signal.

The Raman spectrum is presented as a plot of intensity of the scattered radiation versus the Raman frequency shift. The Raman frequency shift is defined as the wavenumber shift from the exciting line and is calculated by direct subtraction of the absolute wavenumber of the vibration from that of the exciting line. Therefore, Raman bands appear at approximately the same wavenumber shift as the absolute wavenumber of the same adsorption band in the infrared spectrum.

3.2 Study Using Polarized Laser Light

3.2.1 Background Information

The polarizability of a molecule is defined by Eq. 3.1

$$\mu_i = \alpha \epsilon \qquad (3.1)$$

where

μ_i = induced dipole moment

ϵ = electromagnetic field strength

α = polarizability of the molecule

The polarizability is a tensor quantity and as such has components in each of the x, y, z directions of a cartesian coordinate system. As a result, an electric field component in one direction can induce a dipole component in the x, y and z directions as defined by the following equations:

$$\begin{aligned} \mu_x &= \alpha_{xx} \epsilon_x + \alpha_{xy} \epsilon_y + \alpha_{xz} \epsilon_z \\ \mu_y &= \alpha_{yx} \epsilon_x + \alpha_{yy} \epsilon_y + \alpha_{yz} \epsilon_z \\ \mu_z &= \alpha_{zx} \epsilon_x + \alpha_{zy} \epsilon_y + \alpha_{zz} \epsilon_z \end{aligned} \qquad (3.2)$$

which can be written in matrix notation as :

$$\mu = \alpha \epsilon \qquad (3.3)$$

Normally $\alpha_{ij} = \alpha_{ji}$ so that there are six independent components of this two dimensional tensor.

There are two invariant (constant regardless of the

orientation of the molecule) properties of the polarizability tensor:

(1) the mean value α

(2) the anisotropy γ

The mean value can be written as :

$$\alpha = \frac{1}{3} (\alpha_{xx} + \alpha_{xy} + \alpha_{xz}) \qquad (3.4)$$

and the anisotropy as:

$$\gamma = \frac{1}{2} [(\alpha_{xx}-\alpha_{yy})^2 + (\alpha_{yy}-\alpha_{zz})^2 + (\alpha_{zz}-\alpha_{xx})^2 + 6(\alpha_{xy}^2+\alpha_{xz}^2+\alpha_{yz}^2)] \qquad (3.5)$$

These two values can be used for calculation of the depolarization ratio for the different vibrations.

The most common scattering geometry is 90°. The scattering and the laboratory axes are shown in Figure 3.2. There are two configurations in a normal polarized study, referred to as cross configuration and horizontal configuration.

The intensity of the scattered light is proportional to the square of the induced dipole moment and thus for the isotropic and anisotropic scattering; $\mathbf{I}_z$ and $\mathbf{I}_y$ in Figure 3.2,

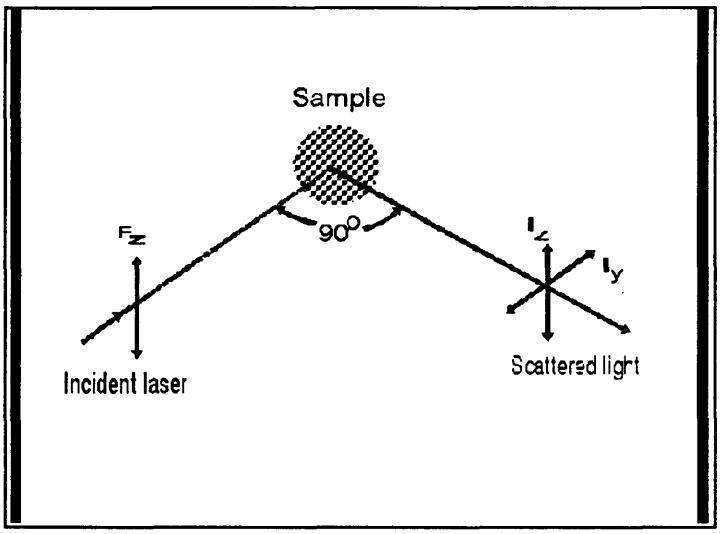

Figure 3.2 90 ° Scattering Geometry

it can be shown:

$$I_z = k\,\alpha_{ii}^2\,\epsilon_z^2 \qquad (3.6)$$

$$I_y = k\,\alpha_{ij}^2\,\epsilon_z^2 \qquad (3.7)$$

The ratio of the intensities of the anisotropic and isotropic scatter is a useful quantity referred to as the depolarization ratio:

$$\rho = \frac{I_z}{I_y} = \frac{1/15\ \gamma^2}{1/45^*\ (45\alpha^2 + 4\gamma^2)} = \frac{3\gamma^2}{45\alpha^2+4\gamma^2} \qquad (3.8)$$

For a vibration not totally symmetrical, that is a vibration which does not generate the totally symmetrical and irreducible representation of the molecular point group, and thus ρ is equal to 3/4. For all other vibrations $0 < \rho < 3/4$. Using this result the value of the depolarization ratio enables the symmetry of a vibration to be determined.

3.2.2 Depolarization Ratio Calculation

In order to calculate the depolarization ratio, the intensity of both directions has to be calculated. The

computer deconvolution technique needs to be used to separate the spectrum into different bands. The integrated area of each band can be calculated using the following expression:

$$Relative\ Intensity = \frac{Integrated\ Area\ of\ Individual\ Peak}{Total\ Integrated\ Area\ of\ The\ Band}$$

However, the observed intensities must first be corrected to remove the temperature-dependent contribution arising from the thermal populations of the excited vibrational levels(Cates and MacPhail, 1991; Walrafen, 1973). The corrected intensities are related to the measured intensity by the equation

$$I^*_r = I_r\, B(\nu, T) \qquad (3.9)$$

where the Boltzmann correction factor $B(\nu,T)$ is given by

$$B(\nu, T) = 1 - \exp\left(\frac{-hc\nu}{k_B T}\right) \qquad (3.10)$$

H is the Planck's constant, c is the speed of the light, ν is the vibrational frequency of the band under investigation, and k_B is the Boltzmann's constant. This

thermal intensity correction makes the calculation of both the depolarization ratio and rotational relaxation time more accurate.

Thus, the depolarization ratio is calculated using the corrected intensity with the following expression:

$$\rho = \frac{I_Z^*}{I_Y^*} \qquad (3.11)$$

where

I_Z^* is the intensity of the depolarized spectrum

I_Y^* is the intensity of the polarized spectrum

3.2.3 Rotational Relaxation Time Calculation

The methodology for studying reorientational dynamics using Raman spectra is the standard(Cates and MacPhail, 1991; Bartoli and Litovitz, 1972; Tarjus and Bratos, 1984; Hills, 1984). Assuming there are no cross correlations between rotation and vibration, the rotational correlation time τ_{rot} can be determined from the difference in the FWHM values of the depolarized spectra and the isotropic spectra of a Raman band according to the equation

$$\tau_{rot}^{-1} = 2\pi c(fwhm_{depol} - fwhm_{isotr}) \qquad (3.12)$$

The isotropic spectrum is obtained by the difference between polarized spectrum and depolarized spectrum with the following relation:

$$I_{isotropic} = I_{Dep.} - \frac{4}{3} I_{Pol.} \qquad (3.13)$$

where

I_{iso} = the intensity of the isotropic spectrum

I_{dep} = the intensity of the depolarized spectrum

I_{pol} = the intensity of the selected polarized spectrum.

3.3 Experimental Setup

There are three components necessary to record any Raman spectrum. First, a convenient exciting source, typically a laser; second, a sample container with well polished-windows for illumination and observation; third, a monochrometer to actually record the spectrum. Auxiliary devices such as light filters, lenses, heating and cooling system, polarizer, and analyzers are used for special purposes. Each component will

be discussed in detail in the following section. The schematic diagram of experimental setup is shown in Figure 3.3.

Solution and solid hydrate samples were studied in a temperature controlled cuvette in the macrochamber of the Raman spectrometer.

Each segment of the system will be discussed in detail in the later sections.

3.3.1 Description of the Laser System

A laser device is the fundamental source of any modern spectroscopic research. Laser excitation was provided by a 5-W Ar^+ CW ion laser(Spectra-Physics Model 2025-5) capable of generating ten visible wavelength and two long wavelength ultraviolet lines. The visible green line with wavelength 514.53 nm was used for all the experiments. The operating power was changed depending on what system was measured. Prior to recording each spectrum, laser power was measured with a Scientech, Inc., Model 361 power meter at the entrance to the macrochamber. Two Pellin-Broca prisms and a spatial filter were used to eliminate the plasma lines. For routine Raman spectra the excitation power employed was 170 *mw* for studying pure THF liquid and THF solution, 340 *mw* for studying THF hydrate due to the scattering from the solid. The output power

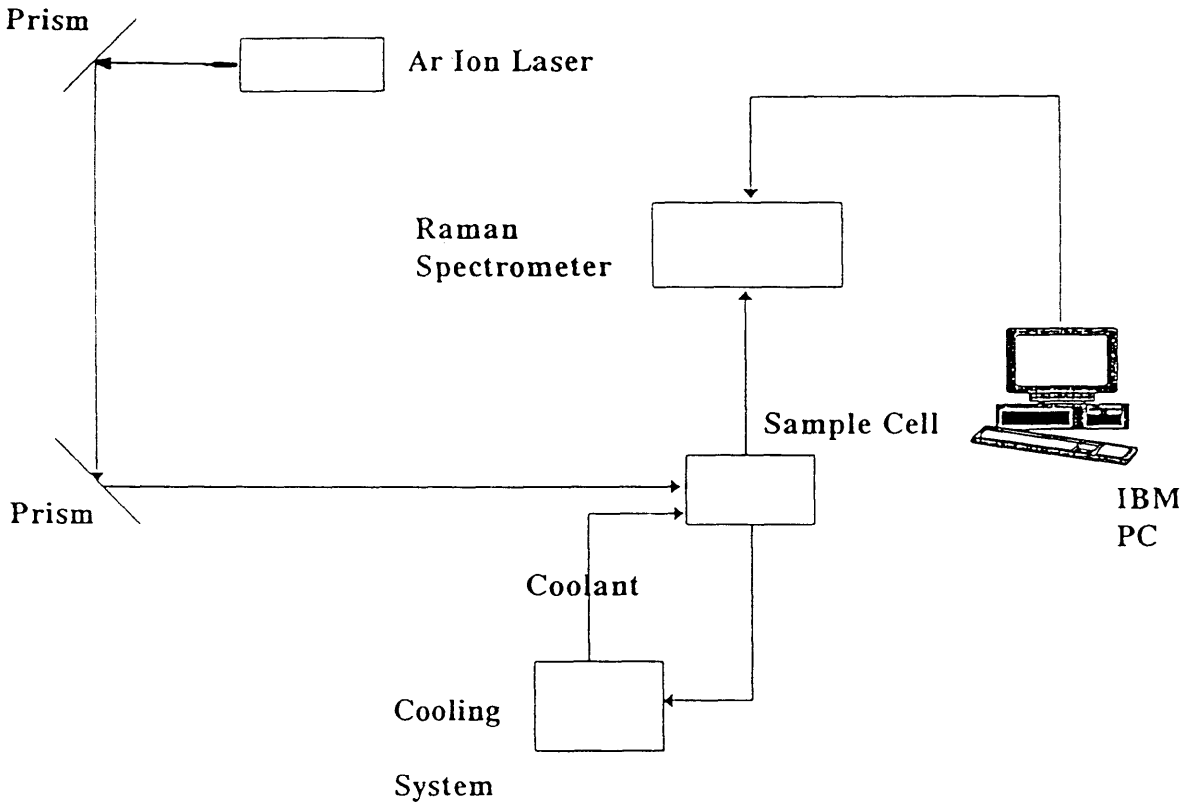

Figure 3.2 Diagram of Experiment Setup

of the ionized-gas laser device is reasonably stable (+/- 1% output power). For the system used in this research, the laser beam is polarized in the vertical direction.

3.3.2 Laser Optical System and Optical Alignment of the Raman System Macrochamber

Almost every laser-Raman instrument seems to have its own unique sampling system and pre-slit optics. However, the basic requirements are the same in each case: to illuminate the sample in such a way that a reasonable amount of signal is produced to be passed efficiently to the entrance slit of the monochrometer. In this research, the optical alignment is similar to most of the other laser spectroscopy optical systems.

In this particular application the macrochamber, with a rectangular configuration, of the Raman spectrometer was used. The 90° scattering geometry was used in this study. Due to the inherent weakness of the Raman effect, the laser beam must be focused on the sample. This was achieved by passing the laser beam through a focusing lens as it entered the macrochamber. The beam was focused on the center of the macrochamber where the sample cell was mounted. Due to the random angle of the scattered light, there were two reflective mirrors inside the

chamber; one was on the laser path; the other was on the path 90° to the laser beam. The purpose of these two mirrors was to collect the scattered light and refocus on the sample to increase signal to noise ratio(S/N). Both mirrors can be adjusted to get the maximum S/N value. In front of the entrance of the monochrometer, there was a focus lens which can be used to focus on the center of the sample. By adjusting all these mirror and focal lens, high S/N ratio can be obtained.

For polarized measurements, a polarization rotator was placed in the laser beam path before it entered the macrochamber. A polarization analyzer, set to pass vertically polarized light, was positioned between the entrance slit of the monochrometer and the focusing lens of the monochrometer. Since the Ar^+ laser beam is vertically polarized, the spectra obtained with this vertically polarized configuration are called depolarized spectra. The overall configuration was called a horizontal configuration because the preferred polarization configuration for the U1000 monochrometer was parallel to the laser polarization direction. Then the polarization of the beam was rotated 90° relative to the original polarization direction before it entered the macrochamber. The spectra obtained referred to as polarized spectra. The overall configuration was referred to as cross

configuration.

Before the polarized spectra of the THF samples were recorded, the system was tested by measuring liquid CCl_4 polarized spectra at room temperature in both directions. The polarized spectra of CCl_4 were in good agreement with literature spectra(SchrÖtter, 1970).

The sample was put in a jacketed cuvette made of glass which is shown in Figure 3.4 with dimensions of length, width and height. The windows were very well polished on the laser beam path so that there was not too much scattering from the windows which increased the S/N ratio. A methanol circulating cooler/heater was used to control the temperature of the sample cell ranging from -27.5 °C to 25°C. The rate at which the methanol was pumped through the jacket was controlled so that the temperature of the cell could be quickly stabilized. There was no stirring inside the cuvette.

3.3.3 Description of the Monochrometer System

As pointed out before, the Raman bands were extremely weak relative to the exciting radiation, and it is required that the monochrometer system has very high discrimination. The basic function of the monochrometer is to select a small spread of the wavelength of the scattered radiation.

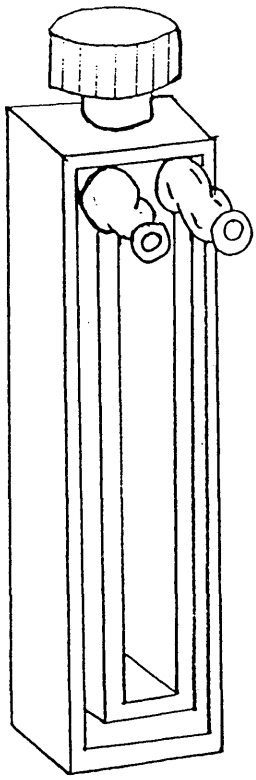

Figure 3.4 Configuration of the jacket cuvette cell

(Cell has horizontal in and outlet tubes to jacket on one side and Teflon stopper on specimen compartment of 4 mm wide. All sides are clear and polished with path length 10 mm. **Type T-54FL**, NSG Precision Cells, Inc., New York)

Spectroscopic measurements were made with an Instruments SA, Inc.(ISA) Ramanor U1000, 1m double-dispersed monochrometer system equipped with different holographic grating systems, i.e, 1800 grooves/mm and 600 grooves/mm at the United States Geological Survey (USGS), Denver Federal Center, Denver, Colorado. The monochrometer uses a sine drive so that dispersion is linear in wavelength. The slits setting for the monochrometer depends on the kind of grating system used during the experiments. The resolution of the spectrum depends on the slit width. Slit settings and spectral resolution are discussed in the section on calibration.

3.3.4 Signal Processing System

The signal processing system was composed of a photomultiplier tube (PMT), an amplification system and an output device. The photomultiplier counts the number of the photons entering the detector over the spread of the wavelength determined by the monochrometer.

The signal was detected with a single-channel, photon-counting system(RCA 31034A PMT cooled to -20 °C and a Pacific Instruments amplifier-discriminator) connected to an ISA Spectralink module which was interfaced to an IBM-AT computer running ISA PRISM software(Burruss *et al.*, 1992)

For time-dependent spectra measurements, the PI(Princeton Instrument) multichannel diode array detector was used. The detector system was called the optical simultaneous multichannel analysis(OSMA) system. The PI diode array detector was coupled with a IBM/486 computer running ST120 software to collect and process data. An important advantage of this type of detector is the ability of real-time continuous display of the spectrum and thus shows the spectrum changes with time. The horizontal axis of the time dependent spectrum is divided into units of pixels. To display a spectrum with the units of wavenumber scale, the system has to be calibrated.

3.4 Experimental Procedure

3.4.1 Solution Preparation

THF at 99.99% purity was used as received from Aldrich Chemical Company without further purification. Water was double distilled. Deuterated water was also obtained from Aldrich Chemical Company and used as received without further purification. The solutions were made up by weight, with the weight percent calculated from the required mole fraction of THF. Table 3.1 shows the mole ratio of THF and H_2O required for the correct molar concentration. The precision of the

Table 3.1 Molar ratio and mole fractions of THF+H_2O solutions

Molar Ratio+	Mole Fraction
4:1	0.8
2:1	0.67
Pure THF	1.00
1:2	0.33
1:4	0.2
1:8	0.11
1:16	0.059
1:17	0.056
1:24	0.04
1:49	0.020
49:1	0.98

+: The first number refers to the moles of THF and the second number refers to the moles of water in the solution.

actual THF mole fraction in the solution is within 1% of the mole fraction shown in Table 3.1 since the THF is a very volatile component.

Solutions of THF with other solvents, e.g., D_2O, CH_3OH, $CHCl_3$, and CCl_4, were prepared using the same method. HDO solutions were made by adding equal amounts of D_2O and H_2O solution.

3.4.2 Calibration Procedure

Calibration of any spectroscopic system is critical to the measurements in terms of the resolution of the position of any vibration frequencies. The mercury line at 546.1 *nm* from fluorescent room lights was used as a standard to calibrate the Raman spectrometer system. It has a position of 1123.4 cm^{-1} relative to the 514.53 *nm* green line of Ar^+ laser.

As using two different gratings, the slit width for each grating was different. For most of the experiments, 1800 groove/*mm* grating was used, the slit width for the monochrometer was set at 200 μm for calibration. For polarized spectra 600 groove/mm grating with 70 μm slit width was used for calibration. These combinations of gratings and slit width yield a spectral resolution of about 2 cm^{-1}. However, during the course of the polarized spectra measurement, the slits

width was set at 140 μm in order to improve the intensity of the signal since the wider the slits width, the more the number of photon entering the monochrometer. These slit widths yield a spectral resolution of about 4 cm^{-1}. The system has to be calibrated at the beginning of each experiment.

3.4.3 Cooling Procedure

As mentioned in Chapter 2, the dissociation temperature for pure THF hydrate is about 5.1 °C. In order to make sure that the solid phase was actually hydrate rather than a hydrate and ice mixture, a simple annealing procedure was used to form hydrate. The cell was first cooled to about -10°C from room temperature. Hydrate formed and then it was warmed to just above the dissociation temperature to let part of the THF hydrate dissociate. After some hydrate mass began to melt, the system was cooled to the required measuring temperature(above 0°C). Once the system reached thermal equilibrium, the measurement was begun. This procedure has a two-fold advantage. First of all, it confirms that the solid is hydrate rather than ice since the temperature is above the ice point. Secondly, after going through the annealing cycle, less scattering from the sample itself is achieved so that a higher S/N value is obtained.

A Plexiglass base and cover for the macrochamber were made to keep the moisture away from the cuvette. Coolant was admitted through the base by two brass 1/4" Swagelok bulk head fittings connected to tubing from the cooler. Streams of dry N_2 gas were directed on the four surfaces of the cuvette to prevent condensation of atmospheric water on the optical surfaces. During the cooling process, the temperature of the methanol cooler was kept constant. The set point for the cooler was slightly lower than the required experimental temperature due to the fact that there was heat transfer between the ambient and the tubing.The temperature inside the cuvette was measured by a K-type thermocouple from Omega calibrated using ice-water mixtures.

A typical Raman spectrum of pure liquid THF at room temperature and 1 atmosphere obtained by this method is shown in Figure 3.4. The spectrum agrees well with the Raman spectrum of pure THF liquid in the literature at room temperature.

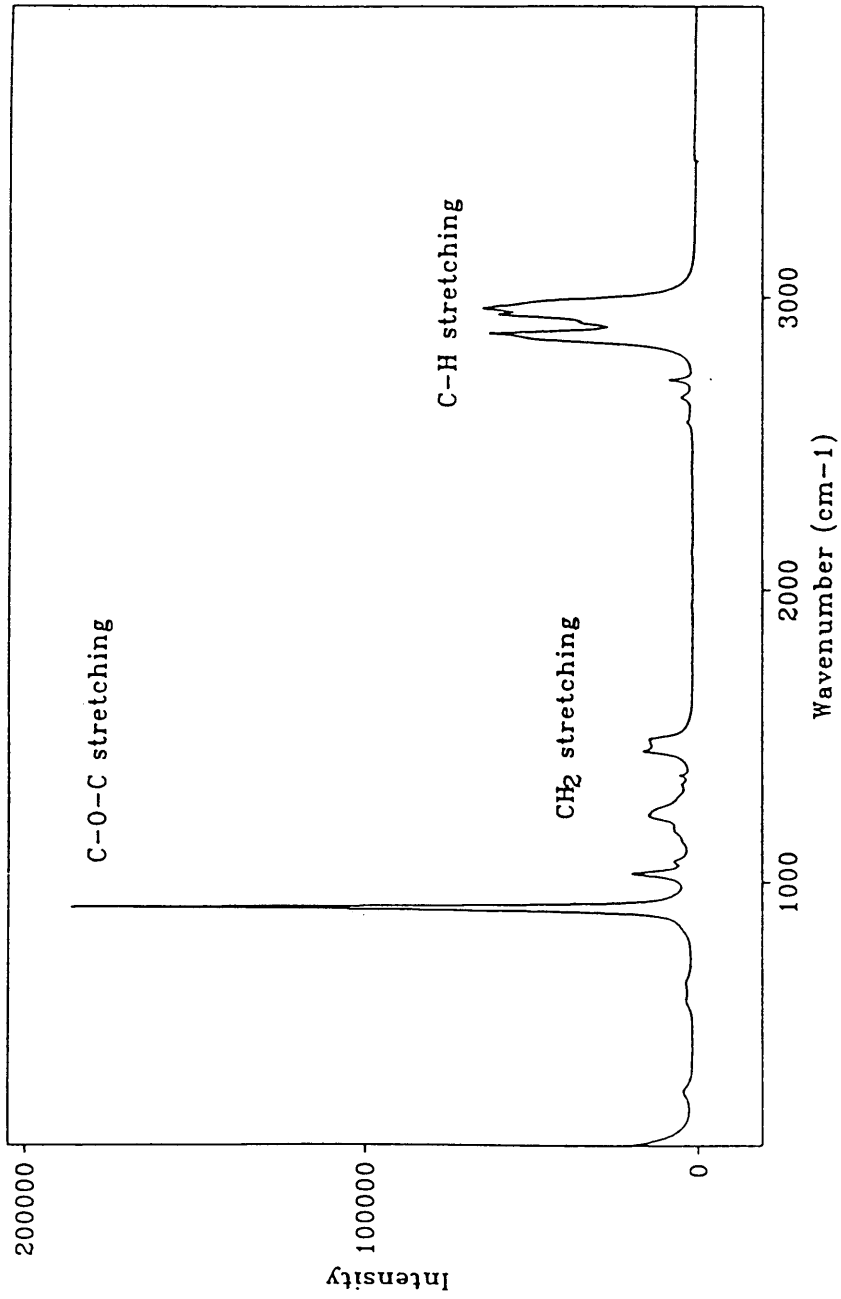

Figure 3.4 Typical Raman spectrum of pure THF liquid at room temperature

CHAPTER IV

EXPERIMENTAL RESULTS

4.1 THF+H_2O, D_2O and HDO Solution Spectra as Functions of THF Concentration

Raman spectra were recorded for different THF concentrations in solvents H_2O, D_2O and HDO. During the first THF+H_2O solution measurement, an obvious change in the THF C-O-C ring stretching region was observed. The C-O-C ring stretching frequency of pure THF as shown in Figure 4.1(a) has been very well defined (Kohlrausch and Reitz, 1940; Luther *et al.*, 1950; Tschamler and Voetter, 1952). A shoulder on the low wavenumber side of THF C-O-C stretching mode in the THF+H_2O solutions is shown in Figure 4.1(b). The position of this shoulder changes with THF concentration in the solution. The spectra of THF+H_2O solutions at molar ratios of 1:8, 1:17, and 1:24 are shown in Figure 4.1(b), 4.2(a), 4.2(b) respectively. Figure 4.3 shows spectra of THF+D_2O and THF+HDO solution at 1:17 mole ratio. There are several spectral features which should be noticed. First of all, there are three important regions in Figure 4.1(a). The region from 850 cm^{-1} - 920 cm^{-1} is THF C-O-C ring stretching region. The very sharp peak that occurs at about 913 cm^{-1} is the THF C-O-C symmetric stretching

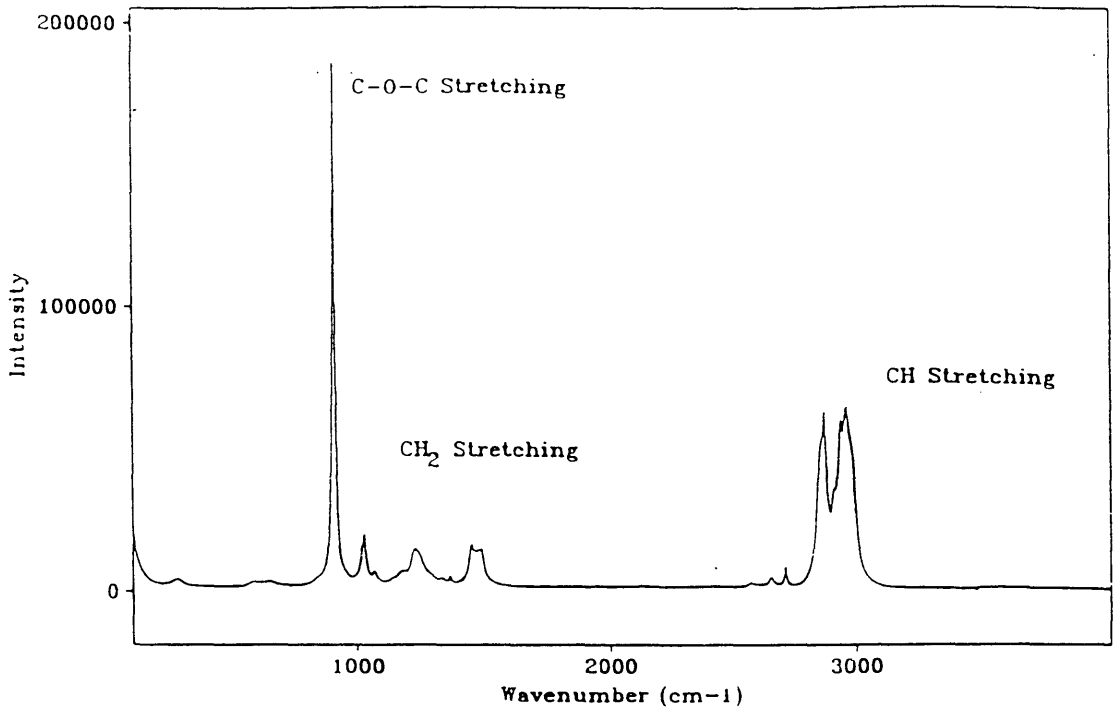

Figure 4.1(a) Spectrum of pure THF liquid at room temperature

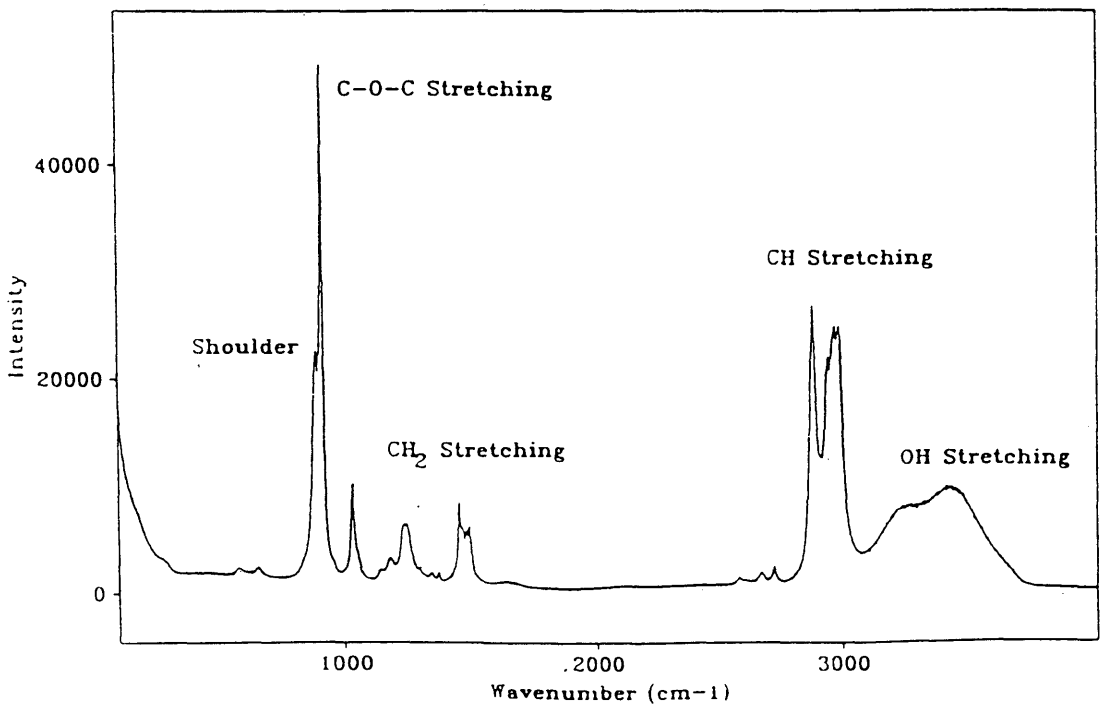

Figure 4.1(b) Spectrum of THF:H_2O solution(1:8 mole ratio) at room temperature

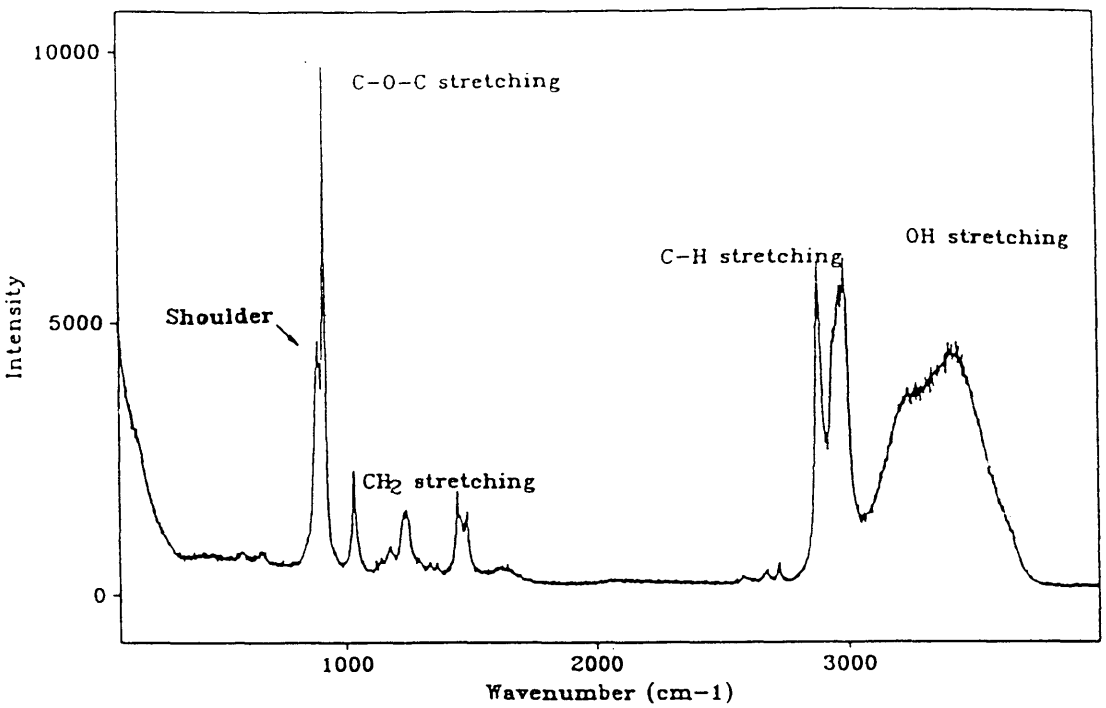

Figure 4.2(a) Spectrum of THF:H_2O solution(1:17 mole ratio) at room temperature

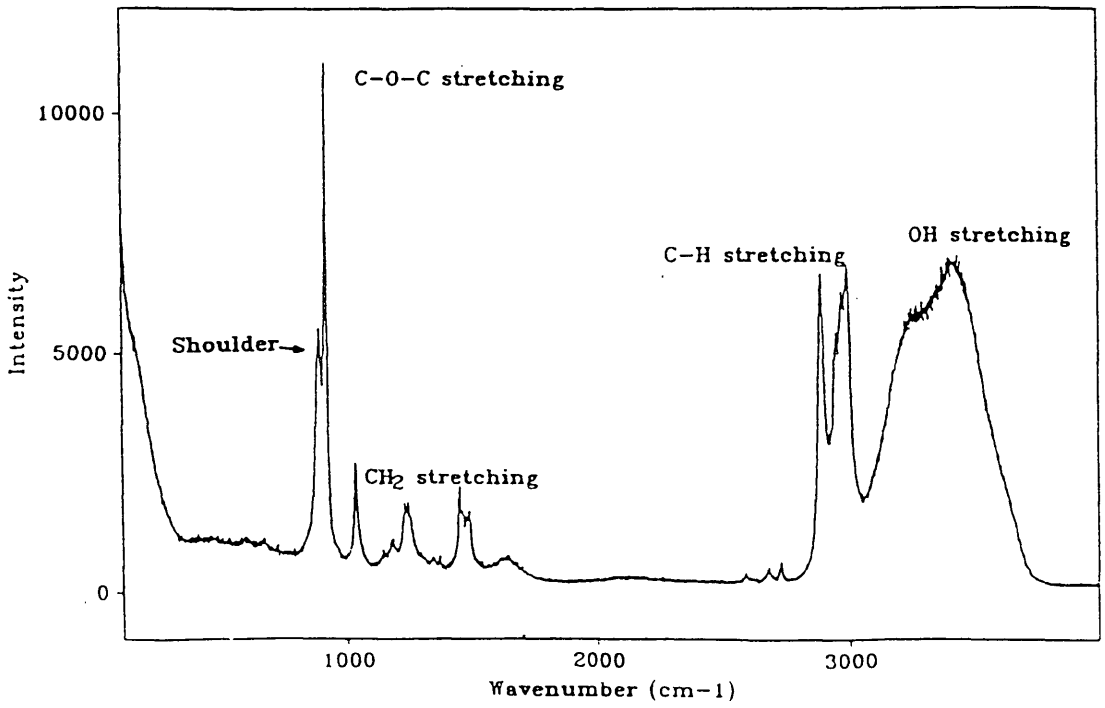

Figure 4.2(b) Spectrum of THF:H_2O solution(1:24 mole ratio) at room temperature

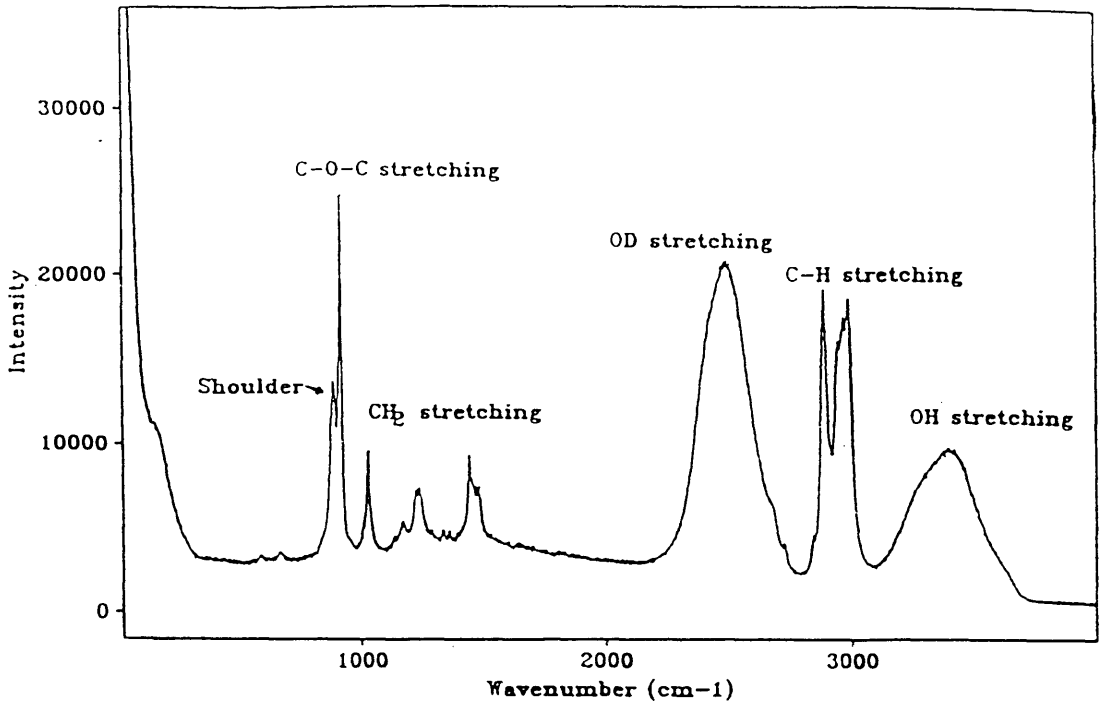

Figure 4.3(a) Spectrum of THF:HDO solution(1:17 mole ratio) at 3.0°C

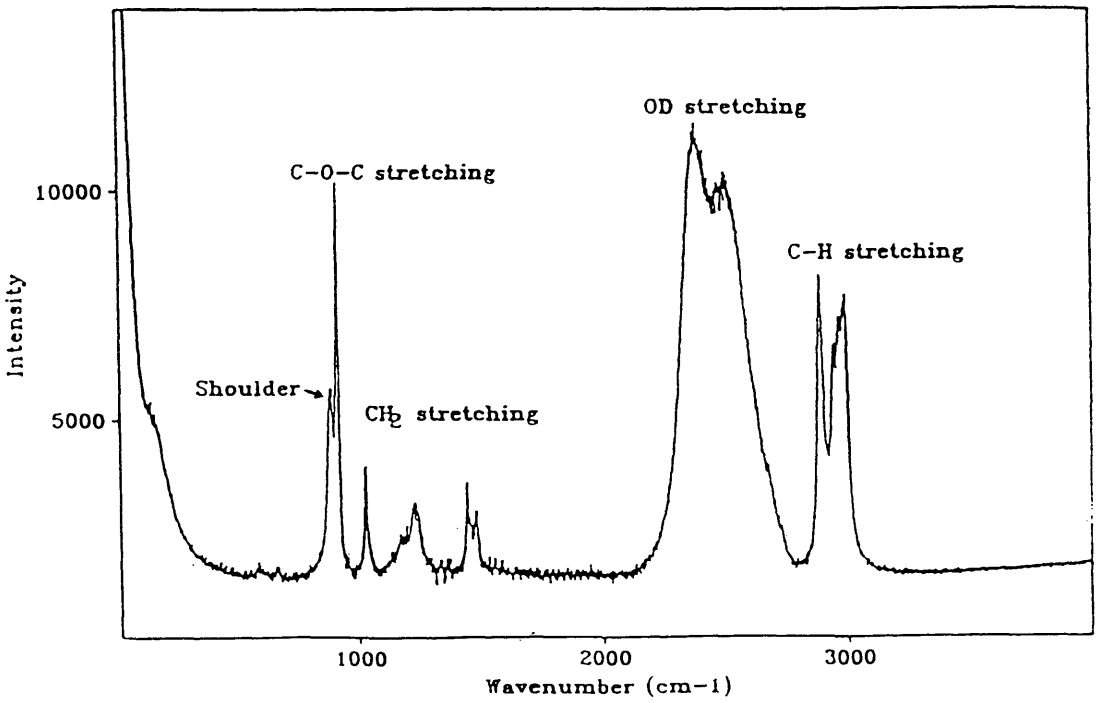

Figure 4.3(b) Spectrum of THF:D_2O solution(1:17 mole ratio) at 3.0°C

mode. Second region is from 940 cm^{-1} to 1600 cm^{-1} which is the THF CH_2 bending mode region. There are several different modes in this region as shown in Table 2.1. The third region occurs at about 2800 cm^{-1} which is called THF CH stretching band. This band is partially overlapped with the water OH stretching band so that the interpretation of the water OH band becomes more complex. Some special treatment of this band needs to be done before the interpretation. This will be discussed in detail in Chapter 5. In Figure 4.1(b), there is another region that is OH stretching region from 2800 cm^{-1} to 3600 cm^{-1}.

Figures 4.3 (a) and 4.3 (b) show the spectra of THF+HDO and THF+D_2O respectively. As shown in Figure 4.3 (a), there are two water intramolecular H-bonding and D-bonding bands, OH stretching and OD stretching respectively. The advantages of doing isotopic substitution are two-fold: first, it is possible to determine the origin of the shoulder near the THF ring stretching mode. Secondly, separating the complicated water OH band to OD and OH bands is very useful for understanding the intramolecular hydrogen bonding between water in the presence of THF molecules. In this research, the OD stretching is not analyzed using the computer decomposition techniques. However, the OH stretching band is fully analyzed for most of the system. In every figure except Figure 4.1(a), close to the THF C-O-C stretching mode at about 908 cm^{-1}, there

appears a small peak which is referred to as shoulder.

4.2 Spectra of THF+H_2O, D_2O, and HDO Solution as Functions of Temperature

Since the pure THF hydrate dissociation temperature is 5.1°C, and the temperature is one of the most important driving forces for hydrate nucleation process, several experiments of the subcooled THF+H_2O, D_2O, and HDO solutions at different temperatures were performed. While the whole temperature range was relatively small (from -10 °C to 25 °C), the phenomena near the THF hydrate dissociation temperature were well covered. The results are shown in Figures 4.4, 4.5 and 4.6.

Figure 4.4 shows spectra of THF+H_2O solution at 0.0 °C temperature and 3.0 °C. These spectra show little change in the position of the THF C-O-C ring stretching mode as well as the position of the shoulder over the temperature range. In other regions of the spectra, there are some subtle changes in the CH_2 vibration and CH stretching region. Changes are obvious in the water OH stretching mode. The overall band shape, which is an indication of the interaction, is changed. Similar changes occur in the spectra of THF+D_2O and THF+HDO solutions with variation in temperature.

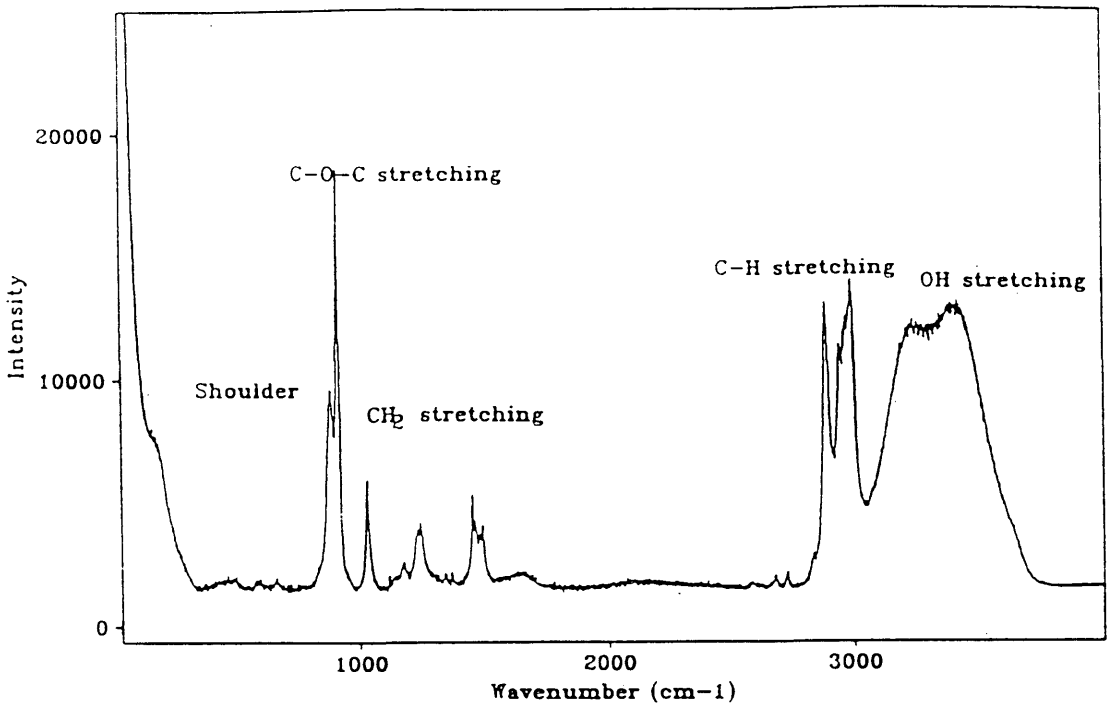

Figure 4.4(a) Spectrum of THF:H_2O solution(1:17 mole ratio) at 3.0°C

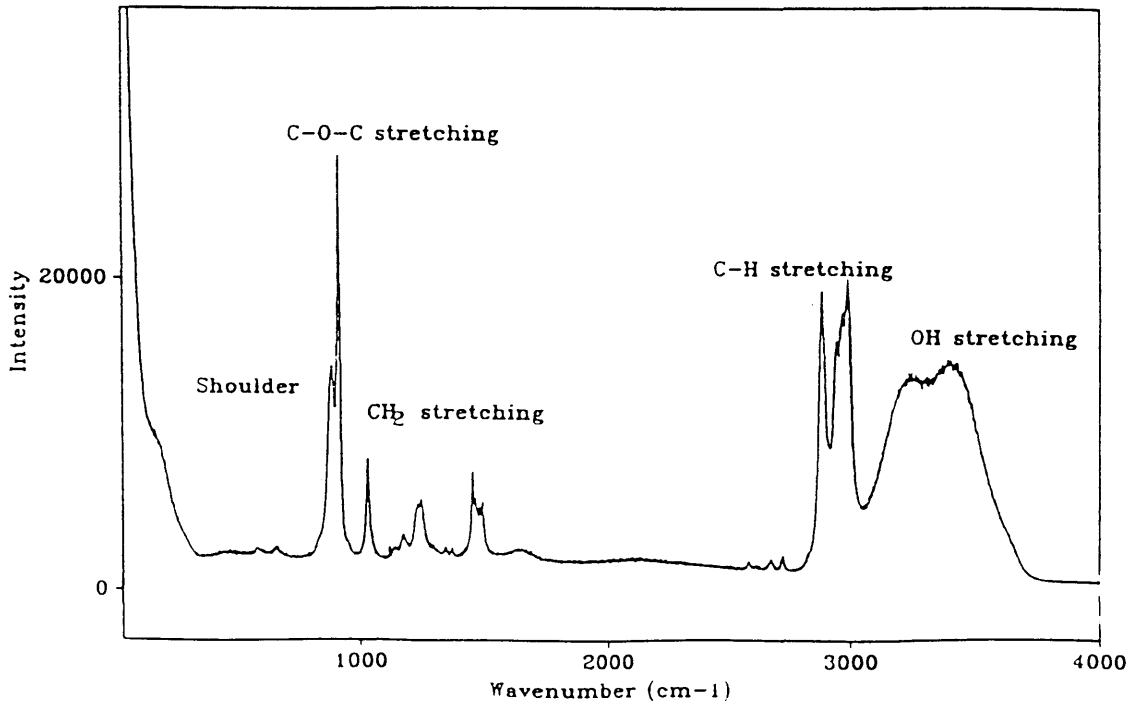

Figure 4.4(b) Spectrum of THF:H_2O solution(1:17 mole ratio) at 0.0°C

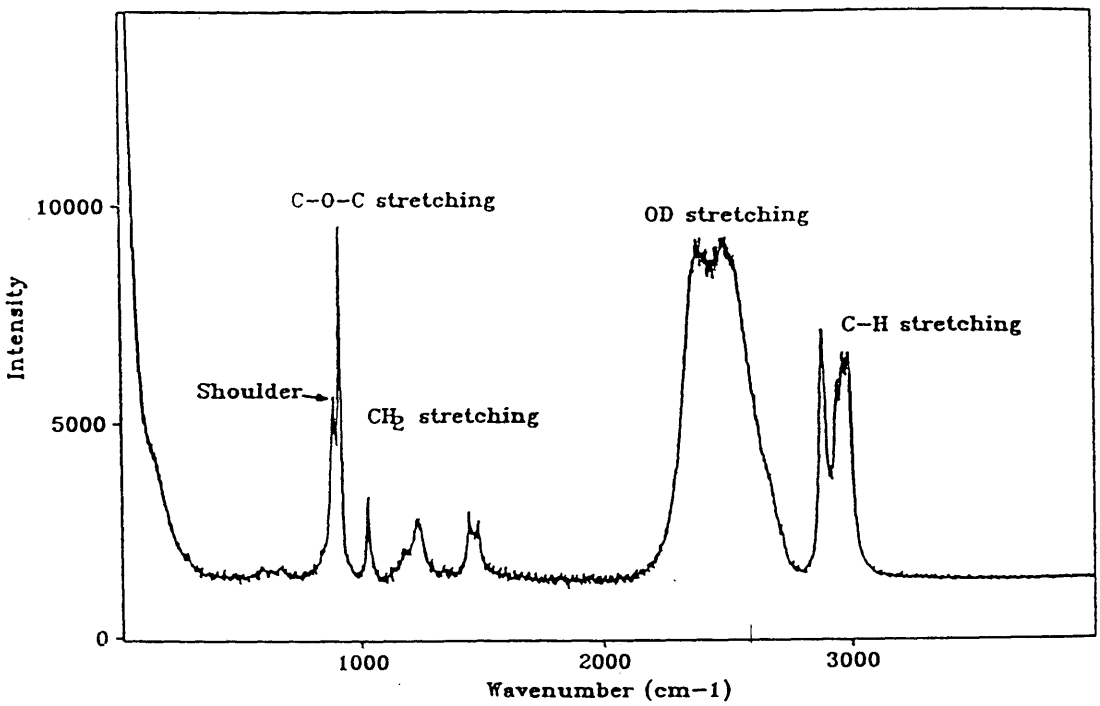

Figure 4.5(a) Spectrum of THF:D_2O solution(1:17 mole ratio) at room temperature

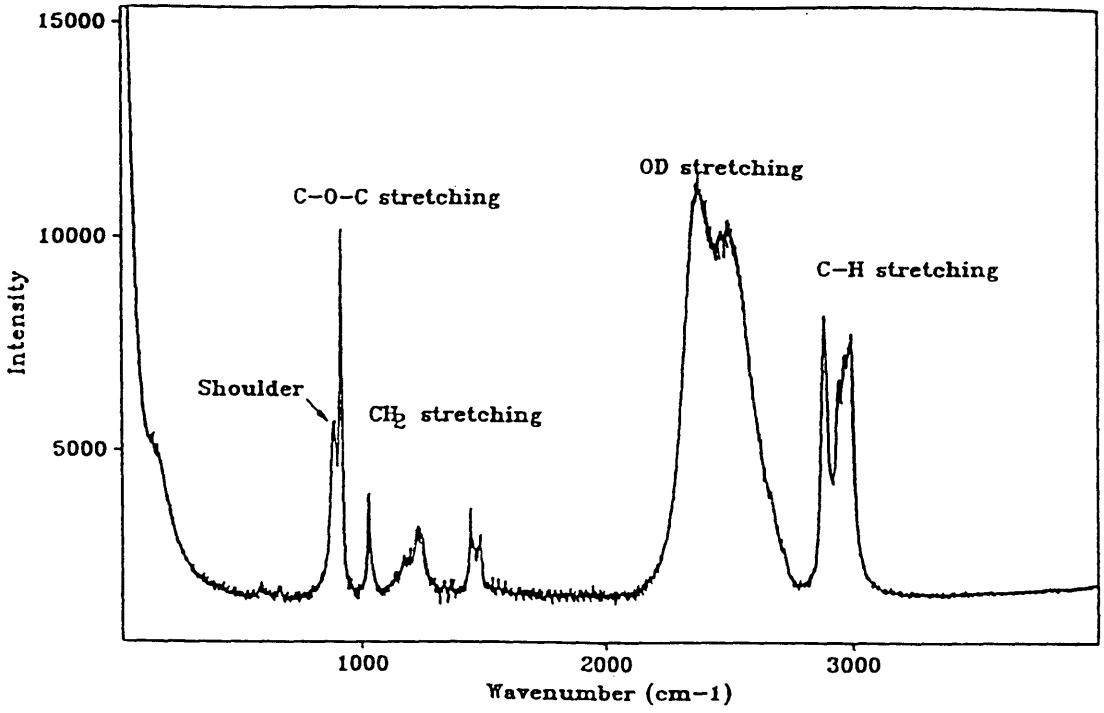

Figure 4.5(b) Spectrum of THF:D_2O solution(1:17 mole ratio) at 3.0°C

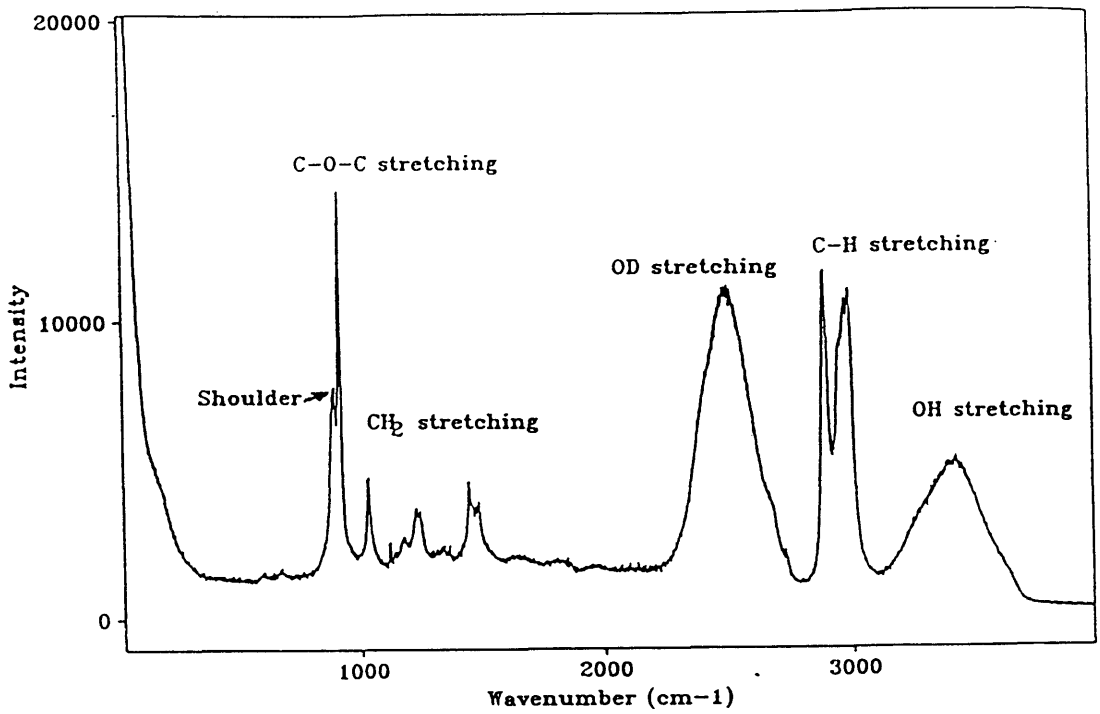

Figure 4.6(a) Spectrum of THF:HDO solution(1:17 mole ratio) at 3.0°C

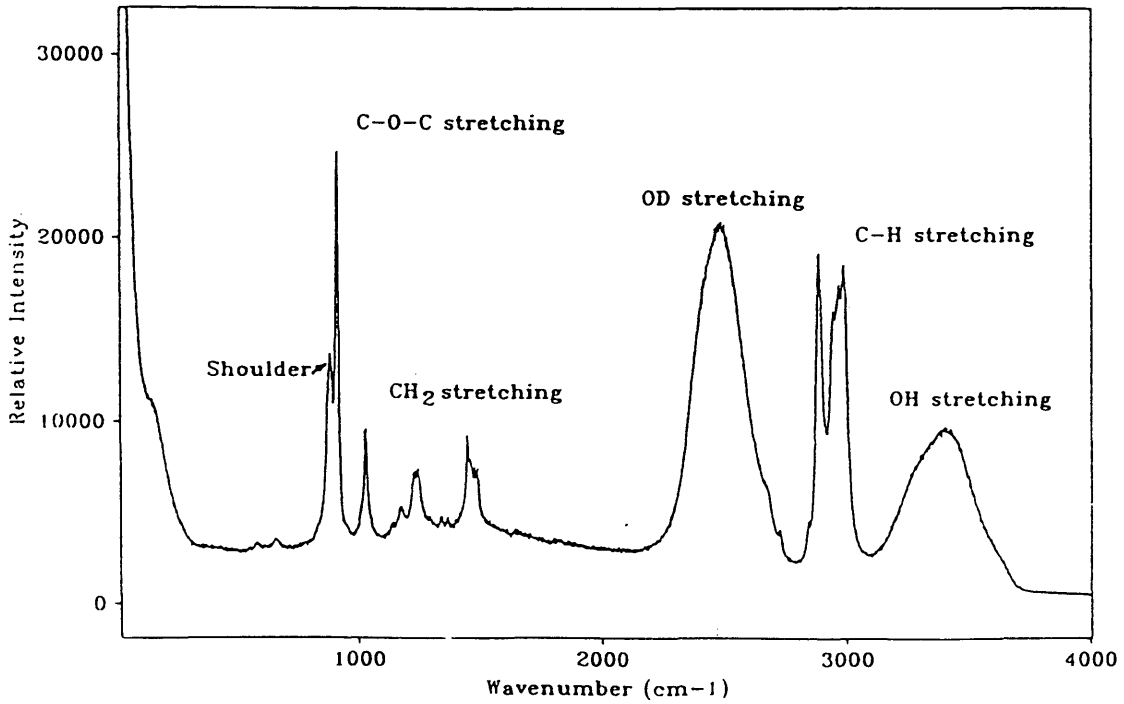

Figure 4.6(b) Spectrum of THF:HDO solution(1:17 mole ratio) at room temperature

4.3 Spectra of THF Hydrate as Function of Temperatures

The formation of the solid hydrate phase causes two significant changes in the spectra: decrease in intensity of the shoulder and the appearance of the low wavenumber lattice vibration mode.

The spectra of THF+H_2O , THF+D_2O and THF+HDO hydrate are shown in Figures 4.7, 4.8, 4.9 and 4.10 respectively. Besides the differences between subcooled solutions and solid hydrates, there are definitely differences between spectral positions of THF molecule C-O-C stretching mode inside the different host lattices, e.g., H_2O, D_2O, and HDO. They are different by about 1 cm-1 to each other.

Spectra of the solid THF hydrate show significantly decrease in intensity of the shoulder and the C-O-C stretching mode compared to the intensities of both modes in the liquid solutions. Changes also occur in the OH stretching region upon formation. The shape of the whole OH stretching band is changed.

In the region below 300 cm^{-1}, there is a water libration mode. In the solid phase, i.e., hydrate and ice, this mode becomes the lattice vibration mode. The position of this lattice vibration mode does change with isotopic substitutions by about 1 cm^{-1} from THF+H_2O hydrate, THF+D_2O hydrate, and

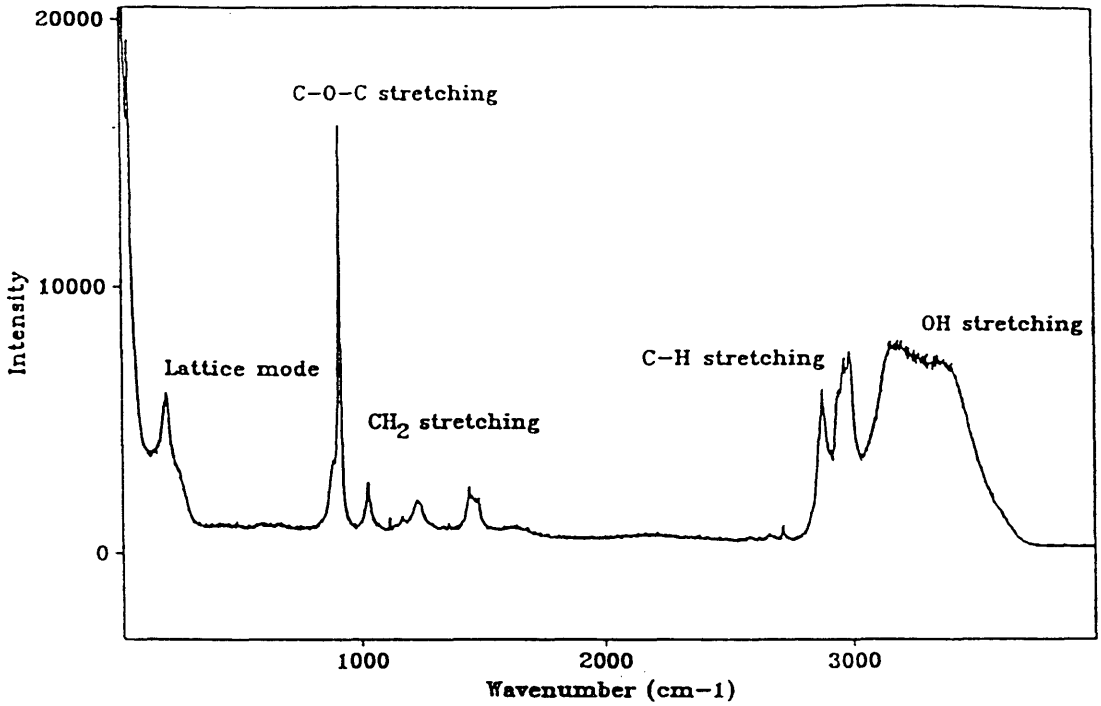

Figure 4.7(a) Spectrum of THF:H_2O hydrate at 3.0°C

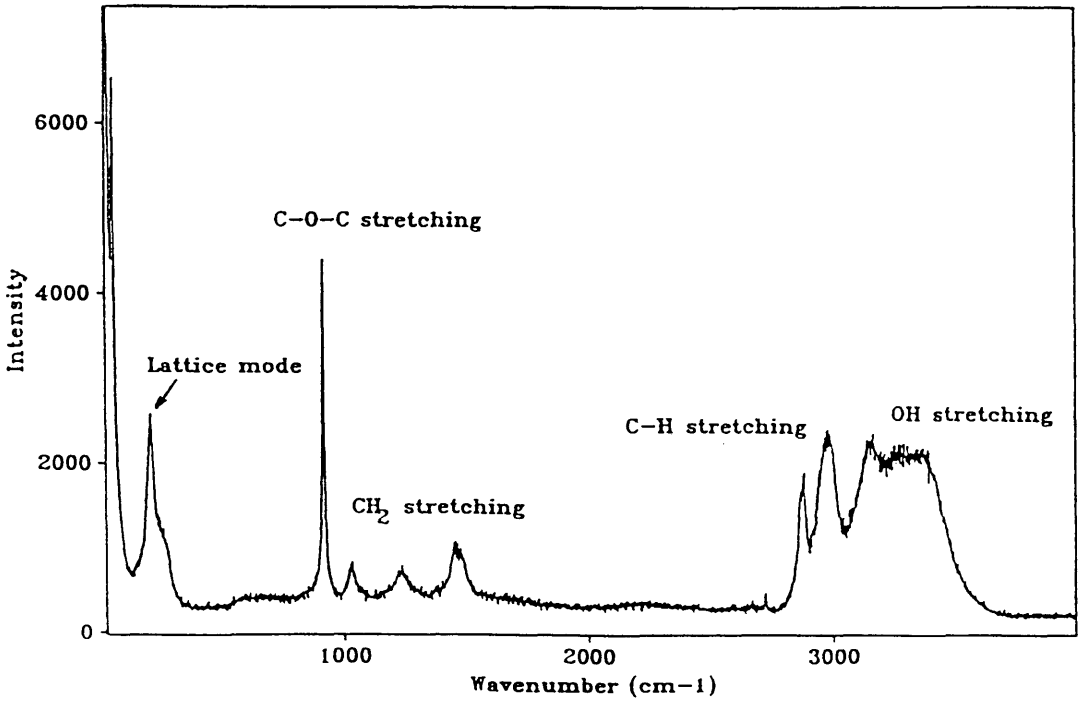

Figure 4.7(b) Spectrum of THF:H_2O hydrate at -6.0°C

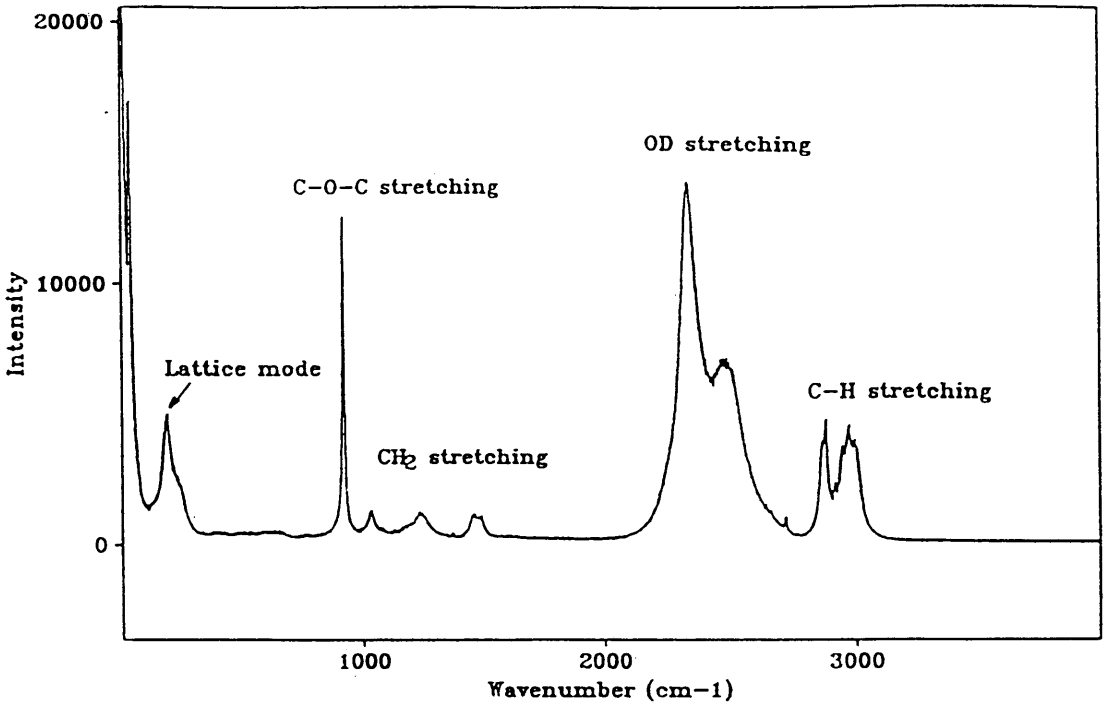

Figure 4.8(a) Spectrum of THF:D_2O hydrate at 4.0°C

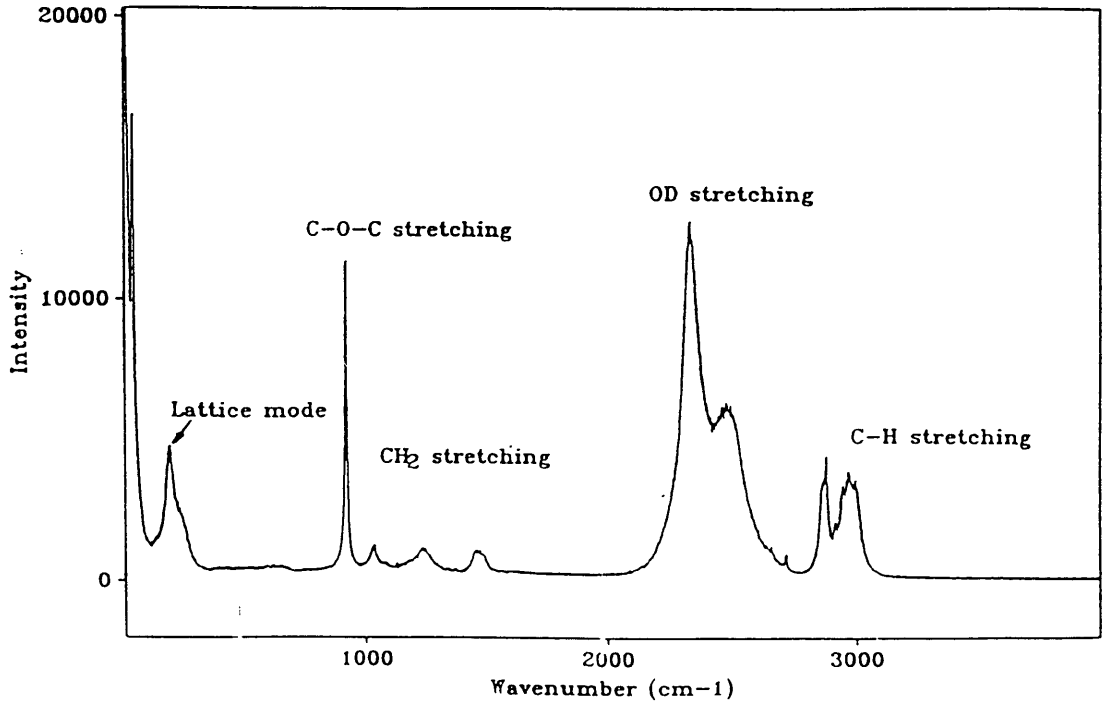

Figure 4.8(b) Spectrum of THF:D_2O hydrate at 0.0°C

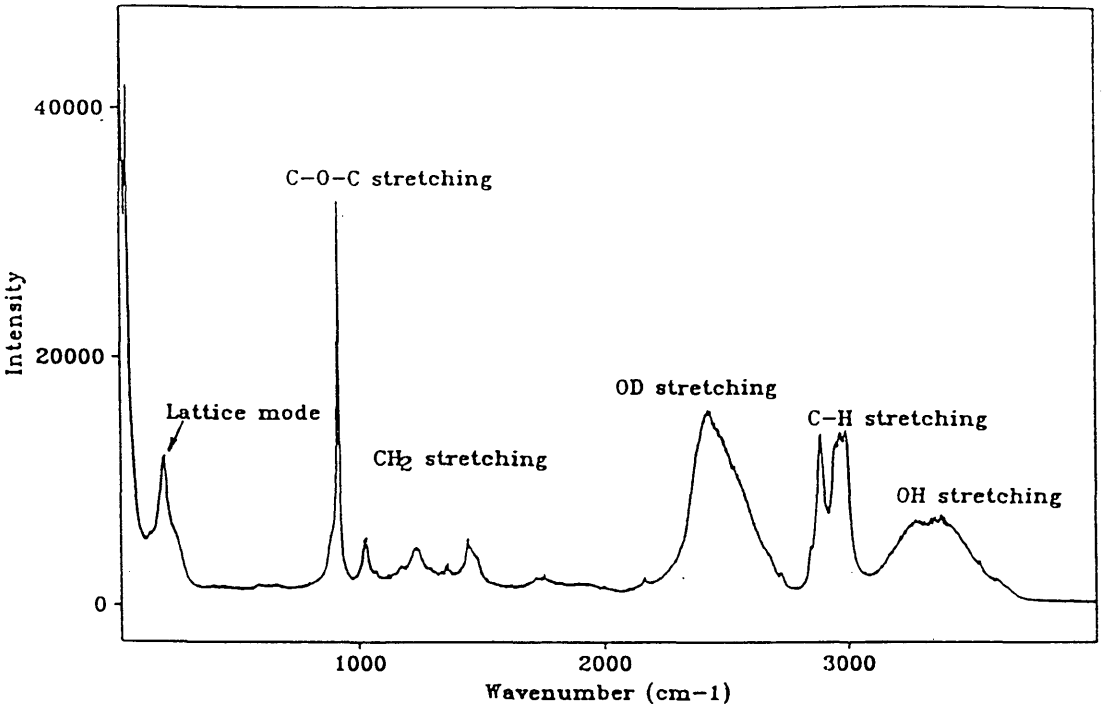

Figure 4.9 Spectrum of THF:HDO hydrate at 4.0°C

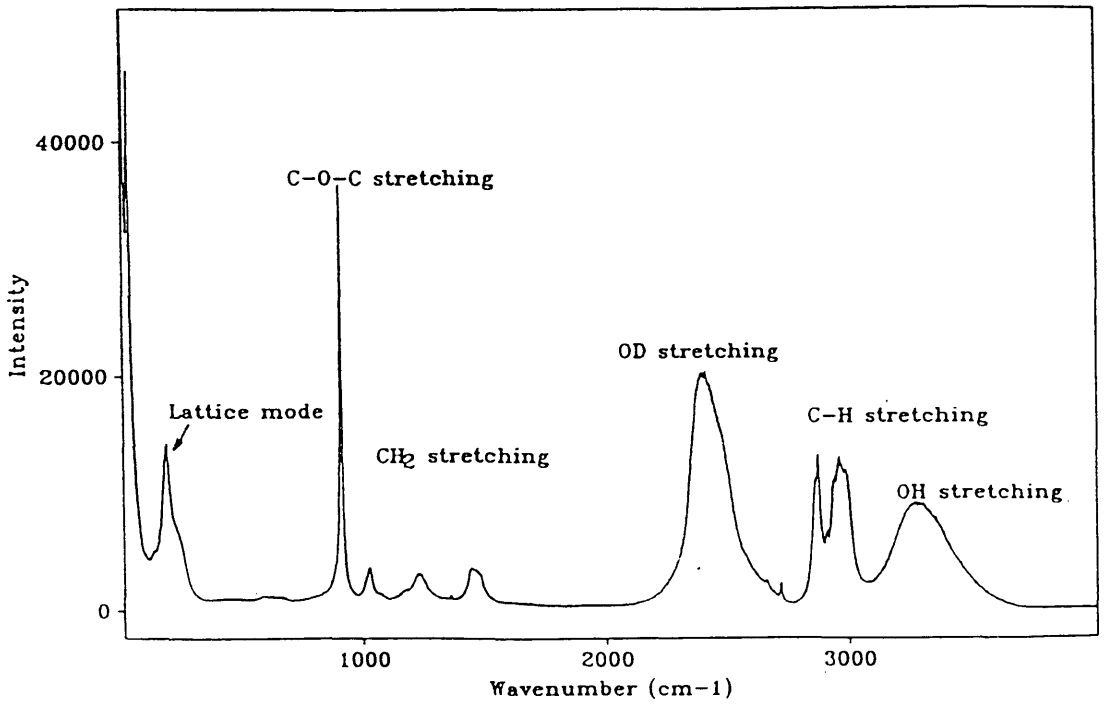

Figure 4.10 Spectrum of THF:HDO hydrate at 2.0°C

THF+HDO hydrate.

4.4 Polarized Spectra of Pure THF , THF+H_2O Solution and THF Hydrate

4.4.1 Actual Polarized Spectra for Pure THF and THF+Water Solution

Typical polarized spectra for both directions for THF+H_2O solution and pure liquid THF are shown in Figures 4.11, 4.12, 4.13 and 4.14. From these spectra, although the C-O-C ring stretching mode is reasonably symmetrical, there is still a fair amount of unsymmetrical vibration component present.

4.4.2 Polarized Spectra of THF Hydrate at Different Temperatures

Polarized spectra were obtained of THF hydrate at different temperatures ranging from -10 °C to +4 °C. Typical spectra were shown in Figures 4.15, 4.16, 4.17 and 4.18. For comparison, the polarized spectra of subcooled THF+H_2O solution and THF hydrate are shown in the Figure 4.19. There are large differences between these two spectra in most of the spectral regions.

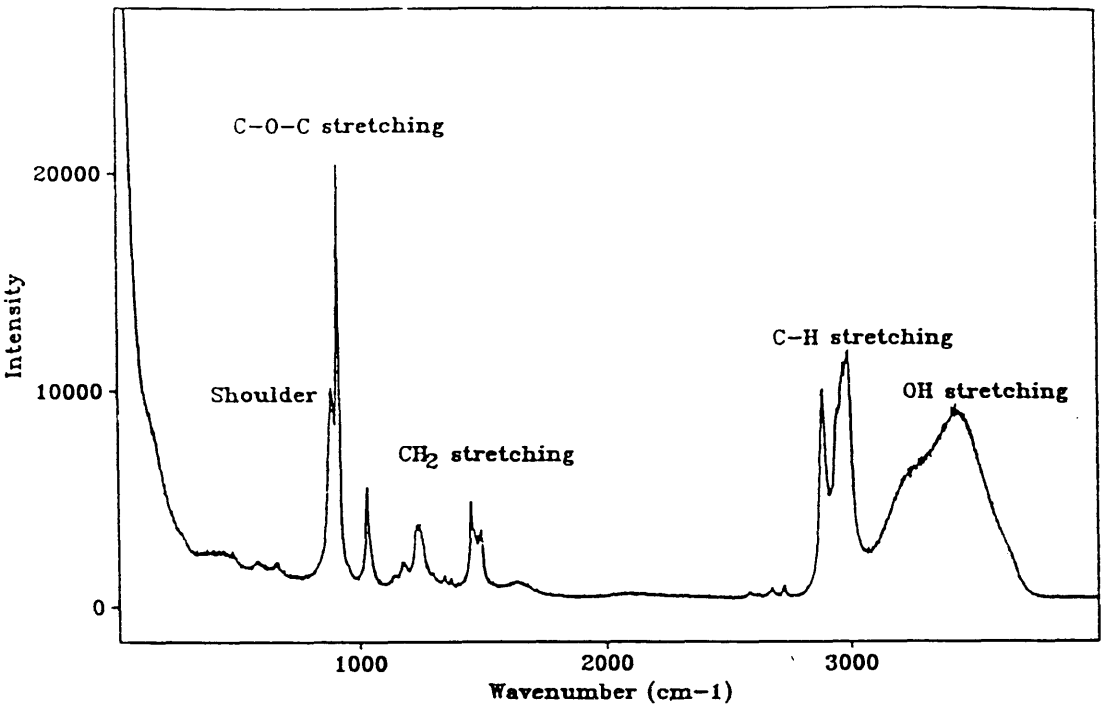

Figure 4.11(a) Polarized spectrum of THF:H_2O solution(1:17 mole ratio) with horizontal configuration at room temperature

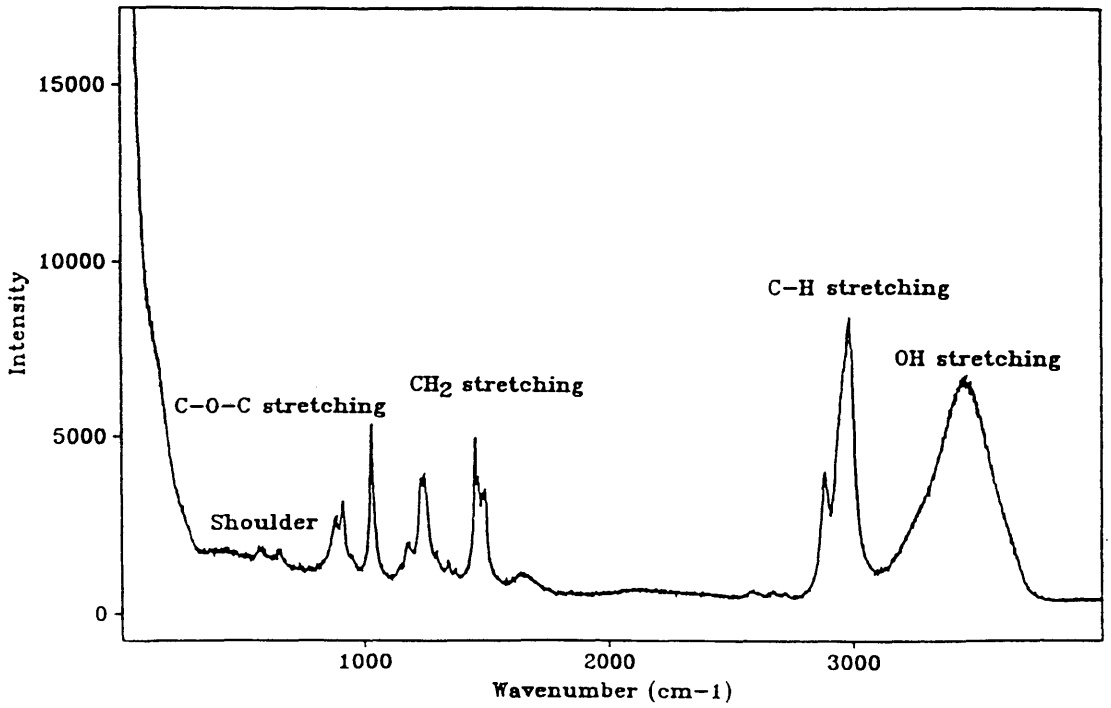

Figure 4.11(b) Polarized spectrum of THF:H_2O solution(1:17 mole ratio) with cross configuration at room temperature

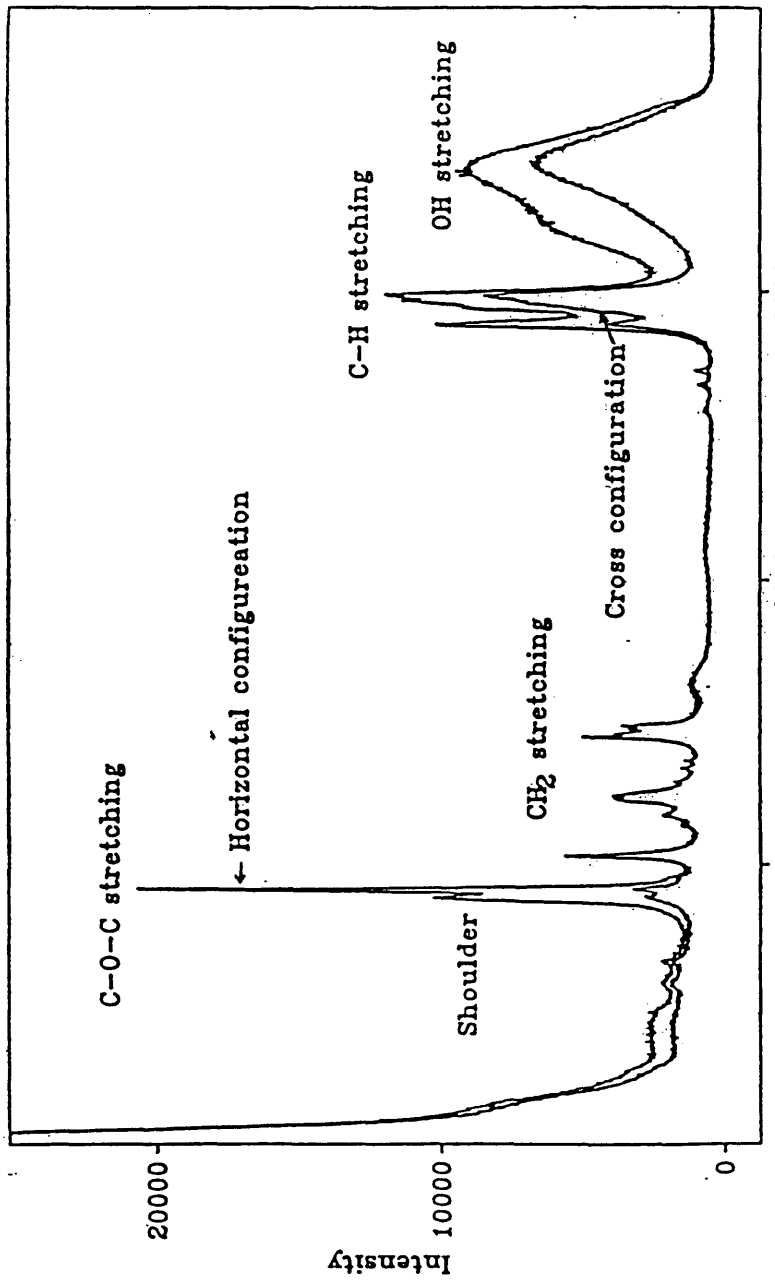

Figure 4.12 Comparison between two polarized spectra of THF:H_2O solution(1:17 mole ratio)

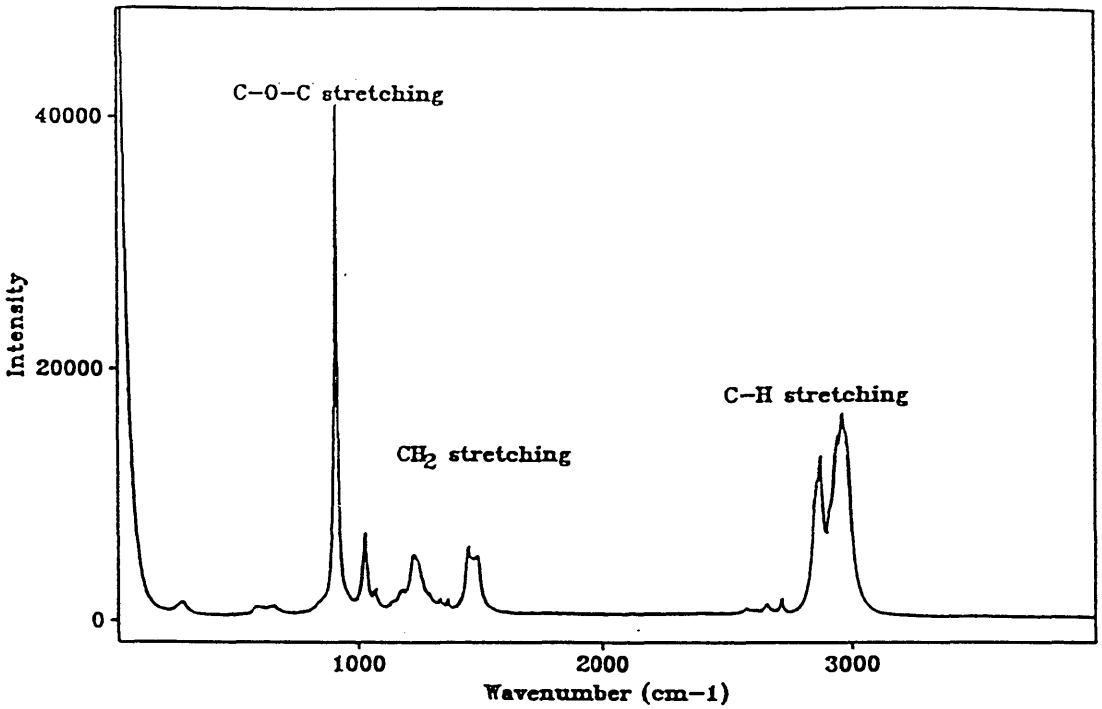

Figure 4.13(a) Polarized spectrum of pure liquid THF with horizontal configuration at 15.0°C

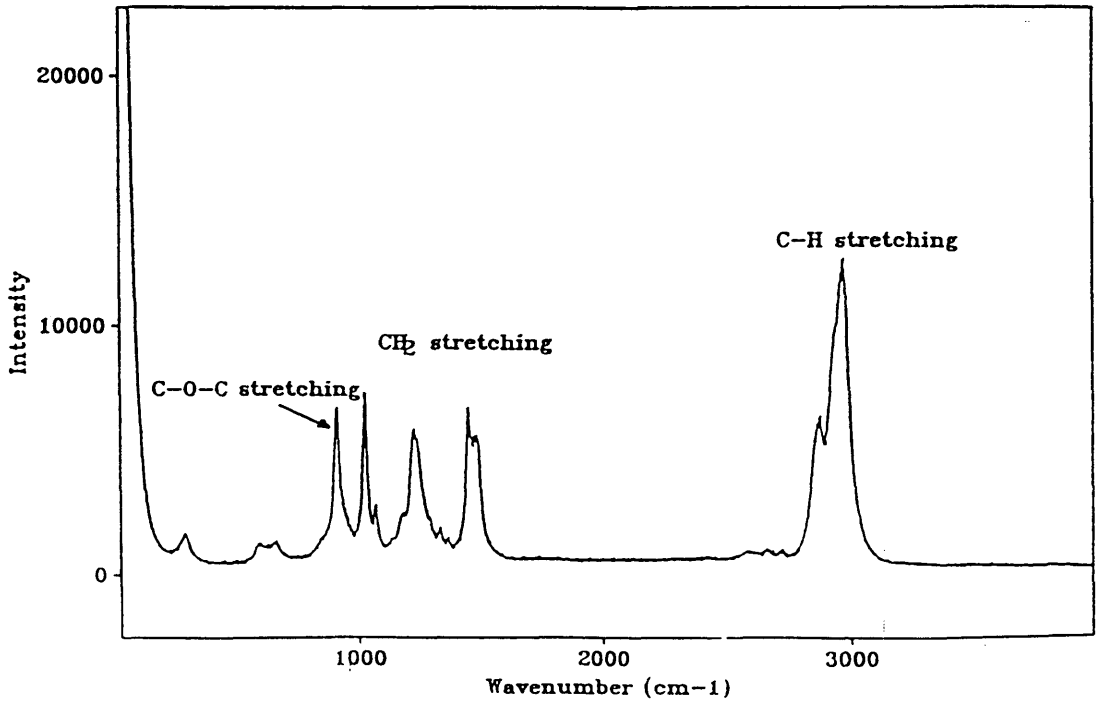

Figure 4.13(b) Polarized spectrum of pure liquid THF with cross configuration at 15.0°C

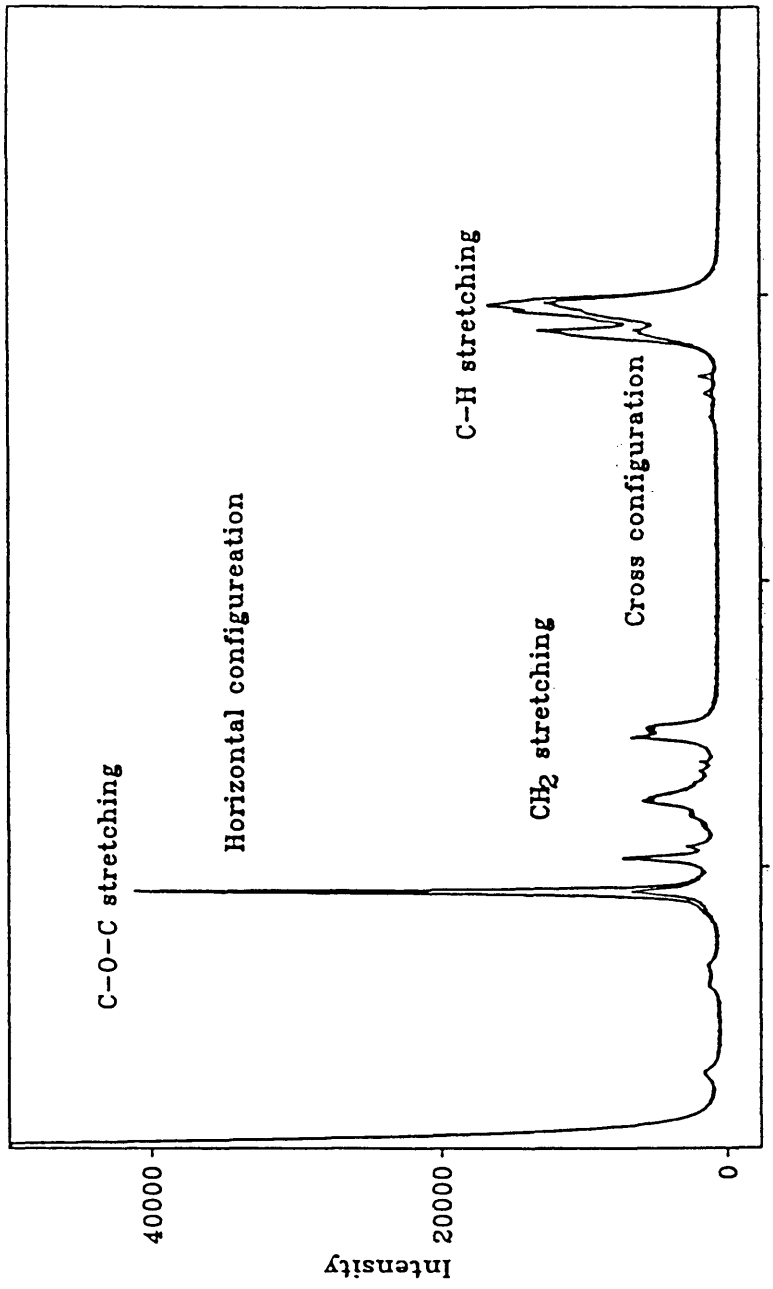

Figure 4.14 Comparison between two polarized spectra of pure liquid THF at 15.0°C

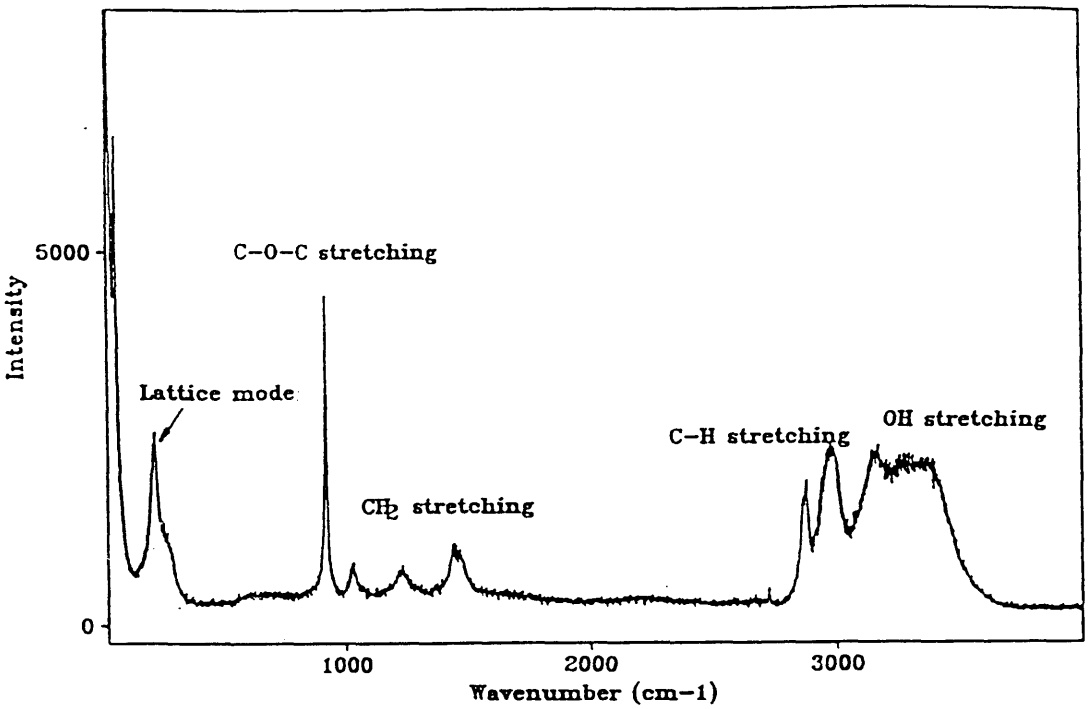

Figure 4.15(a) Polarized spectrum of THF hydrate with horizontal configuration at -6.0°C

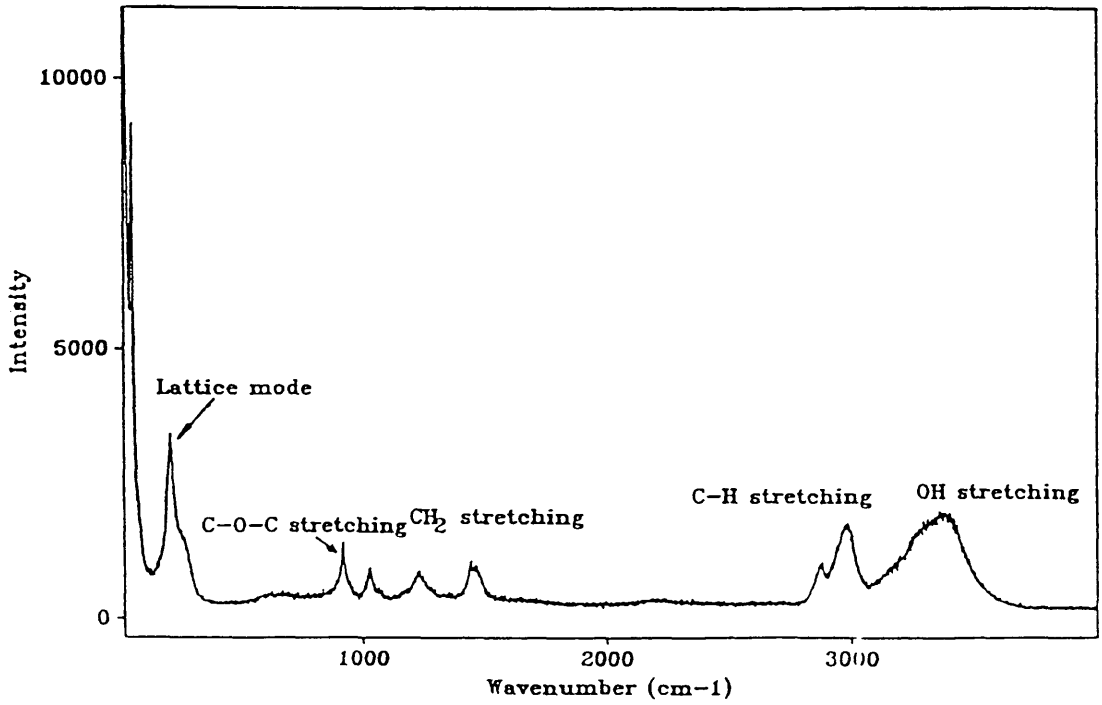

Figure 4.15(b) Polarized spectrum of THF hydrate with cross configuration at -6.0°C

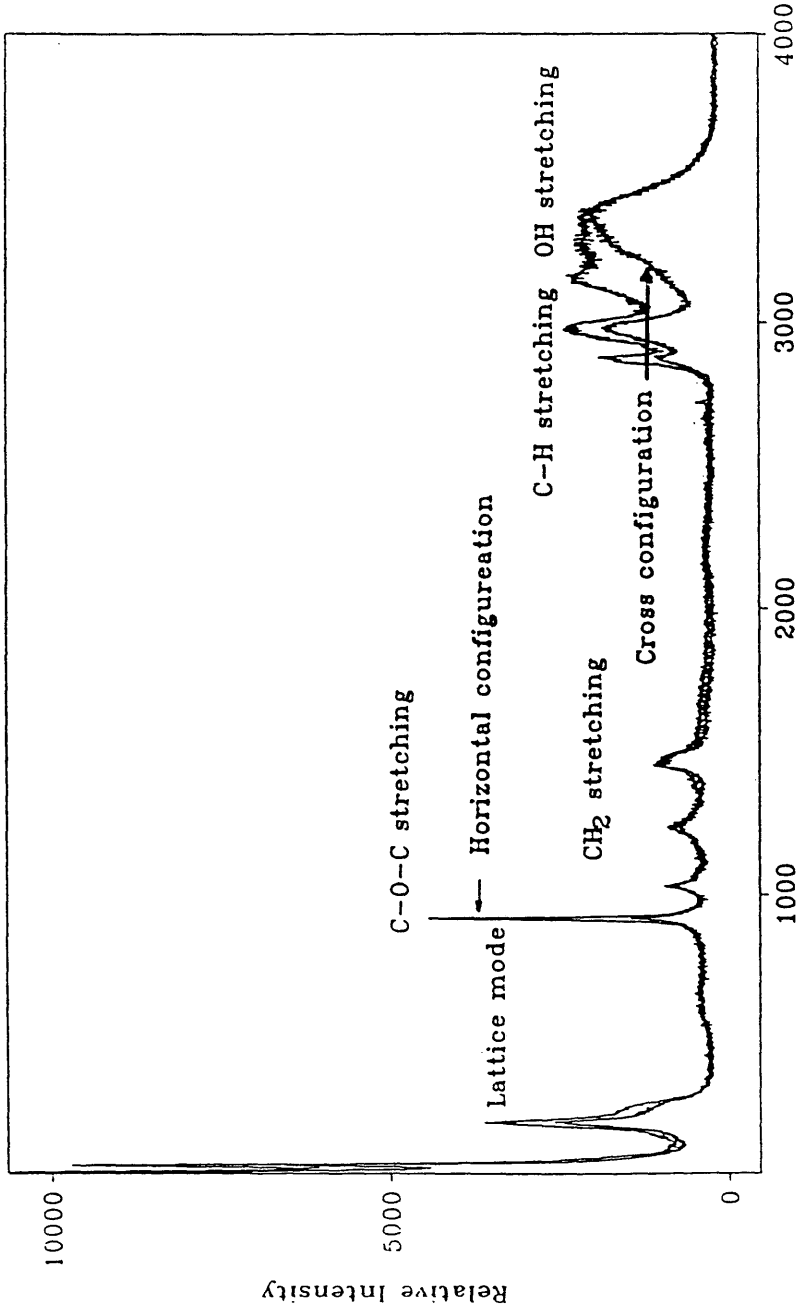

Figure 4.16 Comparison between two polarized spectra of THF hydrate at -6.0°C

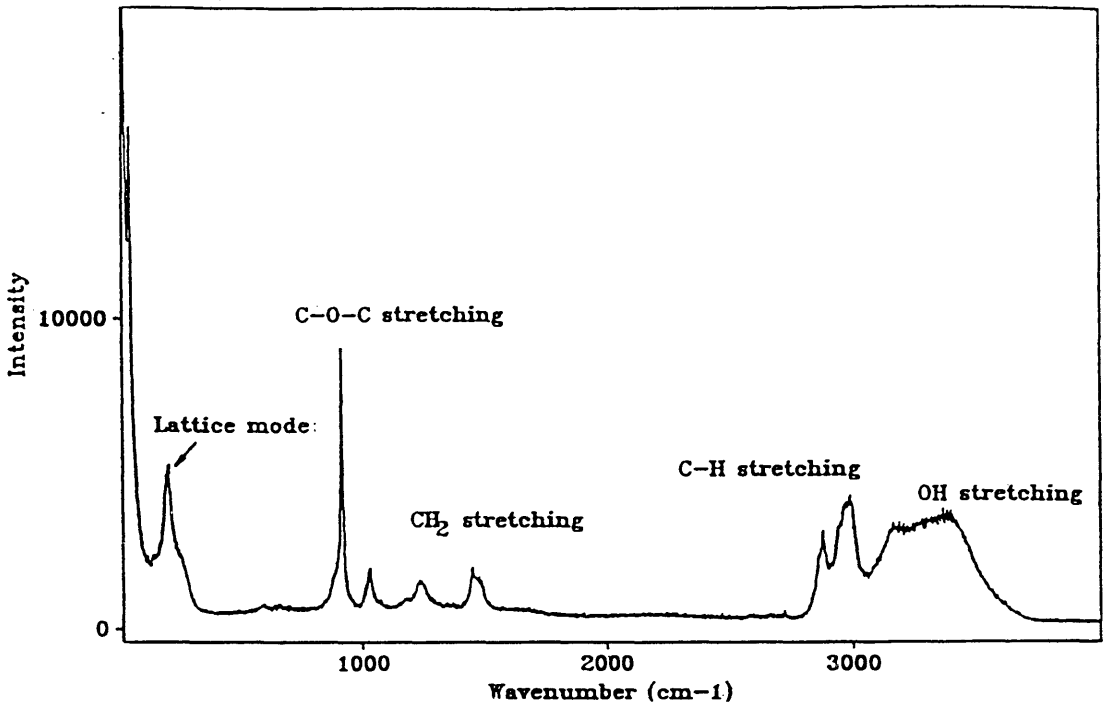

Figure 4.17(a) Polarized spectrum of THF hydrate with horizontal configuration at 2.6°C

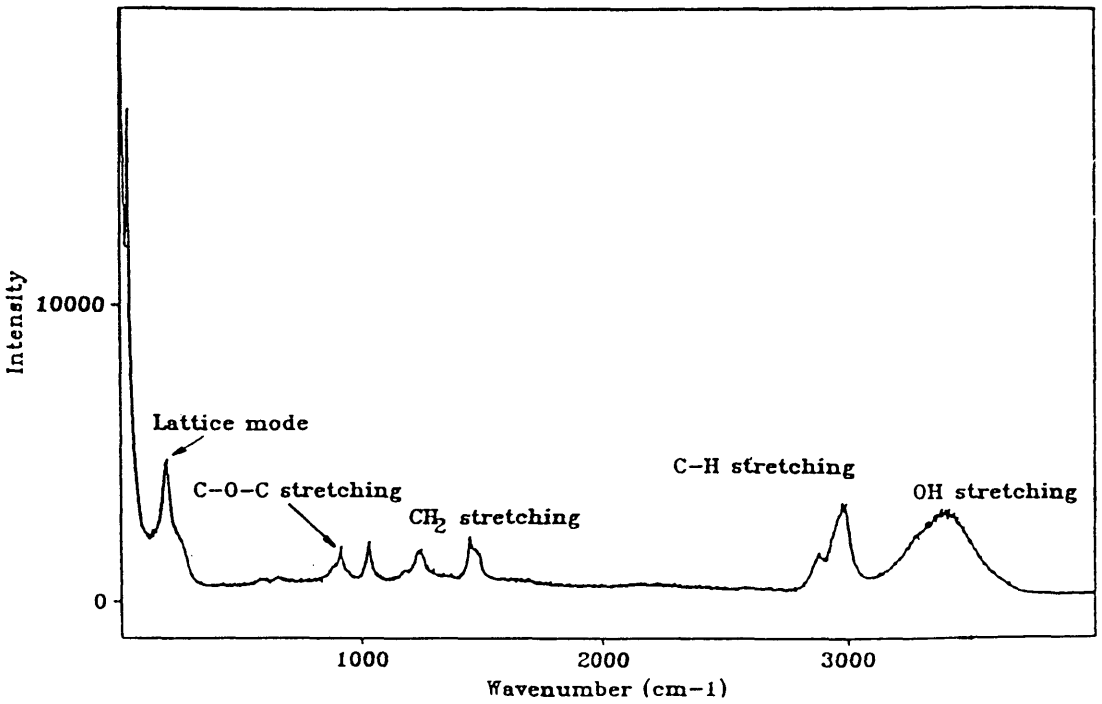

Figure 4.17(b) Polarized spectrum of THF hydrate with cross configuration at 2.6°C

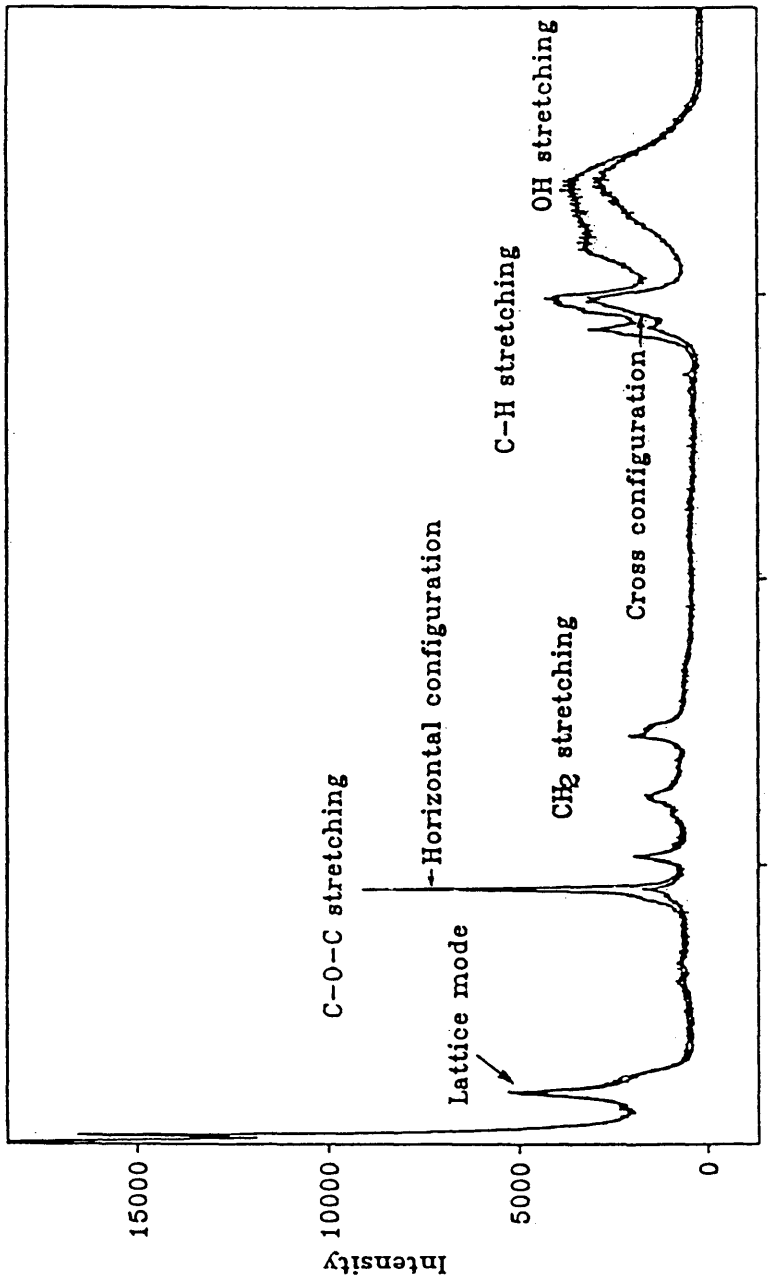

Figure 4.18 Comparison between two polarized spectra of THF hydrate at 2.6°C

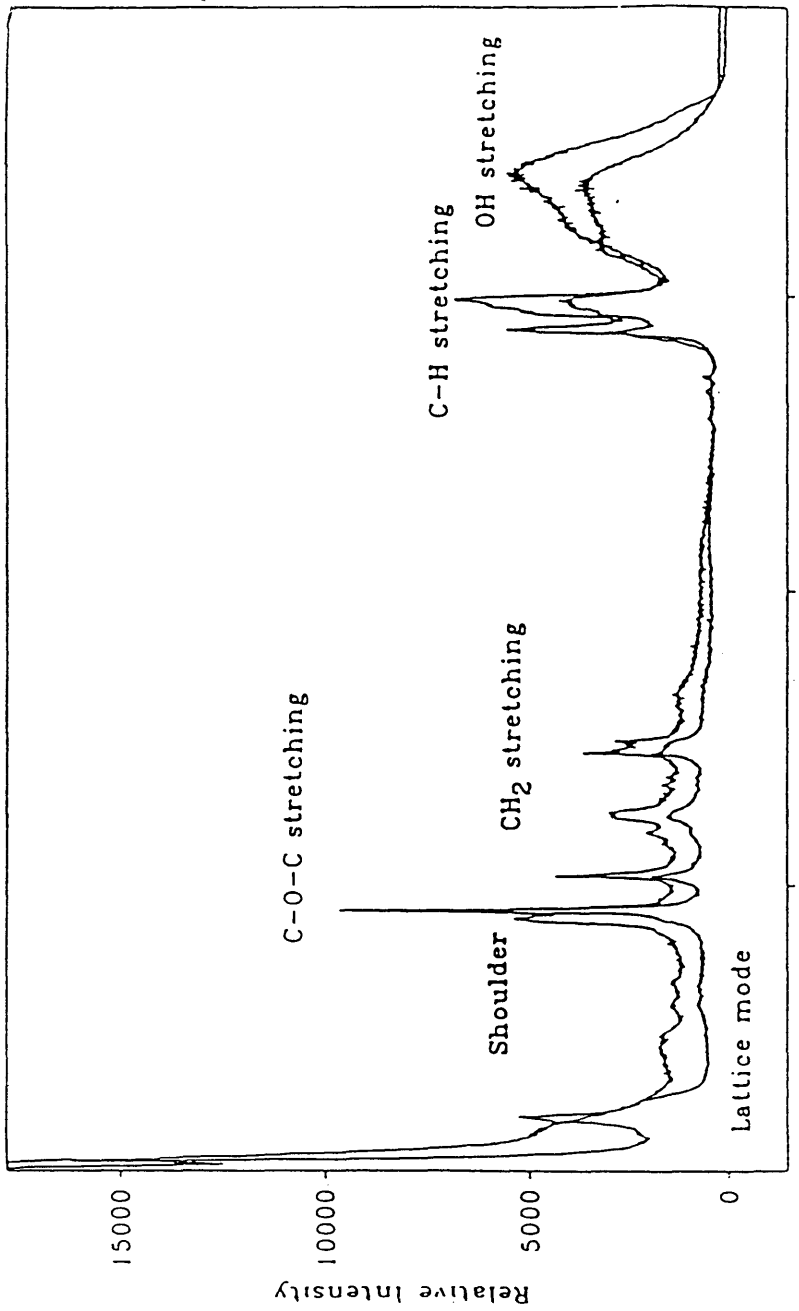

Figure 4.19 Comparison between polarized spectra of THF solution and THF hydrate with horizontal configuration at 2.6°C

4.5 Time Dependent Measurement of THF+H_2O System

A multichannel diode array detector was used to record 100 spectra with a time constant of 0.5 second. Figure 4.20 shows 36 spectra near the point at which the shoulder begins to decrease in intensity. In the 3-D graph in Figure 4.20, the x axis is diode number which is related to the wavenumber, the y axis is relative intensity, and the z axis is time. There are three peaks in the spectra. The most intense peak is the THF C-O-C ring stretching mode at 914 cm^{-1}. The peak on the left side of the C-O-C peak is the shoulder. The peak on the right side of the C-O-C stretching peak is due to the CH_2 bending vibration mode. The gradual decrease of the intensity of the shoulder was observed as the system undergoes a phase transition from subcooled solution to solid hydrate phase.

The important thing needs to be mentioned here are that: first this is a system away from the equilibrium. Secondly, during the course of this experiment, not only the time was changing, the temperature of the system was changing as well. The overall temperature range is from 6°C to -8°C. The temperature driving force was not kept constant. At the same time, the nucleation was induced by external force, i.e., external agitation. It may not be used to draw any quantitative conclusions. However, it demonstrated that Raman

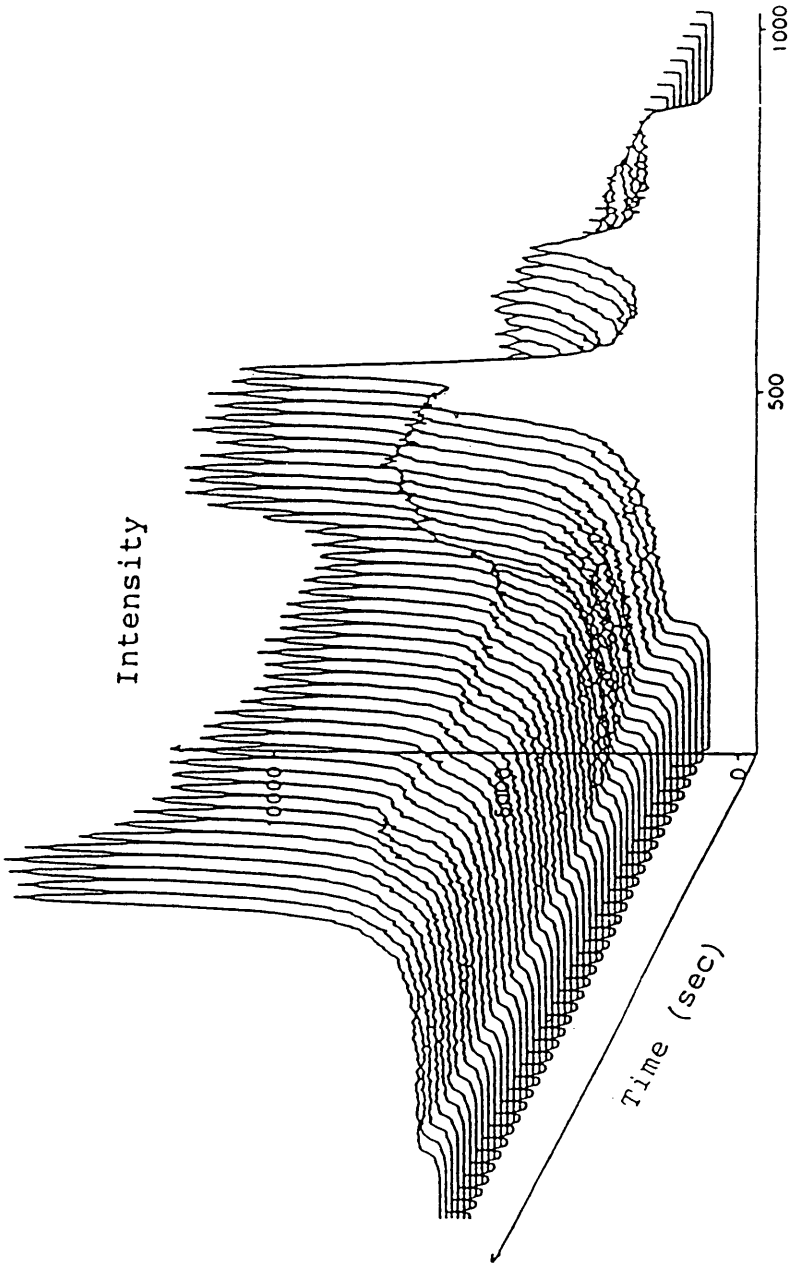

Figure 4.20 3D graph of time-dependent measurement of THF+H_2O system

spectroscopy techniques might be used to determine what happens around the onset of nucleation.

4.6 Spectra of THF+H_2O+Inhibitors Solutions

Kinetic inhibition of natural gas hydrate has been studied extensively in the lab at the Colorado School of Mines(Sloan *et al.*, 1991, 1992). Several compounds that acts as kinetic inhibitors have been identified.

PVP(polyvinylpyrrolidone) and VC713 are two examples of the best kinetic inhibitors. There are published studies of time domain dielectric relaxation in the PVP+H_2O system in the literature(Mashimo, 1977; Iwata, 1973). However, there are no Raman data on THF+H_2O+PVP system. The spectrum of PVP+THF+H_2O solution at room temperature is shown in Figure 4.21.

4.7 Spectra of Solutions of THF with Other Solvents

Not only solutions of THF with H_2O, D_2O, and HDO were studied in this research, but also solutions of THF with other solvents, e.g., $CHCl_3$, and CCl_4 were measured. These spectra are shown in Figures 4.22(a) and 4.22(b). Spectra of pure liquid chloroform and carbon tetrachloride are shown in Figure 4.22(c).

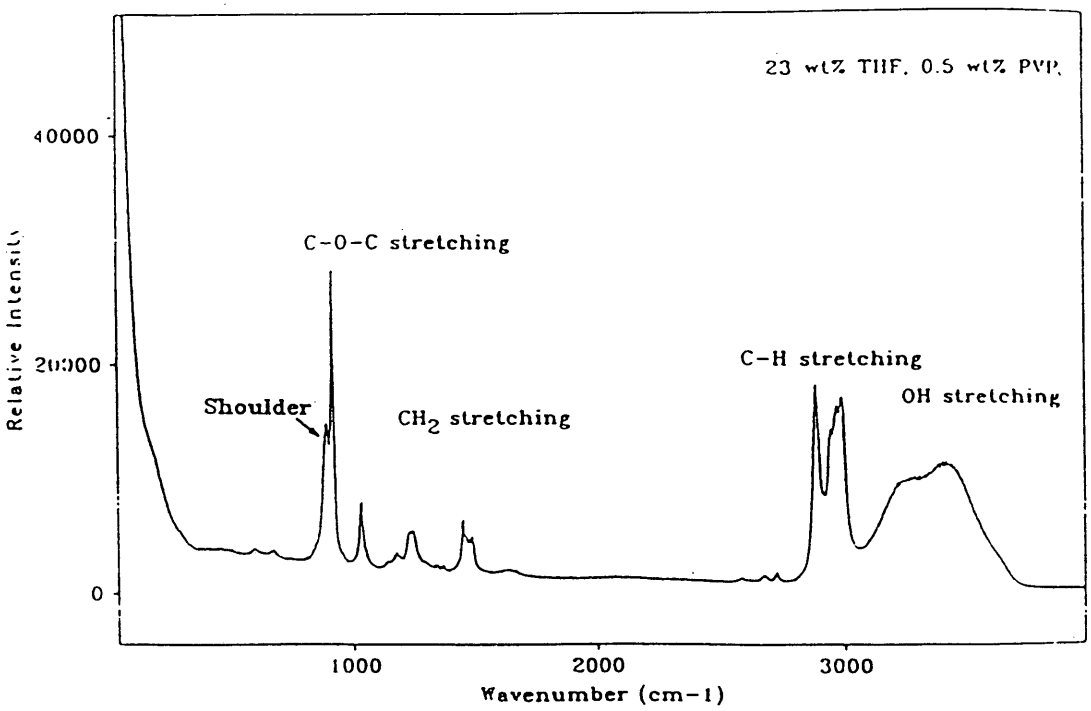

Figure 4.21 Spectrum of PVP+THF+H_2O solution at room temperature

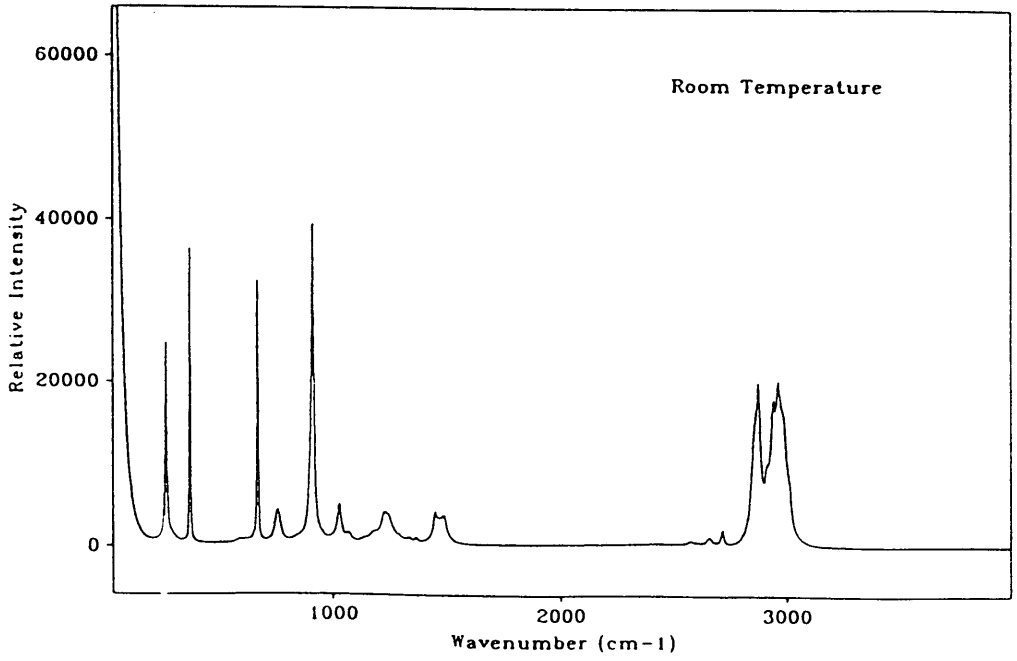

Figure 4.22(a) Spectrum of THF and chloroform solution with 1:1 mole ratio

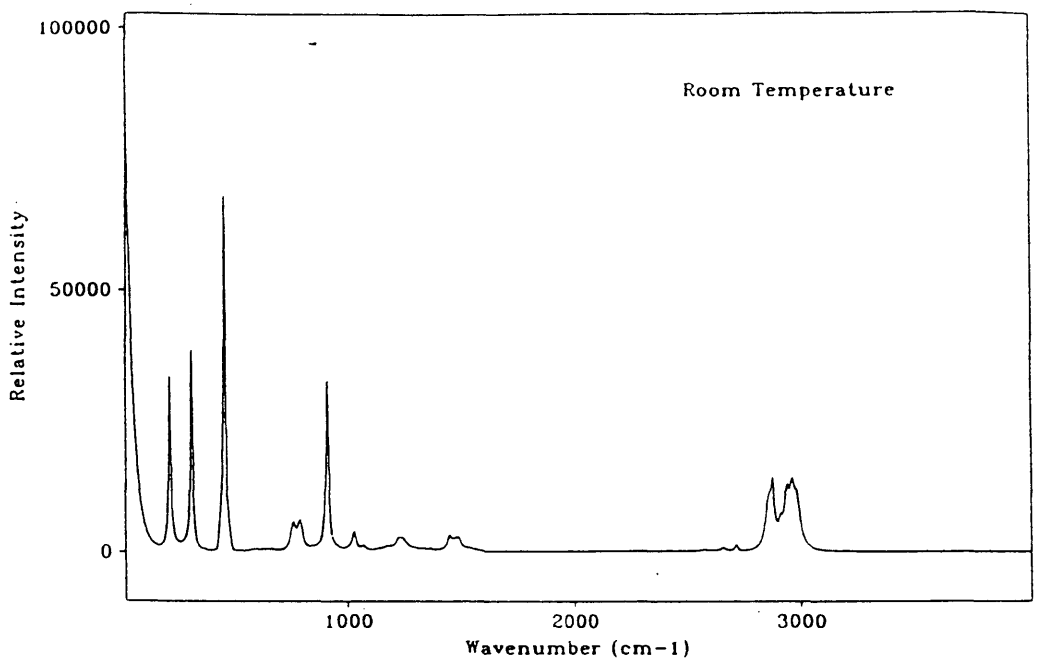

Figure 4.22(b) Spectrum of THF and carbon tetrachloride solution with 1:1 mole ratio

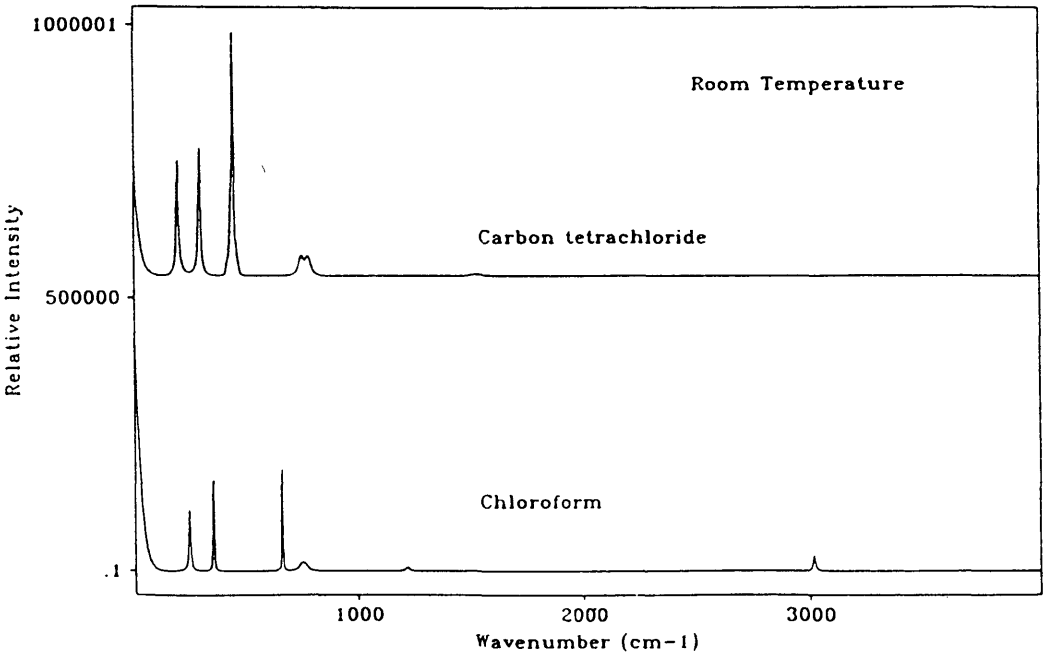

Figure 4.22(c) Spectrum of pure chloroform and carbon tetrachloride liquid

CHAPTER V

DATA ANALYSIS AND DISCUSSION

5.1 Data Analysis Procedure

The molecular spectrum obtained from experiment usually has a fairly complicated shape. It is due to the origin of the complicated molecular vibrational and rotational states in the molecule. A lot of important information can only be obtained by analyzing the complicated band. One efficient way to do this is doing deconvolution of the band and separate the complicated band into several possible and reasonable peaks.

5.1.1 Software Introduction

The software used in the data analysis process is marketed by Galactic under the brand name "Lab Calc". It does standard peak choosing, curve fitting and other mathematical manipulations. Among the several fitting functions in this software, the one chosen was designed for curve fitting specifically.

The general procedure for curve fitting involves the following steps. First, the spectral region must be chosen. As

an example, the region chosen to fit the C-O-C ring stretching region was from 750 cm^{-1} to 1000 cm^{-1}. The second step is to deconvolve the region chosen, to eliminate some of the impossible peaks, especially for spectrum obtained at low S/N ratio. Thirdly, a specific peak function which effectively represents the peak shape, in this case, the peak shape of THF C-O-C stretching mode, must be specified. In most of the fitting procedures for this region, a sum of a pure Gaussian function and a pure Lorentzian function was chosen for the peak shape. However, for OH stretching mode, a pure Gaussian function was used. In order to compensate for the baseline of the peak, a linear baseline was used for the C-O-C stretching region.

5.1.2 Fitting Function Introduction

There are several fitting functions used during the course of data analysis which will be discussed in the following section. Most of the information here is from the operating menu of 'Lab Calc'.

FIT is a set of functions for deconvolving the data by fitting model peaks. **FIT** performs a least-squares fit of a model to the data. The number of peaks, the type of each peak(Gaussian, Lorentzian, etc.), and the type of the

baseline, e.g., linear, or cubic, or spline etc., must be provided to the **FIT**. The results obtained will be meaningful only if the model is correct.

FIT gives a Maximum Likelihood result provided that the errors are randomly distributed with a normal probability distribution. In this case, the parameter estimates derived will be the most probable estimates of the true values. If the errors are not drawn from a normal probability distribution, the results will be least-squares estimates rather than Maximum Likelihood estimates.

FIT automatically adjusts the parameters of the peaks and the baseline, until it achieves the best possible fit between the model and the data. The algorithm works by finding a minimum on M-dimensional surface, where M is the number of parameters which need to be determined. **FIT** finds the minimum which is closest to its starting point.

When using fitting procedures to determine the parameters of the model, three things need to be done prior to the model-fitting:

1. The data should not be smoothed. Smoothing changes the error statistics and often introduces false information into the data.
2. Remove the baseline or adjust any unreasonable baseline.

3. Select the correct model for the data.

5.1.3 Peakshape Catalog of the Fitting Function

FIT provides several peakshape functions. These functions are used to synthesize the peakshape in terms of the peak parameters which are optimized by **FIT**. The total area is the area on the entire interval $(-\infty, +\infty)$ of the fitting. The screen area is defined as the area of the interval displayed on the screen during the fit. The units of total area and screen area are the units of the display, (X units Times Y units)

The Gaussian peak shape is one of the most common peak shapes used in snythesizing the spectra shape. The **Gaus**(Gaussian) peak shape is synthesized from the following equation:

$$peak(x) = Hexp\left[-\frac{(x-C)^2}{(\frac{W}{1.665})^2}\right] \qquad (5.1)$$

where C is the center positions of the peak, H is the peak height, and W is the full-width at half maximum(FWHM). The three parameters C, H, and W are optimized by **FIT**. The peak areas are calculated by $\sqrt{\pi}WH/1.665$

Lrnz(Lorentzian) peakshapes are synthesized from the following equation:

$$peak(x) = H\frac{1}{1+4(x-C)^2/W^2} \qquad (5.2)$$

where C is the center position of the peak, H is the peak height, and W is the full-width at half maximum(FWHM). The three parameters C, H, and W are optimized by **FIT**. Area is π**WH/2**.

The typical **Gaus** and **Lrnz** peakshapes are shown in Figure 5.1(a). Besides the pure **Gaus** (gaussian) and pure **Lrnz** (lorentzian) peakshapes, there is **Sum(Gaus+Lrnz)** and **Prod(Gaus*Lrnz)** which is the direct sum and product of individual peakshapes, respectively. The peakshapes of both are shown in Figure 5.1(b).

5.1.4 Typical Fitting Spectrum and Individual Components

The typical fitting parameters are shown in Table 5.1. The fitting spectra of THF+H_2O solution (1:17 THF to H_2O mole ratio) at room temperature and THF hydrate at 3.0 °C are shown in Figure 5.2 and Figure 5.3 respectively.

From the fitting spectra and original spectra, it is very clear that the difference between them is very small. The X^2

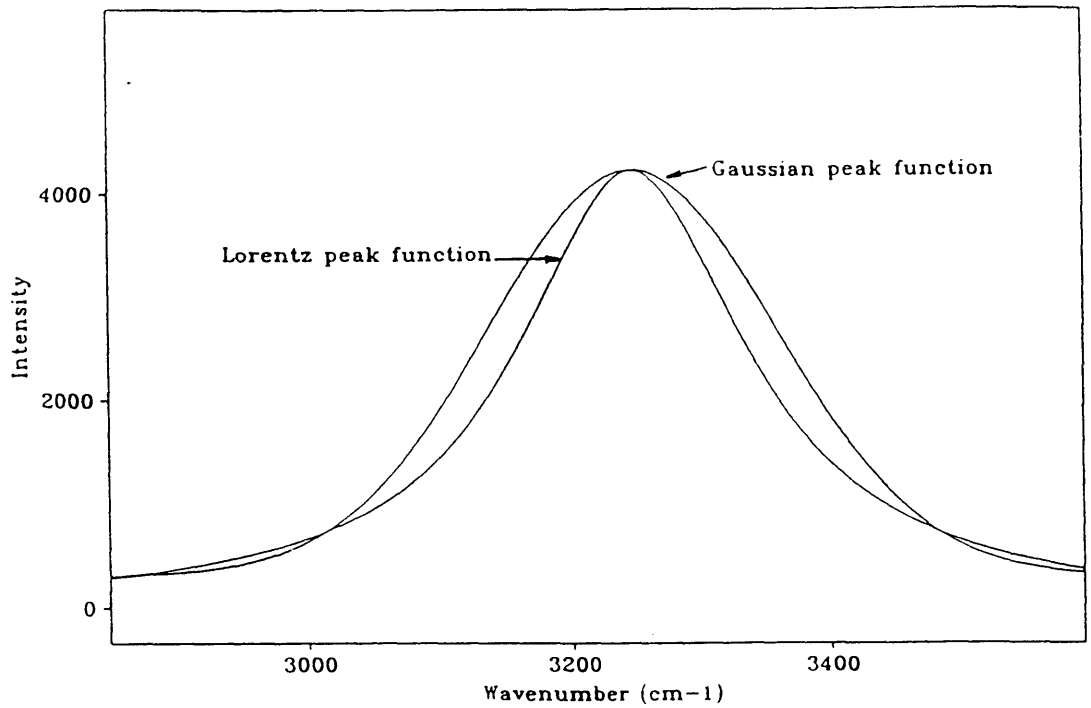

Figure 5.1(a) Pure Gaussian and Lorentz peak shape function

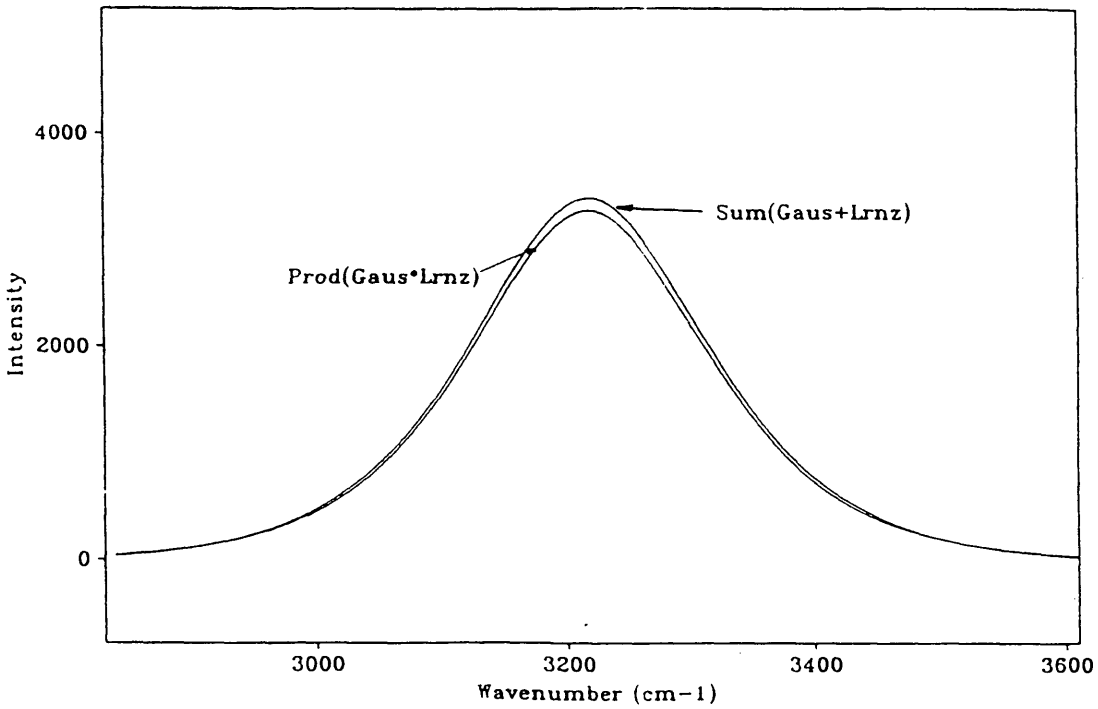

Figure 5.1(b) Sum(Gaus+Lrnz) and PRod(Gaus*Lrnz) peak shape function

Table 5.1 Typical Fitting Parameters Used for Fitting C-O-C Band

Fitting Parameters			
# of Peaks	Peak Shape	Baseline	FWHM(cm^{-1})
2(for solution)	Sum(Gaus+Lrtz)	Linear	13
1(for hydrate)	Sum(Gaus+Lrtz)	Linear	10

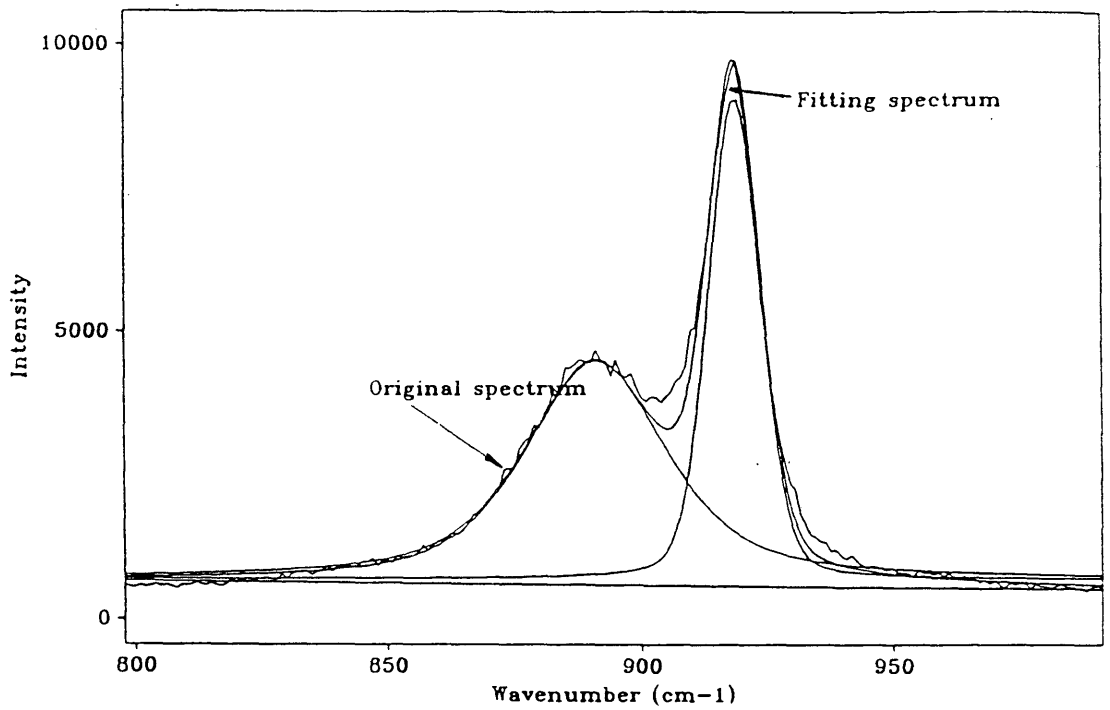

Figure 5.2 Computer fitted spectra and original spectrum of THF:H_2O solution(1:17 mole ratio)

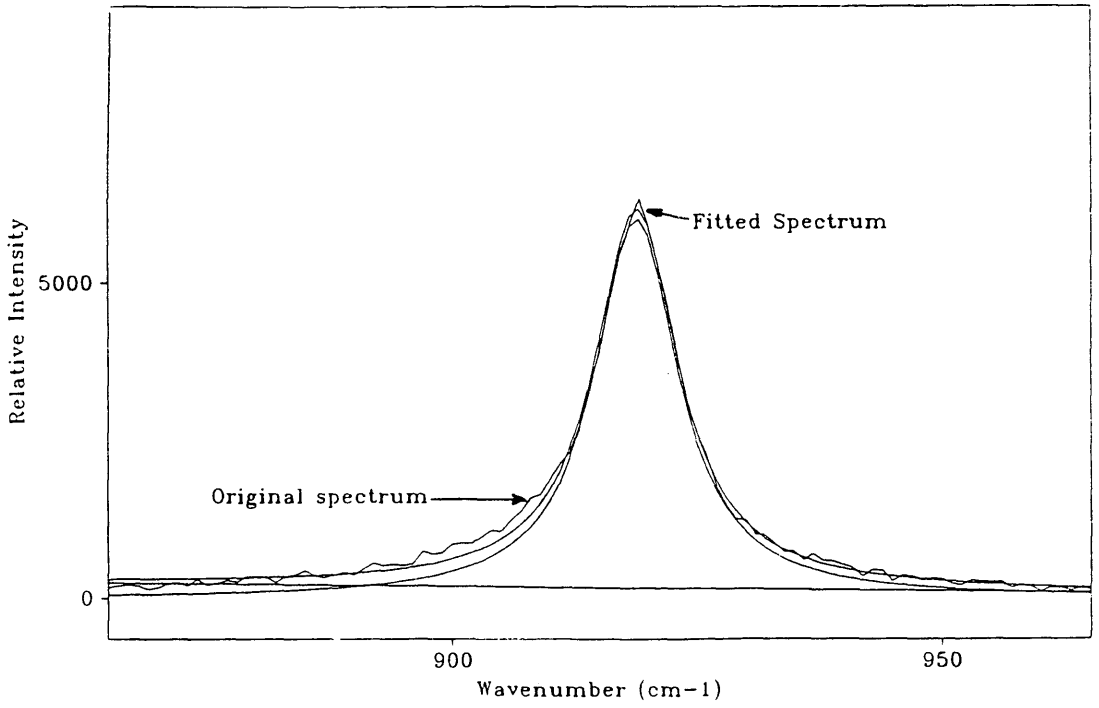

Figure 5.3 Computer fitted spectra and original spectrum of THF:H_2O hydrate at 3.0°C

value, which is a measure of fit, is very small. X^2 is defined by the following equations:

$$X^2=(X_{act}-X_{fit})^2 \qquad (5.2)$$

The typical X^2 for good fitting is about 0.2. All the following fitting values of the spectra were obtained from this same procedure.

5.2 C-O-C Ring Stretching Region

5.2.1 C-O-C Position vs. THF Concentration in Solutions

Based on the experiments conducted on different solvents+THF systems, there appears to be a distinct change of interactions due to the different solute concentrations and the different solvents. The solvents used in this research were water, CCl_4, $CHCl_3$, and methanol. Table 5.2 shows the fitting results for the C-O-C ring stretching and the shoulder positions of THF+H_2O solutions with different THF concentrations. Figure 5.4 shows the frequency shift versus the THF concentration in different solvents.

In the experiments, hydrogen bonding solvents: water, methanol(CH_3OH), and chloroform($CHCl_3$) and non-hydrogen bonding solvent: carbon tetrachloride(CCl_4), were used. In these two

Table 5.2 Computer Fitting Results for C-O-C Stretching Region

Molar Ratio	Molar Concentration	C-O-C Position	Shoulder Position
4:1	0.8	915.99	903.45
2:1	0.67	915.52	906.27
Pure THF	1.0	914.82	907.34
1:2	0.33	916.59	900.72
1:4	0.2	917.29	898.64
1:8	0.11	918.11	894.05
1:16	0.059	918.98	891.41
1:17	0.056	918.80	891.00
1:24	0.04	918.64	889.91
1:49	0.02	918.74	888.95
49:1	0.98	912.97	904.22
1:1 (CCl_4)	0.5	916.00	911.76
1:1 ($CHCl_3$)	0.5	914.40	905.39
1:1 (CH_3OH)	0.5	914.92	905.77
1:79(CCl_4)	0.0125	914.76	907.14

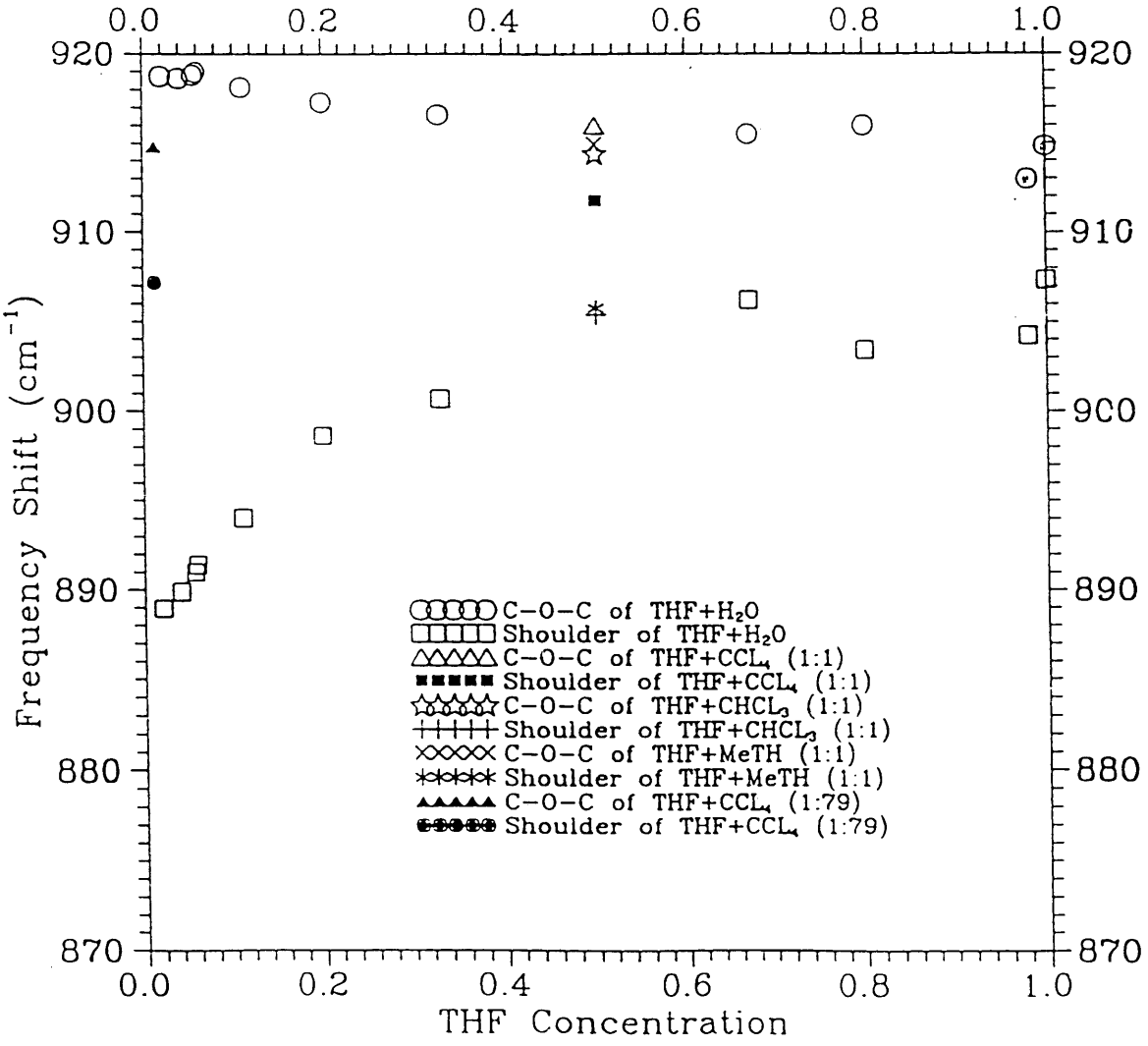

Figure 5.4 THF concentration vs. frequency shift of C-O-C and shoulder in different solutions

different types of solvents, totally different trends of the perturbation of THF C-O-C ring stretching mode were observed. The behavior of THF+CCl_4 does not follow the general trend, as is clearly shown in Figure 5.4. This is evidence that the origin for that particular shoulder is due to the hydrogen bonding interaction between water molecules and the THF molecules, which form some type of complex in the solution.

The relative intensity of the THF C-O-C stretching band is shown in Figure 5.5. The intensity of the shoulder changes with the THF concentration in the solution. The degree of hydrogen bonding between water and THF molecules is increasing as the concentration of THF in solution is increased. As the concentration of THF is increased, the increased THF-water interaction(which is the origin of the shoulder) will cause the increase of the shoulder's relative intensity. This strong interaction might cause local concentration difference which could lead to onset of nucleation.

The positions of both C-O-C stretching mode and the shoulder have different dependence on the solvents and the concentration of the solvents. The C-O-C ring stretching frequency showed very small dependence on the solvent and solvent concentration. However, the shoulder position did show strong dependence on solvent and solvent concentration.

For pure THF, although the shoulder is not visible, the

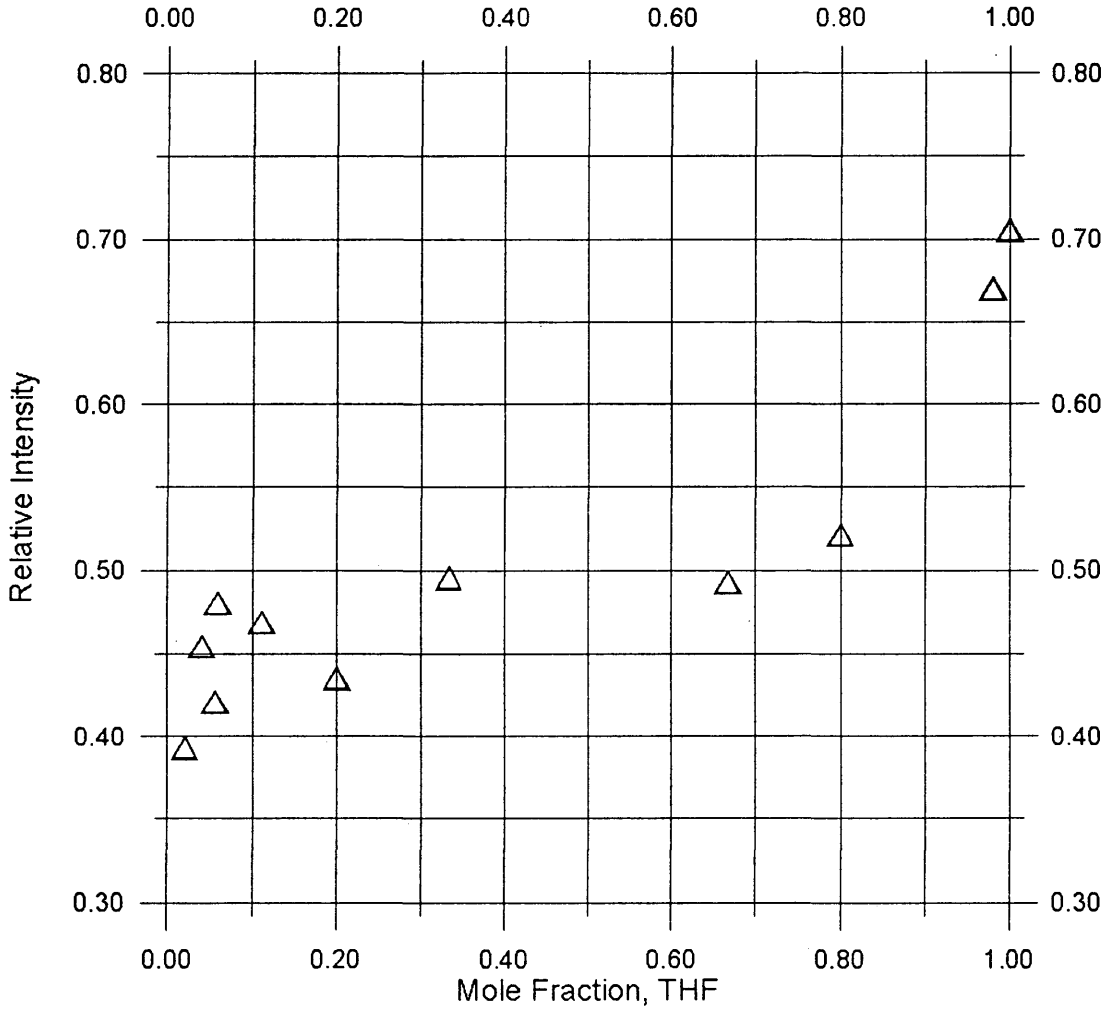

Figure 5.5 Relative intensity of THF C-O-C stretching vs. THF mole fraction

overall shape of the C-O-C ring stretching peak shows that the C-O-C ring stretching mode is partially symmetrical rather than totally symmetrical.

5.2.2 Shoulder Position vs. THF Concentration in Solutions

As determined in Figure 5.4 and Figure 5.5, once THF molecules dissolve into water, methanol and chloroform, a shoulder appears on the lower wavenumber side of THF C-O-C stretching frequency. The position of this shoulder changes with concentration of solvents, as clearly shown in Fig. 5.4.

The frequency of the shoulder close to THF C-O-C ring stretching frequency in solvents such as water, methanol and chloroform follows the same trend, which is counter to that with the solvent CCl_4. This is evidence that the appearance of the shoulder is due to the hydrogen bonding interaction between THF molecule and solvent molecules.

In order to understand the mechanism for the appearance of the shoulder, a series of isotopic substitution experiments were conducted. Isotopes of hydrogen, deuterium, were used to form deuterium oxide and deuterium hydrogen oxide as solvents. As determined in the spectra of Figure 4.1, Figure 4.2, and Figure 4.3, the position of the C-O-C ring stretching does not change for solutions of THF+H_2O, THF+D_2O and THF+HDO; neither

does the shoulder position. However, as the hydrates form, the C-O-C ring frequency shifts for each solvent.

The integrated area and area ratio for both C-O-C stretching mode and shoulder in different solvents are shown in Table 5.3. The expanded spectra of this region is shown in Figure 5.6, Figure 5.7, and Figure 5.8.

As it is shown from the spectra, the most prominent spectral features with the formation of the hydrate is that the shoulder's intensity is greatly reduced. The interaction causing this shoulder is thus greatly reduced during the process of hydrate formation. The expanded spectra are shown in Figure 5.6. This computer fitting spectra for both THF hydrate at 3.0°C and THF+H_2O solution(1:17) at room temperature are shown in Figure 5.2 and Figure 5.3. The following section discusses a possible explanation for the appearance and disappearance of the shoulder.

5.2.3 A Possible Explanation for Characteristics of the Shoulder

The appearance of the shoulder close to C-O-C ring stretching frequency in the liquid phase and the substantial reduction in intensity due to hydrate formation is very reproducible experimentally. What is actually happening in the

Table 5.3 Computer Fitting Results for Integrated Area of C-O-C Stretching Region

Mol. Ratio	C-O-C Area	Shoulder Area	C-O-C Ratio	Shoulder Ratio
4:1	1.25e6	1.15e6	0.521	0.479
2:1	9.70e5	9.99e5	0.493	0.507
Pure THF	2.46e6	1.03e6	0.705	0.295
1:2	1.25e6	1.27e6	0.496	0.504
1:4	5.45e5	7.09e5	0.435	0.565
1:8	6.83e5	7.84e5	0.469	0.531
1:16	7.18e4	7.76e4	0.481	0.519
1:17	1.33e5	1.83e5	0.421	0.579
1:24	1.57e5	1.88e5	0.454	0.546
1:49	8.27e4	1.28e5	0.393	0.607
49:1	1.65e6	8.14e5	0.670	0.330
1:1 (CCl_4)	2.75e5	3.55e5	0.437	0.563
1:1 ($CHCl_3$)	5.27e5	2.51e5	0.677	0.323

Note: The first number of the ratio is the number of moles of THF and the second number of the ratio is the number of moles of the solvents.

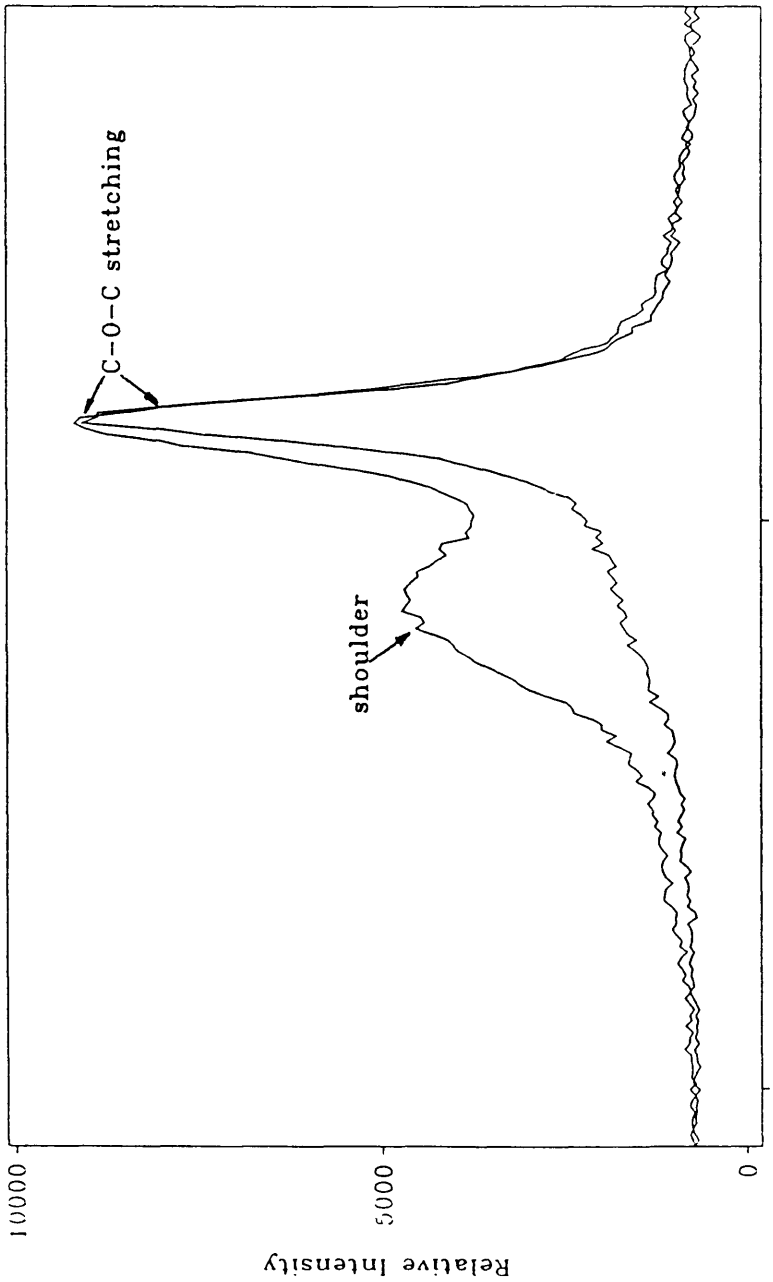

Figure 5.6 Expanded spectra of THF solution and THF hydrate for C-O-C stretching band at -3.0°C

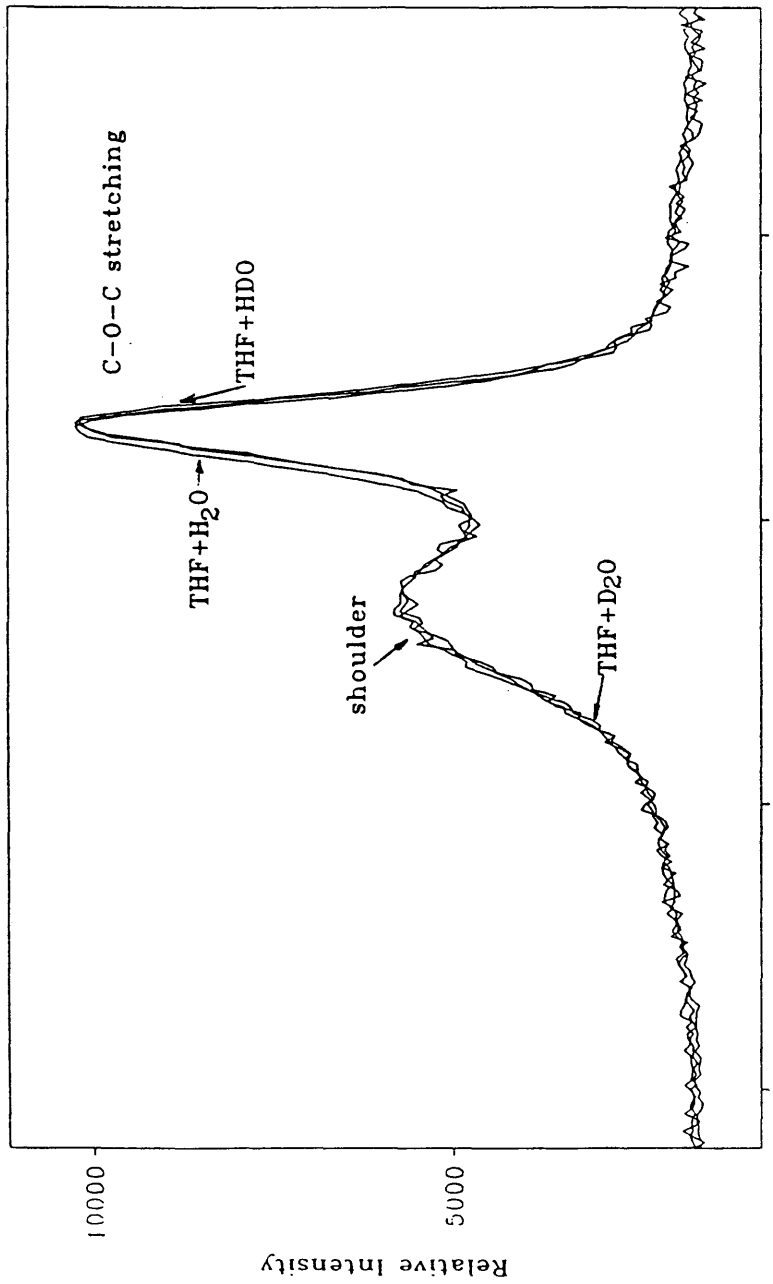

Figure 5.6 Expanded spectra if C-O-C stretching region for THF solutions at 3.0°C

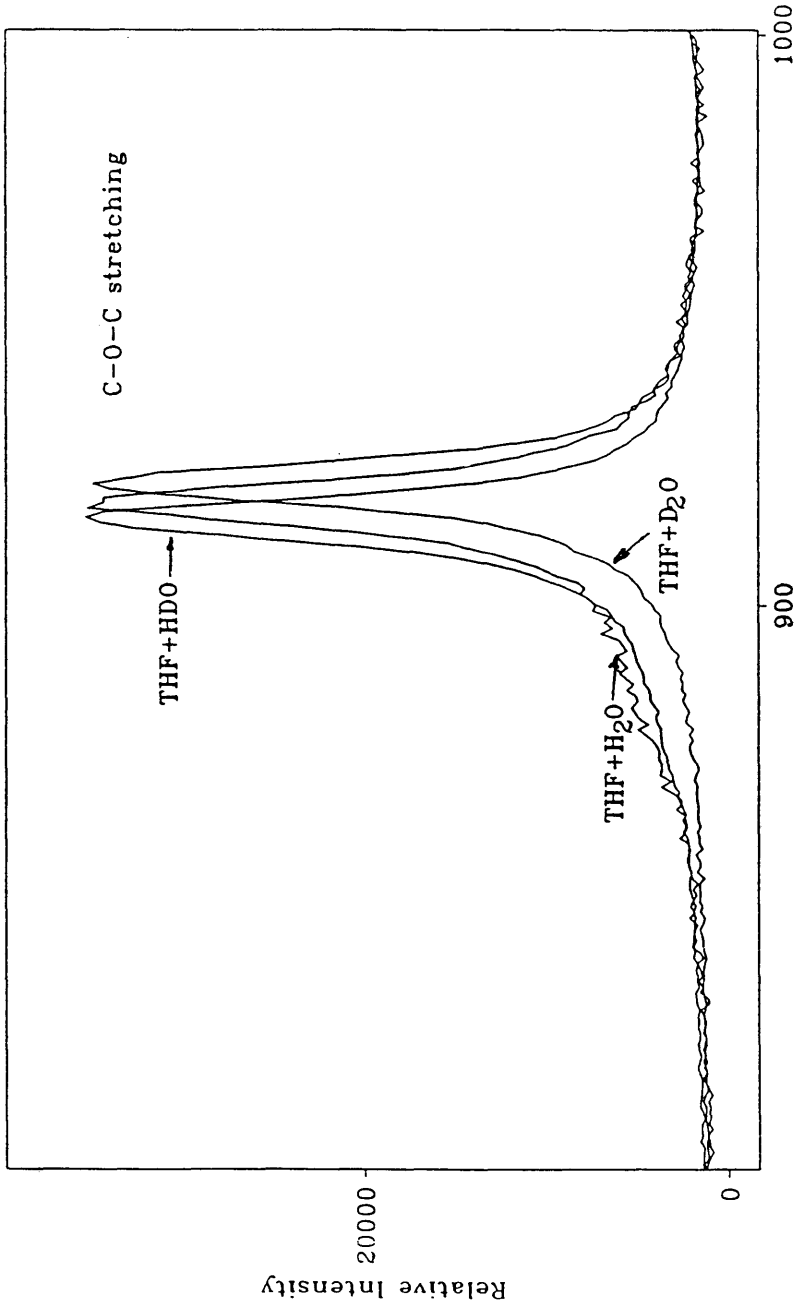

Figure 5.8 Expanded spectra of C-O-C stretching band for THF hydrate at 3.0°C

supercooled solution before hydrate formation is not certain. Based on the experimental evidence of this research and the other theoretical study such as computer simulation, it is well known that nonpolar gas molecules dissolve into water, the water molecules cluster around these apolar molecules to form a hydration shell(Long and Sloan, 1993). In these experiments, THF is a relatively polar molecule with an oxygen atom in the carbon ring, the water molecules will not cluster around a THF molecule. Instead, the THF molecules hydrogen bond to the water molecules.

The experimental evidence in this study shows that the THF molecules and H_2O molecules form a hydrogen bonded complex in the liquid phase. The hydrogen bond between these two molecules is formed by the oxygen atom in the carbon ring and the hydrogen atoms in water molecules. The interaction of the hydrogen bonding is strongly dependent on the type of solvent and solvent concentration. As hydrates form, this hydrogen bond breaks which causes the shoulder to disappear in the hydrate phase. There is no chemical bonding between the host molecules and the guest molecules inside the hydrate cage. The tendency of water molecules to maximize the total number of hydrogen bonds(Franks, 1973) causes the breakdown of the bonding between THF molecule and water molecule upon hydrate formation. This gives the THF free rotation inside the hydrate

cage as shown schematically in Figure 5.9(b).

Although there is no apparent chemical bonding between host molecules and guest molecules, the host structure still has some degree of impact on the guest molecule vibrational frequencies inside the hydrate cage. As shown in Figure 5.7 and Figure 5.8, the C-O-C stretching frequency does change by about 1 cm^{-1} between THF+H_2O, THF+D_2O and THF+HDO solutions.

The formation of the shoulder due to hydrogen bonding is based on the following experimental observations. First, the shoulder frequency of THF+CCl_4 does not follow the general trend of THF+H_2O, THF+Methanol and THF+$CHCl_3$. The difference between these solvents is that the CCl_4 does not have a hydrogen bonding ability while the other three solvents do. This evidence indicates that the appearance of the shoulder is due to hydrogen bonding interaction between the solvent molecules and the solute molecules.

Secondly, based on isotopic substitution experiments, in the liquid phase the shoulder position does not change between THF+H_2O, THF+D_2O, and THF+HDO solutions. This implies that there is a symmetrical bonding pattern between THF molecules and the solvent molecules since only symmetrical bonding can cancel the effect due to the different mass. Figure 5.9 (a) shows the possible hydrogen bonding complex between water molecules and THF molecules.

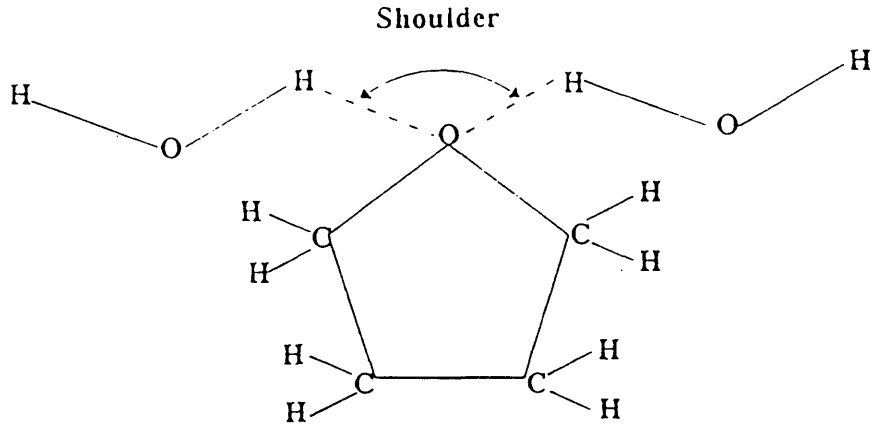

Figure 5.9(a) Possible hydrogen bondinng pattern between THF molecule and water molecules

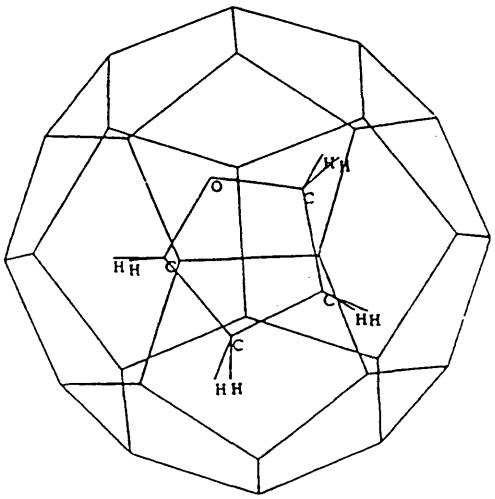

Figure 5.9(b) THF molecule inside the hydrate cage

Once the hydrate forms, the hydrogen bonds between the solute molecules and the solvent molecules are broken. At this point there is only van der Waals type of interaction existing between the THF molecules and water molecules. The THF molecule inside the hydrate cage behaves like a free molecule in the gas phase, as shown schematically in Figure 5.9(b).

5.3. Polarized Spectra Analysis of THF+H_2O Hydrate and Solution

5.3.1 Depolarized Ratio Calculation

Polarized Raman spectra provide precise information about the symmetry properties of normal vibrations. The symmetry property of a normal vibration of a molecule can be determined by measuring the depolarization ratio.

The depolarization ratio ρ is defined as the ratio between the relative intensities of a polarized spectrum and that of a depolarized spectrum. Here the polarized spectrum is referred to as the spectrum obtained using cross configuration, and depolarized spectrum is defined as spectrum obtained using horizontal configuration. The expression is shown in Eq. 3.8 in chapter 3.

In order to calculate the depolarization ratio, the intensities of both directions have to be calculated. The

computer deconvolution technique was used to separate the C-O-C band of both THF+H_2O solution and THF hydrate. Table 5.4 shows the computer decomposed parameters for polarized and depolarized spectra of THF+H_2O solutions, where $I_{//}$ and I_{+} are referred to as intensity of depolarized spectrum and polarized spectrum, respectively. The C-O-C and the shoulder frequency shifts are the frequency shifts of both the C-O-C band and the shoulder relative to the excitation line, i.e., 514.53 *nm* green line, with unit of cm^{-1}. The height is in relative units. The width is also the full-width-at-half-maximum (FWHM) with unit of cm^{-1}.

However, the observed intensities must first be corrected to remove the temperature-dependent contribution arising from the Boltzmann thermal populations of the excited vibrational levels(Cates and MacPhail, 1991). The method is discussed in Chapter 3. The corrected intensities for both C-O-C stretching and shoulder are shown in Tables 5.5 and 5.6.

The calculated depolarization ratios of C-O-C stretching frequency in THF+H_2O solutions are shown in Table 5.5. By using the same method, the depolarization ratio of shoulder in THF+H_2O solution and C-O-C ring stretching frequency is also calculated and is shown in Table 5.6. As shown in these two tables, the depolarization ratio is a function of temperature. The typical value of the C-O-C stretching mode is about 0.2

Table 5.4 Computer decomposed data for polarized and depolarized spectra of THF+H_2O solution

$I_{//}$ (Depolarized)						
Temp. (°C)	C-O-C freq.	Height	Width (cm^{-1})	Should. freq.	Height	Width (cm^{-1})
25.0	917.00	19739	12.53	889.05	9221	33.02
14.4	918.97	9859	12.74	890.27	4837	33.26
10.2	918.74	9977	12.81	889.65	4846	34.33
6.4	918.14	9835	13.28	888.81	5047	33.85
4.6	918.59	10923	13.05	888.93	5368	34.35
3.6	918.71	8791	12.97	889.04	4172	33.69
2.3	919.18	8883	12.98	889.11	4261	33.69
I_{+} (Polarized)						
Temp. (°C)	C-O-C freq.	Height	Width (cm^{-1})	Should. freq.	Height	Width (cm^{-1})
25.0	917.15	1826	17.29	885.85	1339	37.44
14.4	919.39	1493	16.1	889.22	1117	41.71
10.2	919.03	994.4	19.18	886.99	709.3	38.86
6.4	918.79	1269	16.53	886.88	940.3	38.27
4.6	919.72	1412	16.37	886.94	1017	35.9
3.6	920.96	1393	18.09	887.87	1016	42.99
2.3	920.18	1211	14.12	888.27	858.1	40.91

Table 5.5 C-O-C depolarization ratio in THF+H_2O solution

Temp (°C)	I//	I+	Boltzmann coeff.	I// Corr.	I+ Corr.	Ratio
25	296147	49613	5.26E-6	1.55801	0.26101	0.17
14.4	152401	37774	5.44E-6	0.82954	0.20561	0.25
10.2	151846	29959	5.53E-6	0.83899	0.16553	0.20
6.4	150880	32991	5.6E-6	0.84553	0.18488	0.22
4.6	168392	36315	5.64E-6	0.94932	0.20473	0.22
3.6	133975	39620	5.66E-6	0.75792	0.22414	0.29
2.6	138963	26188	5.67E-6	0.78859	0.14861	0.19

Table 5.6 Shoulder depolarization ratio in solutions

Temp (°C)	I//	I+	Boltzmann coeff.	I// Corr.	I+ Corr.	Ratio
25	411341	78771	5.26E-6	2.1640	0.4144	0.20
14.4	222111	73262	5.44E-6	1.2090	0.3988	0.33
10.2	223639	43317	5.53E-6	1.2357	0.2393	0.20
6.4	237611	56540	5.6E-6	1.3316	0.3169	0.24
4.6	250844	57362	5.64E-6	1.4142	0.3234	0.23
3.6	186729	68655	5.66E-6	1.5636	0.3884	0.35
2.6	196835	55148	5.67E-6	1.1170	0.3130	0.28

and for shoulder is about 0.25. The computer decomposed parameters for polarized and depolarized spectra of THF+H_2O hydrate are shown in Table 5.7. For the polarized spectra of hydrate, one peak fitting gives much better result than two-peak fitting. So, only one peak fitting routine is used for polarized spectra of hydrate. The calculated depolarization ratios for the C-O-C ring stretching mode are shown in Table 5.8 with mean value at 0.65.

As shown in these tables, the depolarization ratio of C-O-C stretching mode is different in THF solution and in THF hydrate. The depolarization ratios of that in THF solution have lower value than that in THF hydrate. C-O-C stretching mode in THF hydrate is more depolarized because the depolarization ratios are larger than 0.5. However, those in solutions are between 0.1 and 0.5. This implies that the stretching modes inside the hydrate cage is depolarized while in solution it is neither totally polarized nor totally depolarized. The difference is due to the environmental difference between solution and hydrate. There are more associations between molecules in the solution than these in the hydrate. The perturbations of these associations to C-O-C stretching mode cause the distortion of this stretching mode.

As for the shoulder, due to the fact that there is hardly a shoulder present in the hydrate phase, only the

Table 5.7 Computer decomposed data for polarized and depolarized spectra of THF hydrate

$I_{//}$						
Temp. (°C)	C-O-C freq.	Height	Width	Should. freq.	Height	Width
-6.0	919.11	3649	9.32	911.18	432.1	34.3
-4.2	919.01	4276	11.93	914.53	1066	36.6
-2.2	919.09	4666	11.34	913.46	1005	38.75
0.0	917.87	4878	11.89	913.33	1232	36.01
1.5	919.48	9732	9.61	915.34	2697	29.11
2.6	917.81	6530	13.08	898.79	1071	57.27
I_{+}						
Temp. (°C)	C-O-C freq.	Height	Width	Should. freq.	Height	Width
-6.0	918.44	912.7	27.06	No data since only one peak fitting was used.		
-4.2	918.20	837.4	31.65			
-2.2	917.87	846.2	37.61			
0.0	917.28	757.3	33.58			
1.5	918.90	1202	34.2			
2.6	917.93	798.3	28.08	883.95	282.8	42.75

Table 5.8 Depolarization ratio of C-O-C stretching mode in THF hydrates

Temp (°C)	$I_{//}$	I_{+}	Boltzmann coeff.	$I_{//}$ Corr.	I_{+} Corr.	Ratio
-6.0	5.35e4	3.88e4	5.86E-6	0.31	0.23	0.65
-4.2	6.46e4	4.14e4	5.82E-6	0.38	0.24	0.73
-2.2	7.00e4	5.00e4	5.78E-6	0.41	0.29	0.64
0.0	7.36e4	4.00e4	5.74E-6	0.42	0.23	0.71
1.5	9.95e4	6.46e4	5.7E-6	0.57	0.37	0.54
2.6	1.16e5	3.24e4	5.68E-6	0.66	0.18	0.28

depolarization ratio of the shoulder in the liquid is calculated. They have the same characteristics as the C-O-C stretching mode. This vibrational mode is neither totally polarized nor totally depolarized.

For the last value of the depolarization ratio, the value is off from the other data points. This is attributed to the fact that close to the THF hydrate dissociation temperature, there is more lattice relaxation and vibration than at the other temperatures.

5.3.2 Rotational Relaxation Time Calculation For Hydrate and Solution

The rotational correlation time τ_{rot} is calculated using the methodology mentioned in the previous chapter. It is determined from the difference in the FWHM values of the depolarized spectra and the isotropic spectra of a Raman band.

The calculated isotropic spectrum for THF+H_2O solution at room temperature is shown in Figure 5.10 and the computer decomposed parameters for isotropic spectra of THF+H_2O solution and THF+H_2O hydrate are shown in Table 5.9 and Table 5.10 respectively. The calculated rotational relaxation times for THF molecules in solution and inside the hydrate cages are shown in Table 5.11 and Table 5.12 respectively.

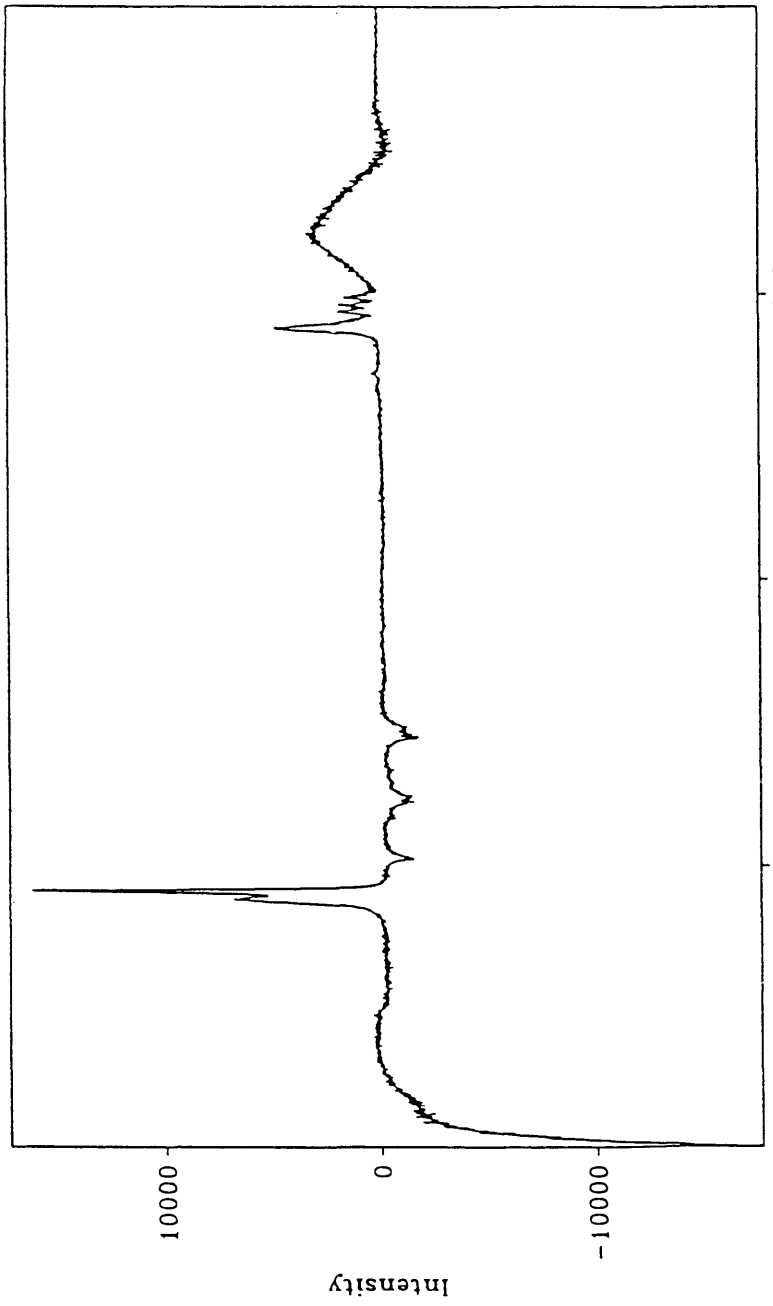

Figure 5.10 Isotropic spectrum of THF:H_2O solution(1:17 mole ratio) at room temperature

Table 5.9 Computer Decomposed Data for isotropic spectra of THF+H_2O solution at different temperatures

Temp. (°C)	C-O-C freq.	Height	Width	Should. freq.	Height	Width
Room Temp.	917.038	1.46e4	12.43	889.73	6642	34.88
14.4	918.95	6585	12.72	890.73	2954	33.96
10.2	918.77	7270	12.65	890.25	3489	36.4
6.4	918.07	6787	13.4	889.50	3462	35.61
4.6	918.64	7582	13.03	889.06	3577	36.95
3.6	918.38	5751	12.53	890.07	2513	34.75

Note: 1. The unit for C-O-C freq., width and shoulder freq. is frequency shift with unit cm^{-1}.

2. There is no real unit for the height. It is a relative height.

Table 5.10 Computer Decomposed data for isotropic spectra of THF+H_2O hydrate at different temperatures

Temp. (°C)	C-O-C freq.	Height	Width	Should. freq.	Height	Width
-6.0	919.179	2676	8.802	910.715	229.5	11.28
-4.2	918.993	4721	9.448	908.023	427.0	8.269
-2.2	919.09	5396	10.27	906.359	380.1	16.27
0.0	917.797	5688	9.093	908.262	442.0	19.11
1.5	919.353	8903	9.382	908.623	817.4	13.00
2.6	917.845	6868	9.806	897.012	518.9	42.84

Table 5.11 Rotational relaxation time for THF molecule in the water solution with molar ratio 1:17

Temperature (°C)	Rotational Relaxation Time (sec)
Room Temp.	3.27E-12
14.4	4.71E-12
10.2	2.44E-12
6.4	5.08E-12
4.6	4.77E-12
3.6	2.86E-12

Table 5.12 Rotational relaxation time for THF molecule inside the hydrate cage

Temperature (°C)	Rotational Relaxation Time (sec)
-6.0	8.72E-13
-4.2	7.17E-13
-2.2	5.82E-13
0.0	6.5E-13
1.5	6.41E-13
2.6	8.71E-13

As expected, the relaxation time for THF molecules inside the hydrate cages is shorter than that of the THF molecules in the solution. There are more associations in the liquid phase than that in the hydrate phase as stated before. The THF molecule behaves more like a free molecule inside the cage.

In conclusion, the THF molecule inside the hydrate cage still has a interaction with the hydrate lattice to some extent. This interaction is much less than that in the solution phase.

CHAPTER VI

ANALYSIS OF OH STRETCHING BAND

6.1. Liquid Water OH Stretching Band

Liquid water has a intense, complex and broad band from 2800 cm^{-1} to 3800 cm^{-1}. This is the water intramolecular OH stretching band. The OH stretching vibrations are very sensitive to the presence and nature of hydrogen bonding in liquids and solids. Therefore, this band is closely related to the 3D network like hydrogen bonding structure which is responsible for most of the water structure and special properties(Rahman and Stillinger, 1973; Walrafen, 1973). Understanding and correctly interpreting this band is essential in order to understand hydrate formation mechanisms and hydrate kinetic inhibition mechanisms.

At room temperature, liquid water OH band is the most difficult to interpret among OH bands of the different states of water. It is the broadest band among all the different water states. In the literature, there were two basic approaches to the interpretation of this band. One is Walrafen's approach (Walrafen, 1973; Walrafen *et al.*, 1990), in which he postulated that there were several components that contribute to the water OH band. These contributions are

separated by the isosbestic point, defined as follows: any contribution below the isosbestic point is due to unbroken hydrogen bonding, while any contribution above the isosbestic point was due to broken hydrogen bonding. Three Gaussian bands were deconvolved by computer analysis techniques. Overall, Walrafen's approach favored the mixture model of water. The second approach is Scherer's(Scherer, 1989), in which he postulates that there is a Fermi resonance present in the OH band. Fermi resonance is defined as that several fundamentals combine together to generate an overtone with an energy as high as these fundamentals(Woodward, 1970). The higher wavenumber bands in the O-H stretching region are these due to the Fermi resonance of the lower water OH bending band around 1640 cm^{-1} with the O-H stretching bands. Scherer(1989) did not agree with the presence of isosbestic point in OH band. Overall, Scherer's approach favors the continuum model of water.

The Walrafen's approach was adopted for the following reasons. First, recent computer simulation and vibrational spectroscopy results are more in agreement with the mixture model than the continuum model. Secondly, separating OH stretching bands into unbroken hydrogen band and broken hydrogen band is easier and more reasonable to interpret the Raman results obtained.

Figure 2.5 shows a Raman spectrum of pure water at room temperature. This spectrum shows all three distinct features: the OH stretching band from 2800 cm^{-1} to 3800 cm^{-1}. the relatively weak OH bending band around 1640 cm^{-1}; and the low frequency libation mode with wavenumber below 310 cm^{-1}. This work is mainly concentrated on the OH stretching band. Two methods were used to deconvolve the OH band. The first method used 3 peaks each with a pure Gaussian shape. The results are shown in Figure 6.1. The second used 4 peaks. The results are shown Figure 6.2. The 3-peak fitting procedure gave better results based on the comparison with Walrafen's result of the peak positions and FWHM values(Walrafen, 1973). The peak around 3260 cm^{-1} is attributed to the unbroken hydrogen bonding contribution (referred to as UHBC or peak 1). The other two peaks, at about 3450 cm^{-1} and 3600 cm^{-1} respectively, are due to the broken hydrogen bonding contribution (referred to as BHBC or peak 2 and peak 3).

No attempt was made in the study to measure the absolute intensity of an individual vibrational mode or band. The relative intensity is used to define the relative importance of each contribution to the overall band structure. It is also used as a measurement of the effect of additives, such as polymers and salts, to change the water structure.

Aqueous ionic solutions have been studied for a long time

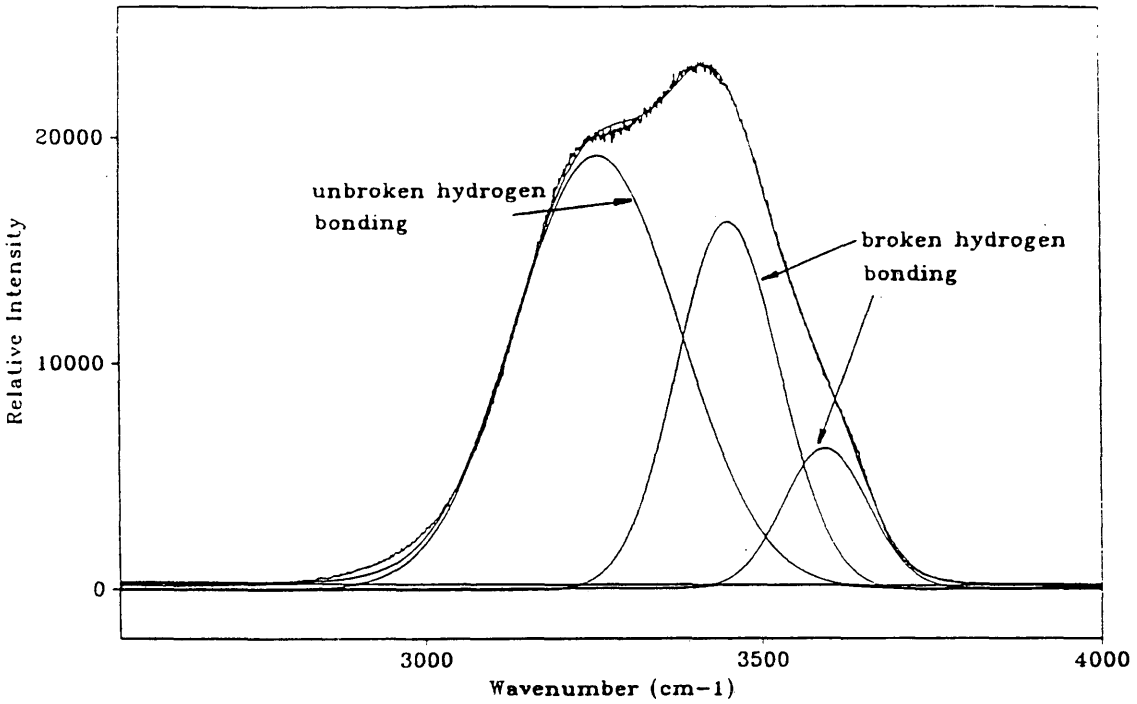

Figure 6.1 3-peak fitting of pure liquid water at room temperature

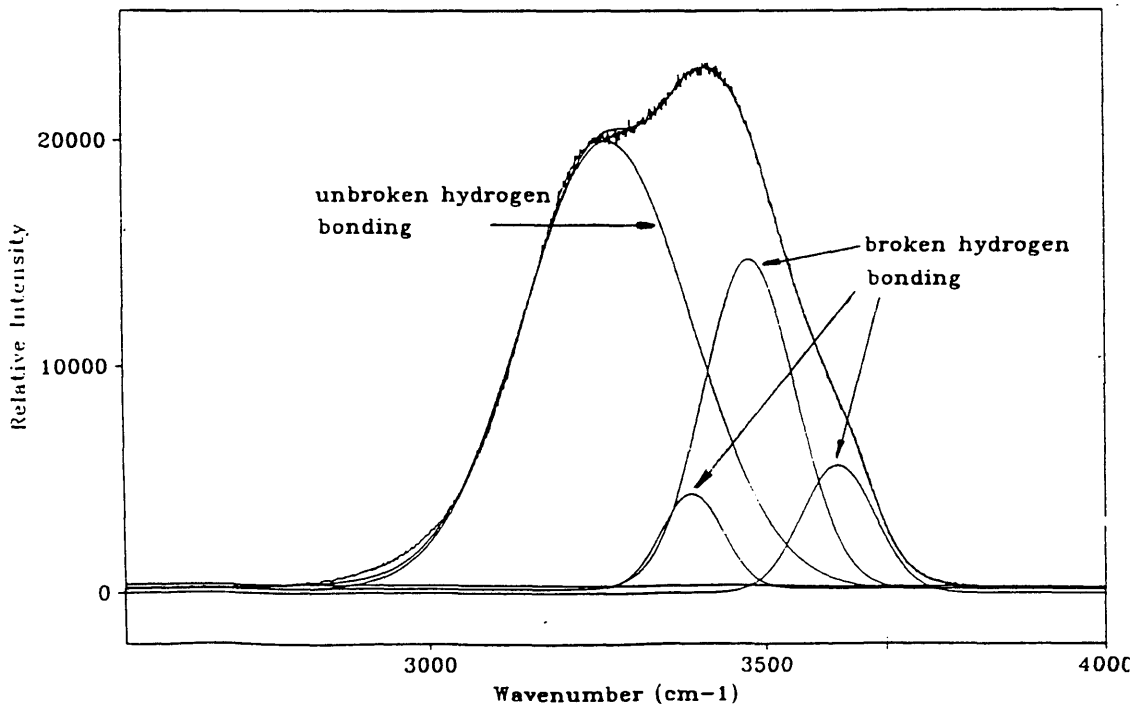

Figure 6.2 4-peak fitting of pure liquid water at room temperature

(Walrafen, 1973; Walrafen, *et al.*, 1985; Terpstra, *et al.*, 1990). Salts have the tendency to decrease the contribution of hydrogen bonded species and increase the contribution of broken hydrogen bonded species(Irish, 1971; Terpstra, *et al.*, 1990). This effect is consistent with the fact that salts can be used as a freezing point depression agent. The water structure is altered with the presence of salt so that conditions are not favorable for ice formation. Thus, salt can also be used as a thermodynamic inhibitor for hydrate inhibition. The mechanism is the same as methanol inhibition in the sense that both materials shift the equilibrium line of the hydrate formation.

6.2. THF+H_2O Solutions with Different THF Mole Fractions

The analysis of the OH band of these solutions is complicated by the overlap between the water OH band and the THF CH stretching band. The THF CH band must be subtracted from the original spectra in order to have a smooth water band profile. The pure water band was used as a reference spectrum to reconstruct the shape of the THF+H_2O solution spectra after removing the THF CH stretching bands in the spectra range from 2545 cm^{-1} to 3100 cm^{-1}. The whole OH band was covered from 2545 cm^{-1} to 4000 cm^{-1}. A comparison between the spectrum both before

and after the mathematical manipulation was conducted. As shown in Figure 6.3, there was no destruction of the peak features of the OH band in THF solutions. The comparison between the pure liquid water spectrum and the THF+water solution spectrum is shown in Figure 6.4.

The frequency shift of each peak versus the mole fractions of THF in the solution is shown in Figure 6.5. The relative intensity of these peaks is shown in Figure 6.6 against the THF mole fractions in the solution. The results for pure liquid water are also plotted on these figures with THF mole fractions equal to zero. All these measurements are done at room temperature.

As shown in Figure 6.5, the positions of peak 2 do not change as the concentration of THF changes. The position of peak 1 shows two distinct trends. As the THF concentration increases, the center position of peak 1 shifts towards the higher wavenumber until the concentration increases to about 1:2 THF to water mole ratio. At higher THF concentration, the position of this peak moves towards the lower wavenumber direction.

Frequency shift is a measure of the energy of the particular vibrational mode. In this case, the energy of the intramolecular hydrogen bond is an obvious function of the THF concentration in the solutions. The maximum value for the

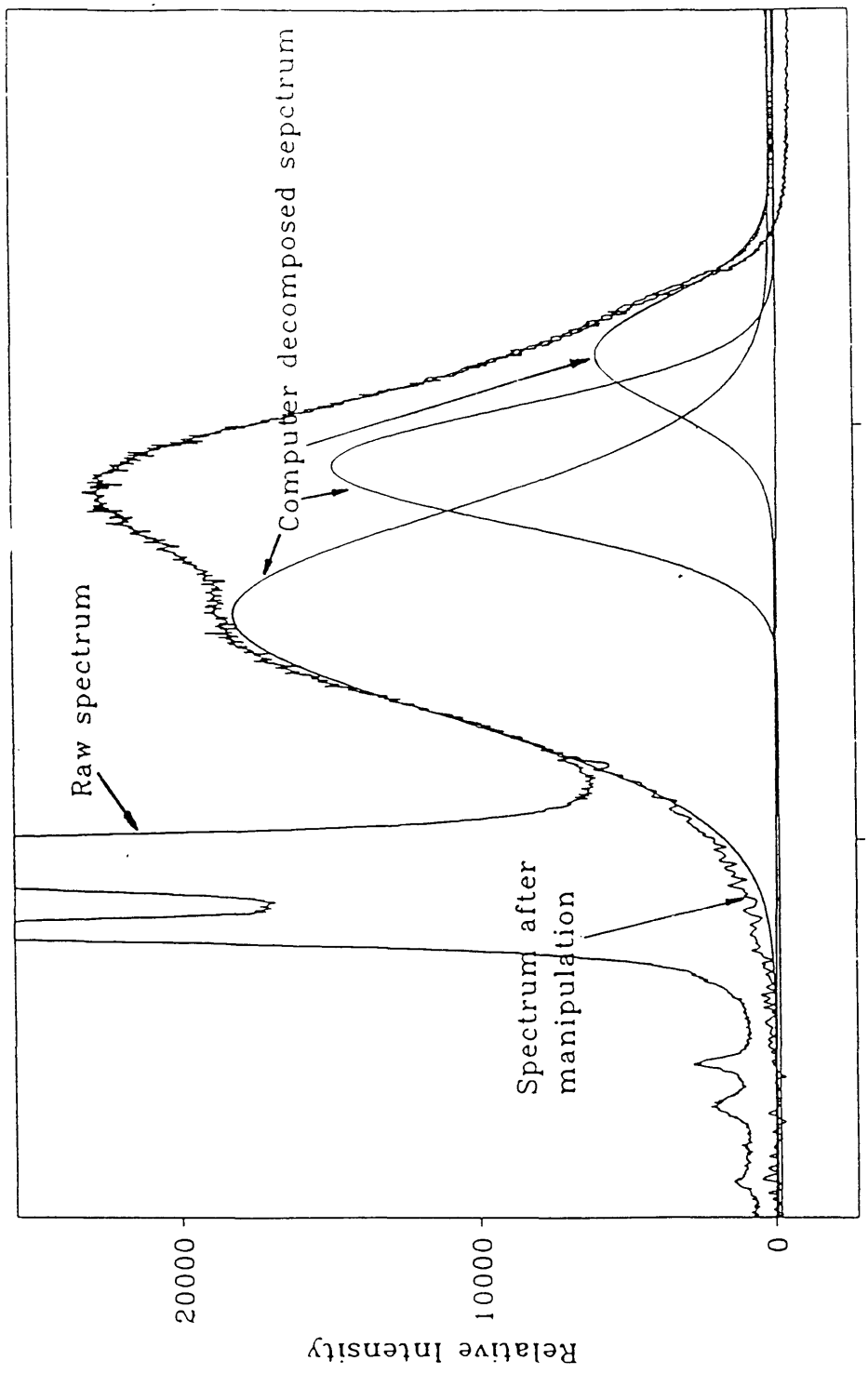

Figure 6.3 Comparison between raw and computer decomposed spectra

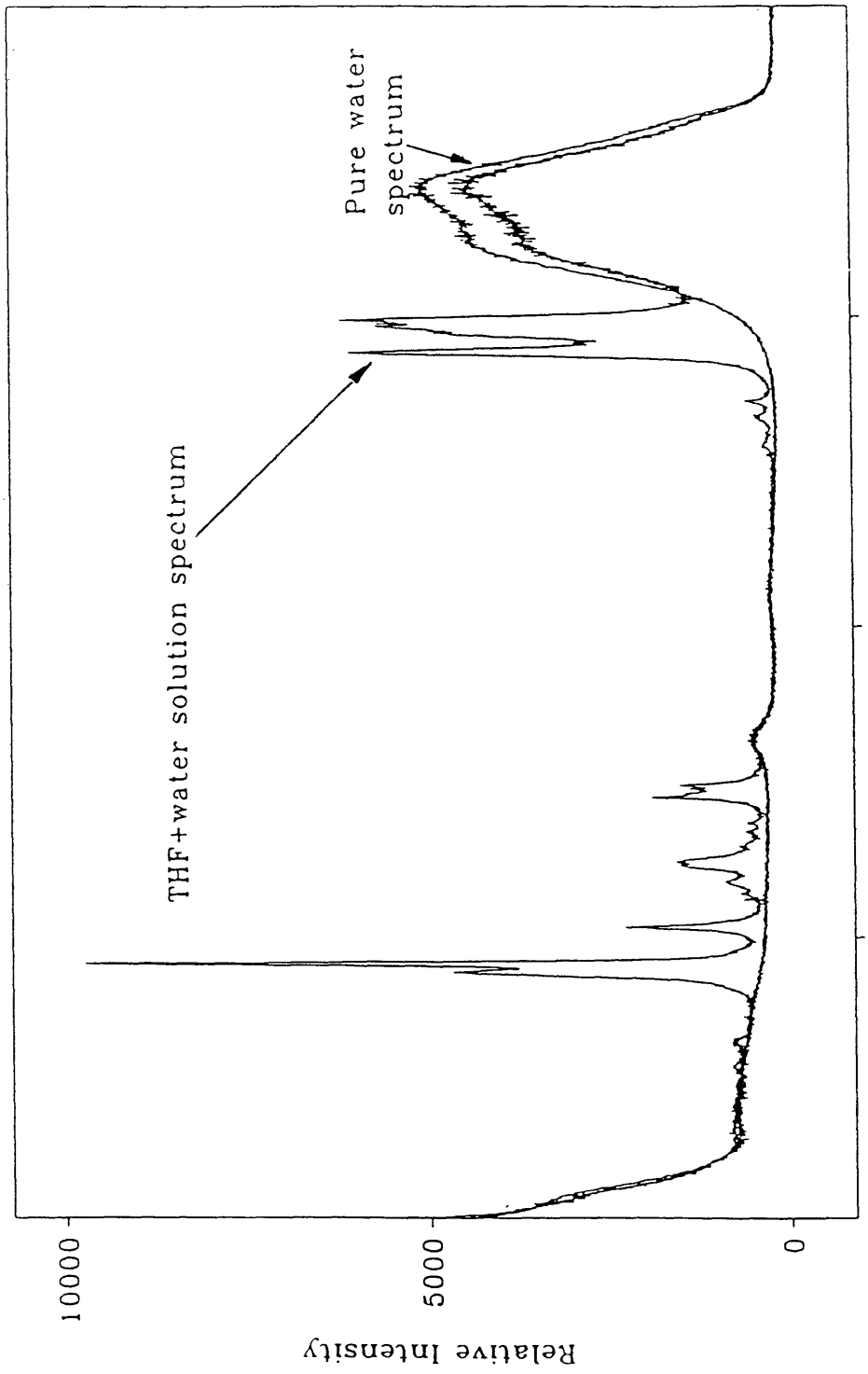

Figure 6.4 Comparison between pure water spectrum and THF+Water solution spectrum

frequency shift for peak 1 (which is the hydrogen bonding contribution) is at about 1:2 THF to water mole ratio. This suggests that at this concentration, the interaction between THF and water is the strongest.

As shown in Figure 6.6, the relative intensity, which is a measure of the relative contribution of individual component to the overall band, has different features. Peaks 1 and 2 have strongly opposite trends. As the THF concentration increases from zero, the peak 1 contribution also increases. Based on the experimental results, it is assumed that a very small amount of THF causes more hydrogen bonding between water-water molecules and water-THF molecules resulting in an increased relative intensity of the unbroken hydrogen bonding contribution. The contribution by broken hydrogen bonding decreases for the same reason. As the THF concentration increases to the point of about 1:2 THF to water mole ratio, there is an sudden change in the trend. This corresponds to the changes shown in Figure 6.5. The 1:2 THF to water mole ratio complex appears to be the most favorable configuration in this solution. The THF hydrate composition is 1:17 THF to water mole ratio. This suggests that the hydrate formation is a process of breaking and forming bonds. The hydrogen bonds formed between THF molecules and water molecules have to be broken before hydrate formation.

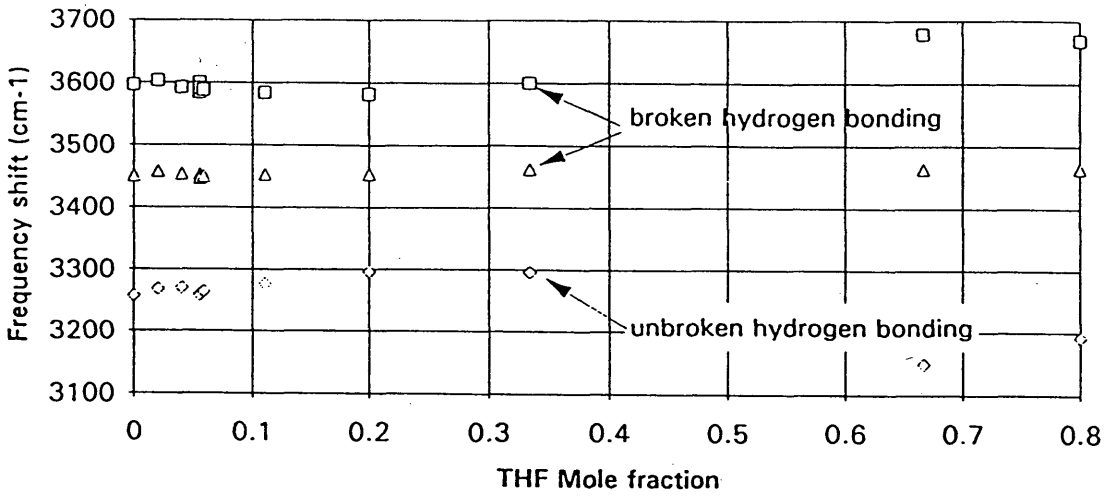

Figure 6.5 Frequency shift vs. THF mole fraction in solutions

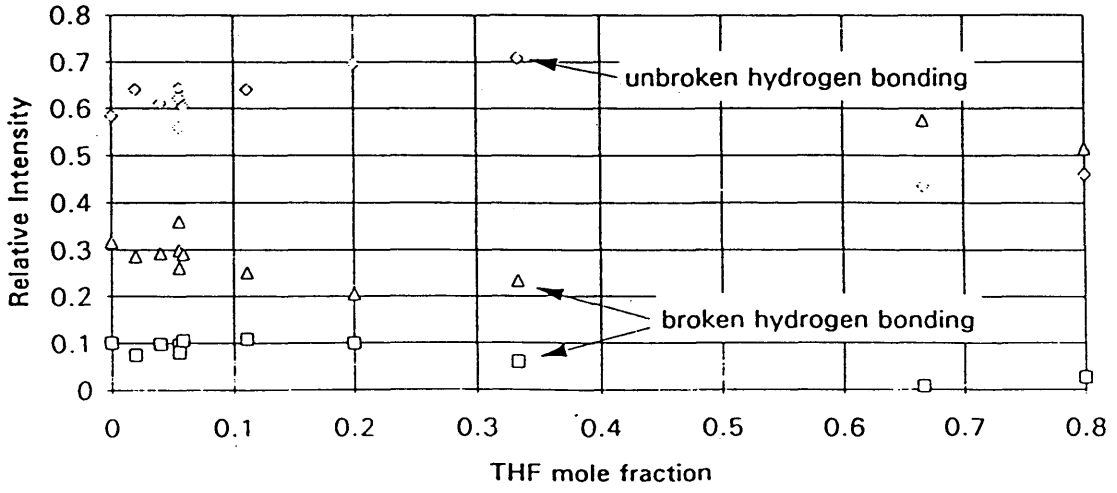

Figure 6.6 Relative intensity vs. THF mole fraction in THF+Water solutions

6.3. OH Stretching Band of THF+H_2O Hydrate

The THF+H_2O hydrate OH band was also decomposed into three components. The frequency shift of peaks 1, 2 and 3 versus the temperature are shown in Figure 6.7. The relative intensity of these peaks vs. temperature is shown in Figure 6.8.

At the present the data points are limited to a 10 °C range, and the following discussion may only be valid within this range. On cooling the hydrate to around 0°C, the Raman shift of all three peak shift to lower wavenumber. However, the relative intensity of peaks 1 and 3 moved to a maximum value point, the relative intensity of peak 2 moved to a minimum value point. This phenomenon may be attributed to the fast relaxation of the clathrate hydrate lattice near 0.0°C which causes an increase in the unbroken hydrogen bonding contribution. Around 0.0°C, the frequency of peaks 1, 2, and 3 shift to a lower wavenumber which indicates a decrease in the energy of the interaction. The number of the unbroken hydrogen bond is increasing due to the fact that lowering temperature will increase the degree of hydrogen bonding and decrease the strength of hydrogen bonding.

Summarizing the above discussion, it can be stated that in the absence of any additives such as polymers or salts, the

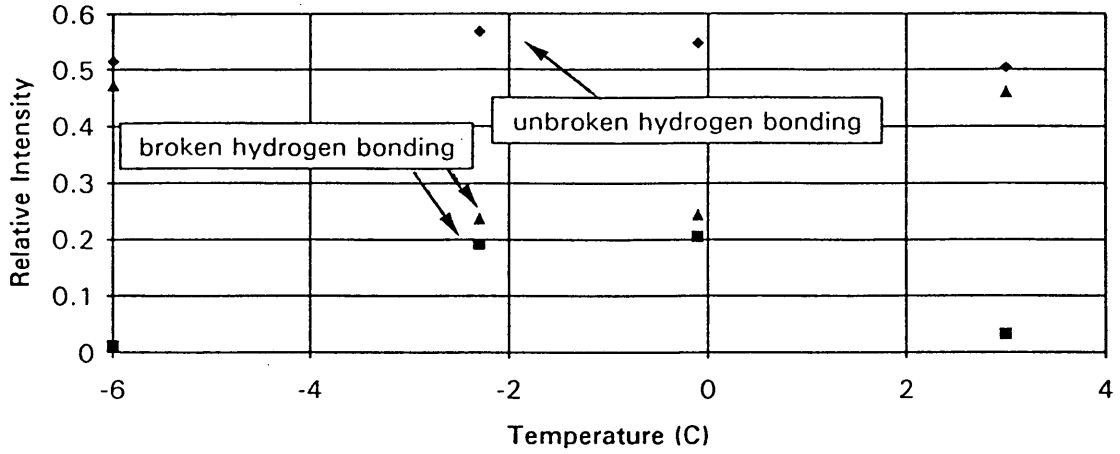

Figure 6.7 Relative intensity vs. temperature for THF hydrate

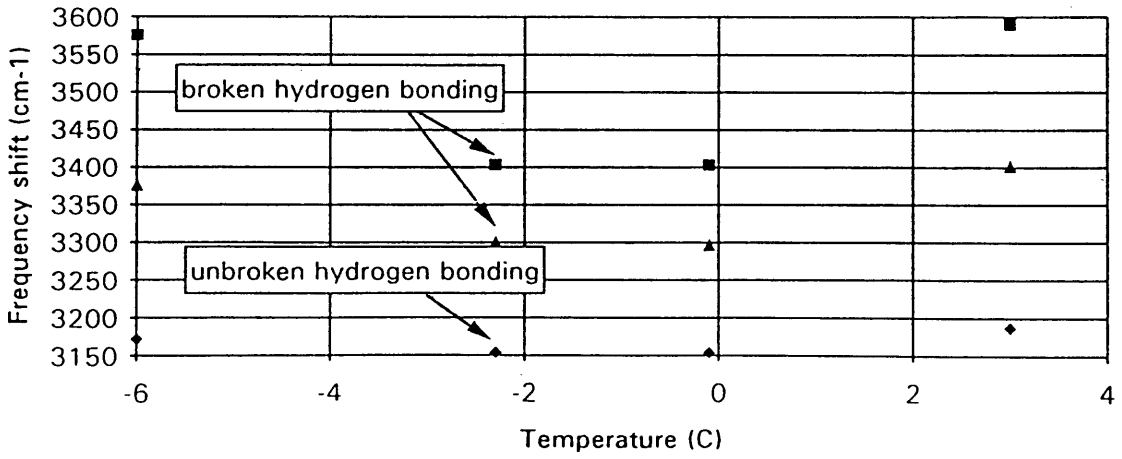

Figure 6.8 Frequency shift vs. temperature for THF hydrate

configuration of water molecules is organized in the way favoring hydrate formation. If this configuration of the water structure could be altered by additives, e.g., polymers, surfactant or salts, to certain degree, the inhibition effect would occur. There may be several mechanisms for polymer inhibition, however, changing the liquid water structure at subcooled conditions may be a very good way because the nucleation for hydrate formation process has to happen under the proper condition, either at the gas-liquid interface or in the bulk liquid phase.

6.4. THF+H_2O+Inhibitors System

Several polymers have been tested both in the laboratory and in the field. Their success suggests that using kinetic inhibitors will substantially reduce the operating costs now associated with annual methanol usage.

Three types of inhibitors are being tested in this research. They are PVP(Polyvinylprolidine), VC713 and PVCap(Polyvinyl Caprolactum), respectively. PVP and PVCap are homopolymers and VC713 is terpolymer of PVP. The structures of both PVP and VC713 are shown in Figure 6.9. The OH band of PVCap solution is presented here without further discussion.

The OH bands of these spectra were also deconvolved into

VC-713

Chemical Name: 2-PROPENIC ACID,2-METHYL-,2-(DIMETHYLAMINO)ETHYLESTER, POLYMER with 1-ETHENYLHEXAHYDRO-2H-AZEPIN-2-ONE & VINYLPYRROLIDONE

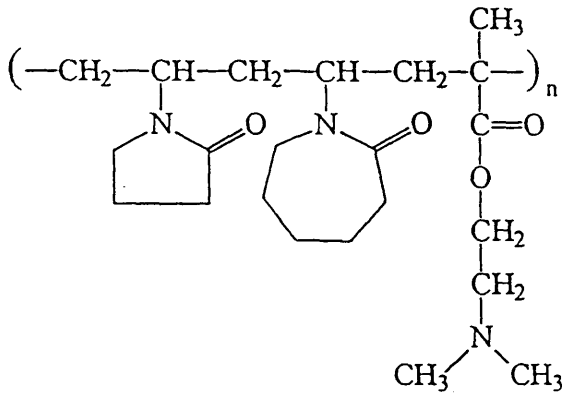

PVP

Chemical Name: POLYVINYLPYRROLIDONE

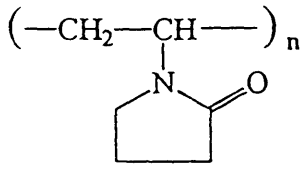

Figure 6.9 Structure of PVP and VC713

three peaks using the same techniques mentioned before. The results are shown in Figure 6.10, 6.11 and 6.12 respectively.

6.4.1 VC713+THF+H_2O System

From extensive testing in the lab, VC713 has been proven to be a very good kinetic inhibitor for hydrate inhibition(Sloan, *et al.*, 1993). The systems have been studied include VC713+THF+H_2O solutions with or without salt. The concentrations of each component are:

23 wt% THF; 0.5 wt% VC713; 3.5 wt% salt (if present)

The salt used in all the systems is ASTM sea salt with the standard composition that can be found in handbooks.

The spectra of this system with and without 3.5 wt% salt are shown in Figure 6.13. As shown in this figure, there are changes in terms of the overall features of the spectrum. The deconvolution analysis has been used for both OH stretching band and C-O-C ring stretching band. The results for OH will be discussed in detail. The results for C-O-C ring stretching show that the polymer does not have significant effect on the vibrational frequencies of solute molecules in the solution which implies that the interaction between polymer molecule

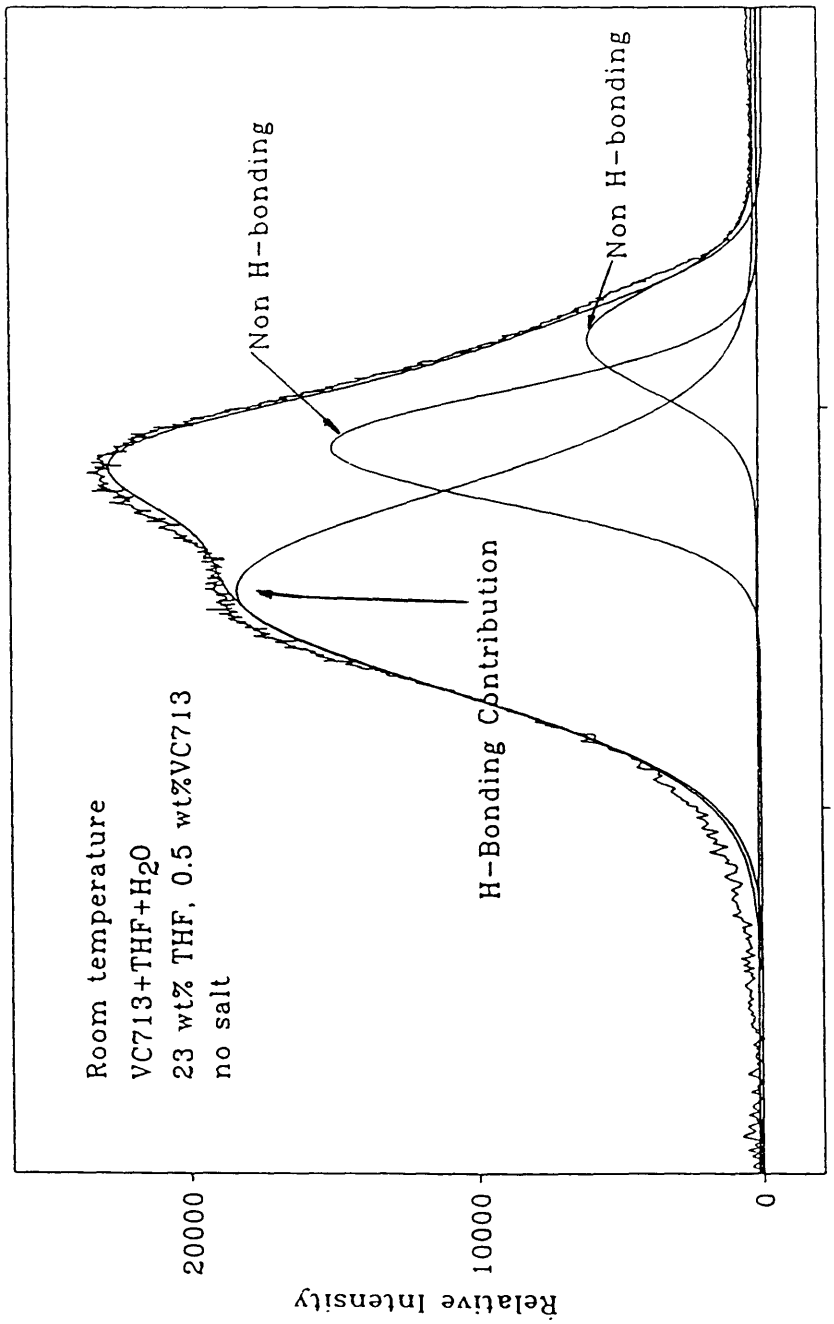

Figure 6.10 Original data and computer deconvoluted spectra for VC713 solution

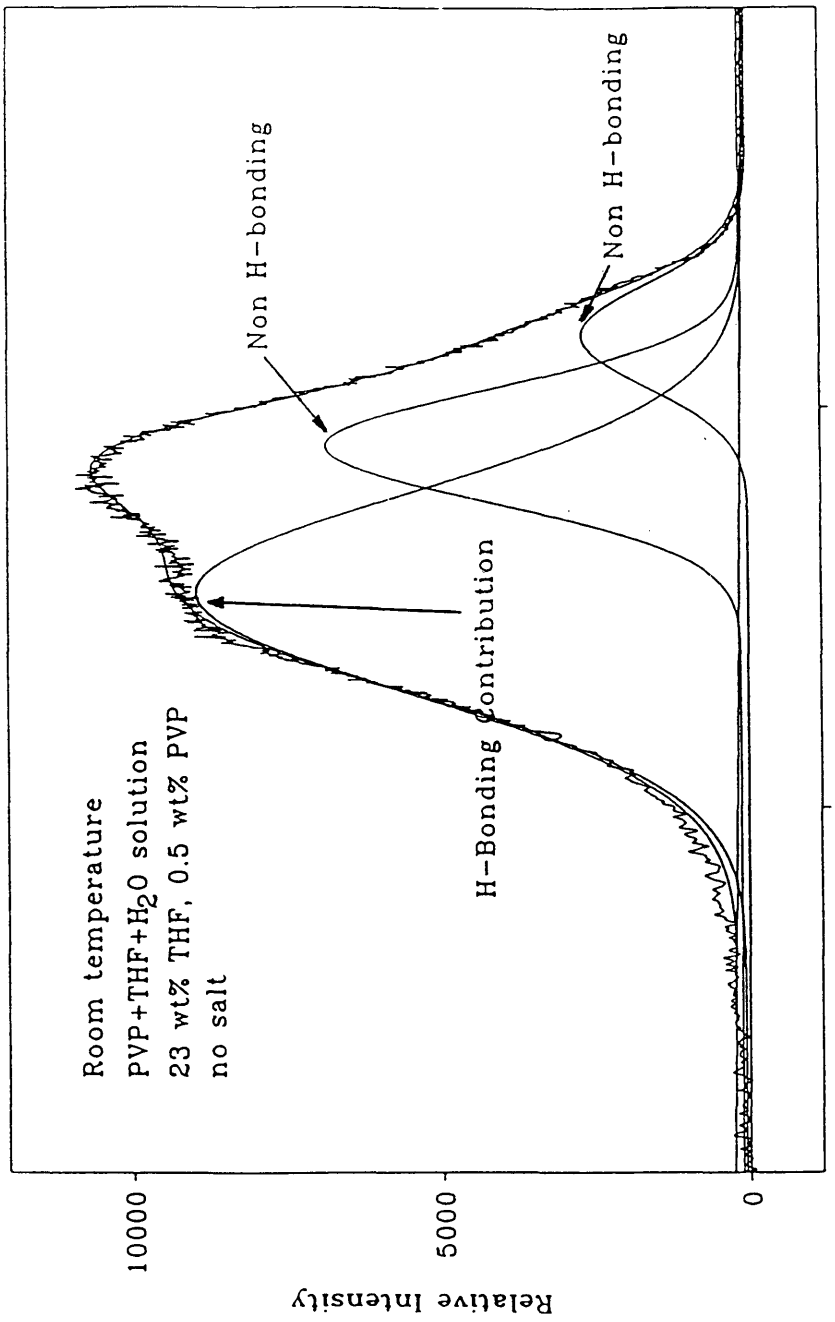

Figure 6.11 Original data and computer deconvoluted spectra for PVP solution

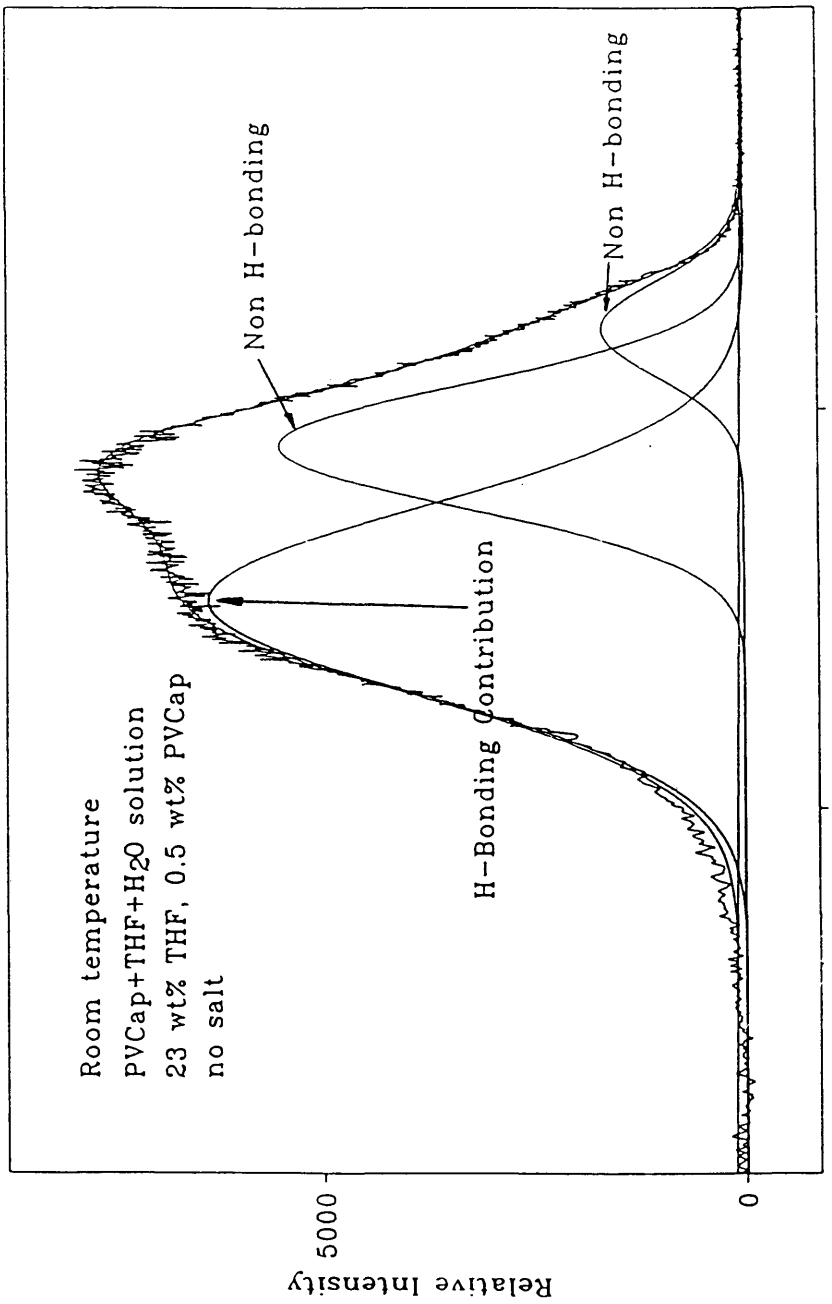

Figure 6.12 Original data and computer deconvoluted spectra for PVCap solution

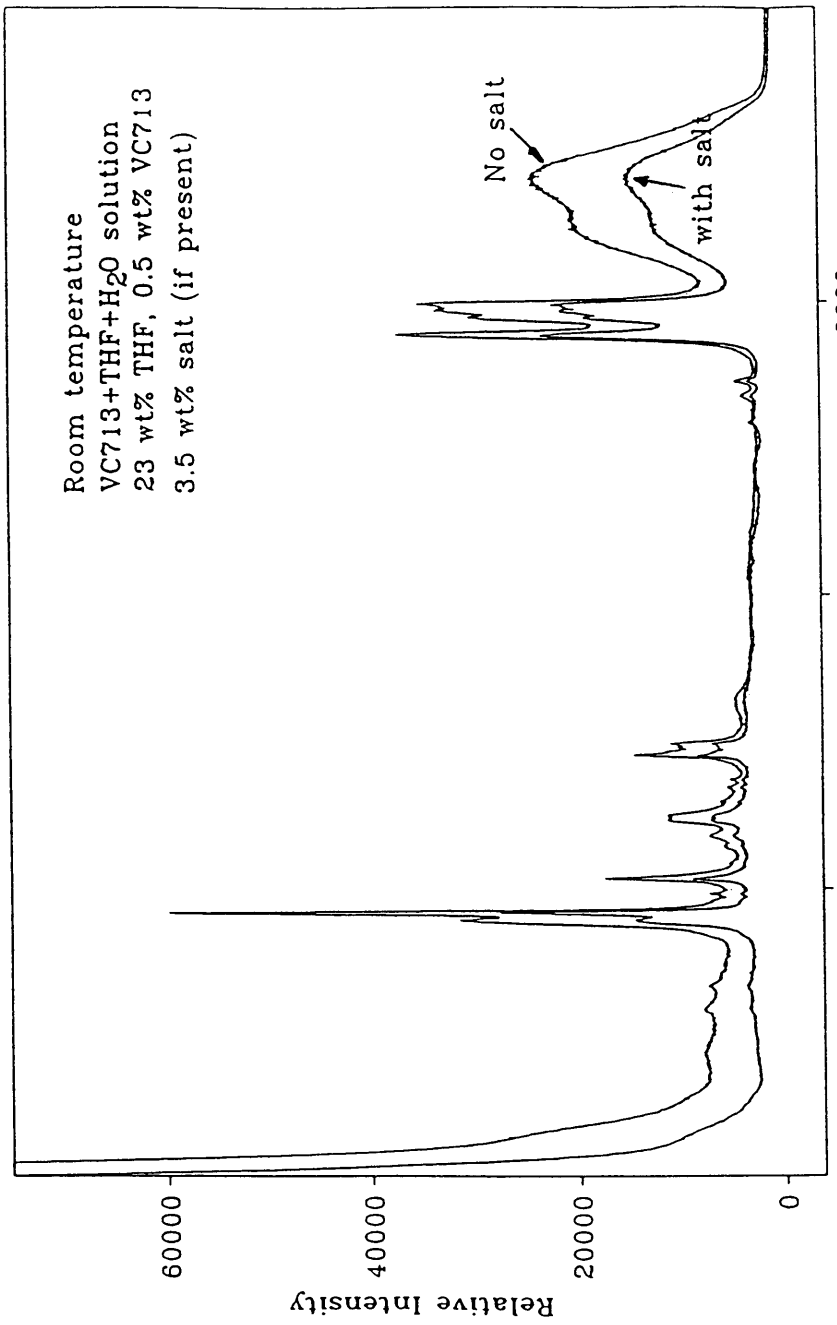

Figure 6.13 Comparison between spectra with and without salt for VC713 solution

and solute molecule is negligible.

In comparison of the positions of the different peaks, there are some differences between pure water and VC713 solution. The hydrogen bond population, which is represented by the relative contribution of each component to the whole band, and the hydrogen bond strength, which is represented by the frequency shift, are shown in Figure 6.14 and Figure 6.15 respectively.

From Figure 6.15, the center position of the unbroken hydrogen bonding band for both systems (with or without 3.5 wt% salt) seems to move towards the high wavenumber direction. The center position for the broken hydrogen bond, which is not shown in that figure, seems to move to the lower wavenumber direction. With the presence of the VC713, the strength of the hydrogen bond is stronger. The interaction induced by polymer increases the overall hydrogen bond energy. Whether this increase is due to the direct hydrogen bonding between VC713 molecules and water molecules or due to water-water molecules is not clear at this point.

In comparison of the relative intensity, there was an increased contribution of unbroken hydrogen bonding for the VC713 solution. As mentioned above, the presence of VC713 in the solution might have the following two effects: induce one or several water molecules clustered around the polymer

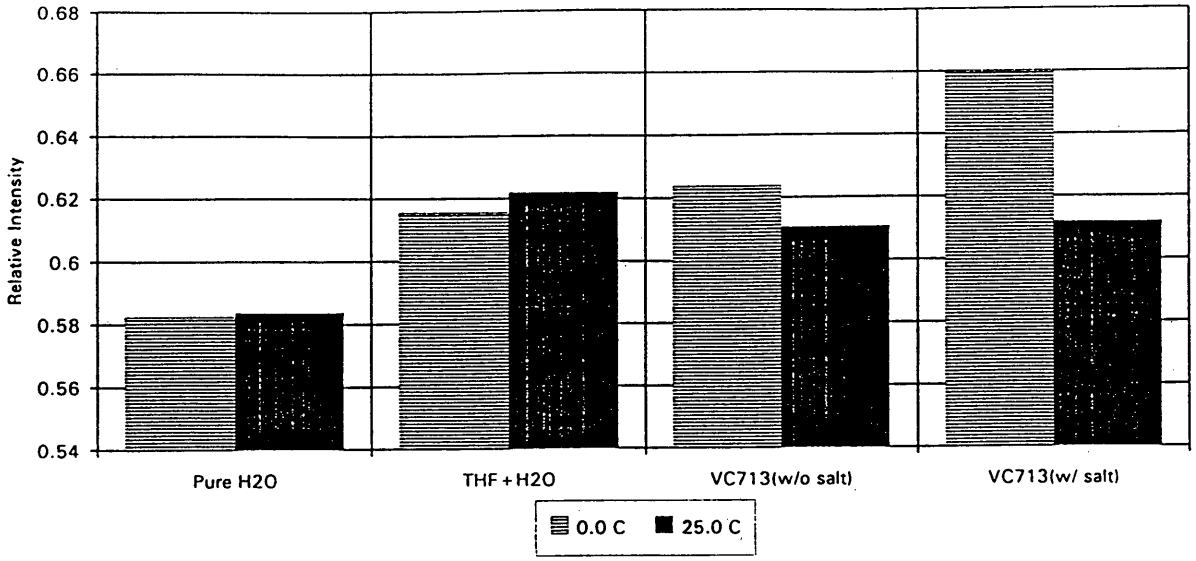

Figure 6.14 Hydrogen bond population for VC713 system

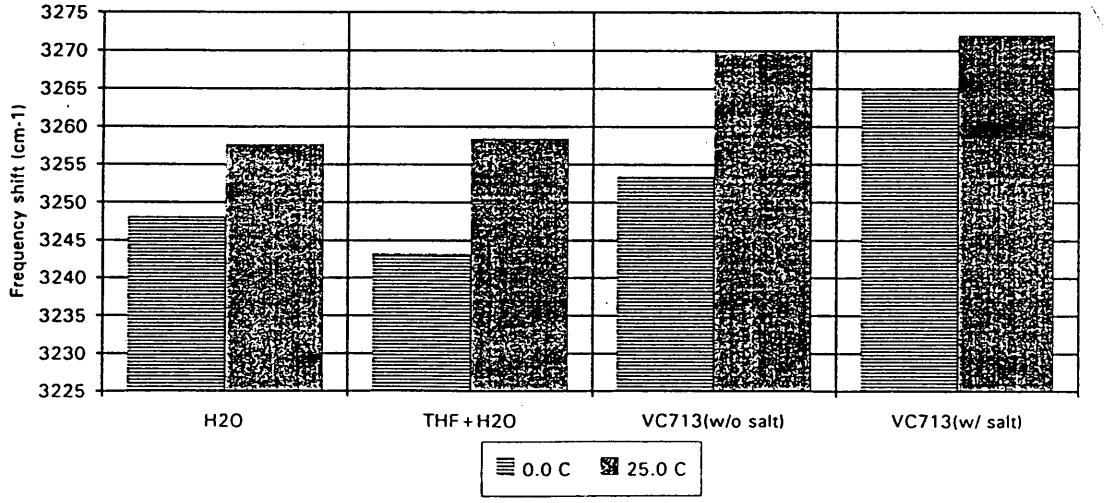

Figure 6.15 Hydrogen bond strength for VC713 system

segments, or H_2O molecules which are hydrogen bonded to the O atom in VC713 cause the increase of unbroken hydrogen bonding contribution. This process might not be very clear in the process of hydrate formation since most people would think that the more hydrogen bonding, the easier to form hydrate. It is evident that for pure hydrate and ice, there are more hydrogen bonds than pure water. However, will more hydrogen bonding help hydrate formation or hinder hydrate formation? From the experimental results obtained thus far, increasing the population of hydrogen bonds present in the subcooled solution may not be the only factor for inhibition mechanism, the configuration of the hydrogen bond in the whole solution may also be very important. The contribution of broken hydrogen bonding, especially peak 2, in this system was greatly reduced compared to both pure liquid water and THF-water solution.

The salt presence enlarges the population and strength of hydrogen bonding in the inhibitor system. This can be explained in the following way. Salt is known as a water structure breaker(Irish, 1971). The presence of salt will decrease the population of the unbroken hydrogen bonding and increase the population of broken hydrogen bonding. That is why salt can be used as a thermodynamic inhibitor since it takes water molecules away from each other. With salt and

VC713 present together, the requirement by VC713 to form more hydrogen bonds is satisfied by the contribution due to salt. This leads to an implication that the hydrate formation process is an two-step process: bond breaking and bond forming. VC713 enters this process at some point which leads to the inhibition of hydrate formation.

In conclusion, the OH band change for VC713 is significant. An increase in population and strength of hydrogen bond effectively decreases the possibility of water molecules forming a lattice-like structure , since it has to break the bond formed by water molecules under the presence of VC713. This can only be done under some conditions, particularly lower temperature and higher pressure. The above explanation is probably accounts for the inhibition function of VC713.

6.4.2 PVP+THF+H_2O System

PVP is another water soluble polymer found to have a good inhibition effect(Sloan *et al.*, 1991, Sloan, *et* al., 1992). It has only the 5-member ring of the VC713 molecule as the structural unit. Thus it is a homopolymer. The spectra of PVP+THF+H_2O system with and without 3.5 wt% salt are shown in Figure 6.16.

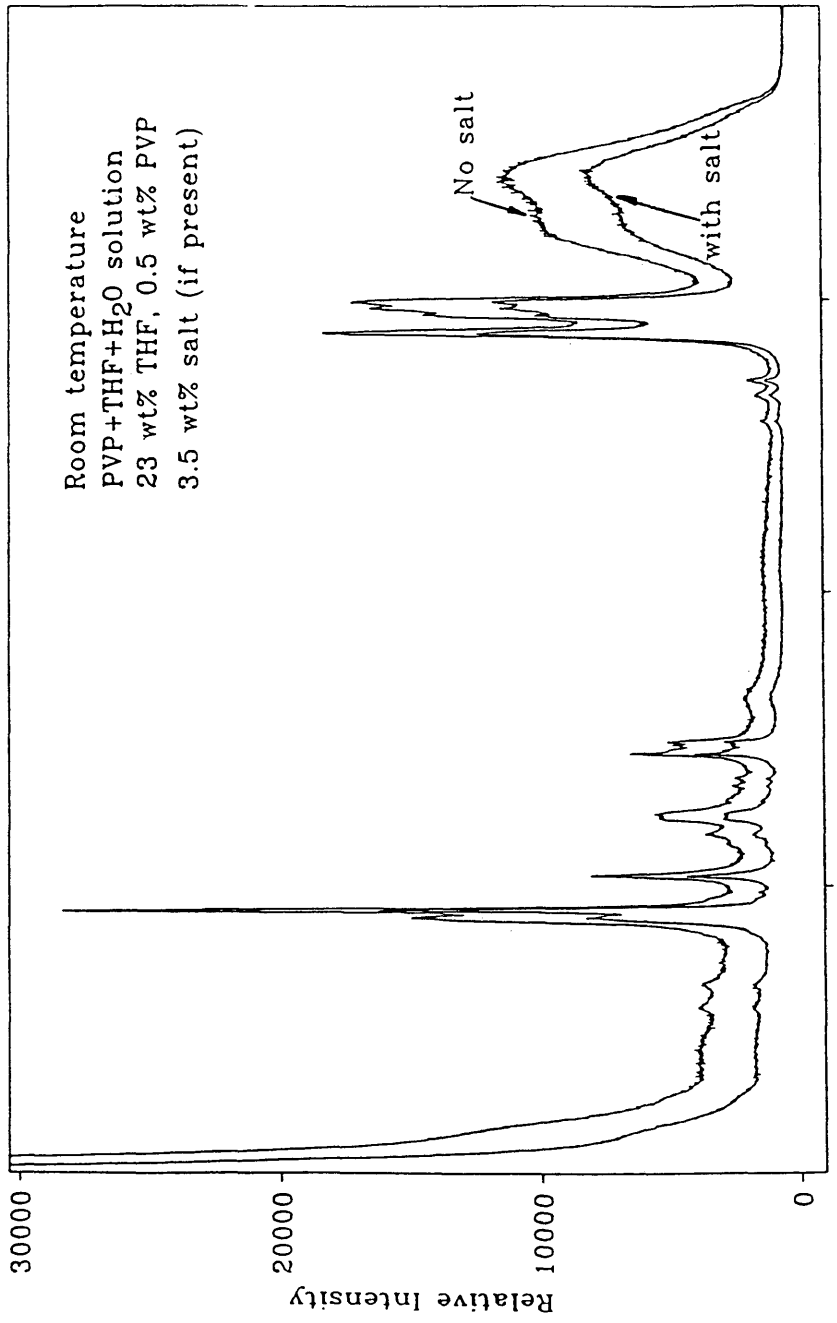

Figure 6.16 Comparison between spectra with and without salt for PVP solution

Although VC713 shows enhanced structure with the presence of salt, the effect of PVP is different. With the presence of the salt, there is neither significant increase of the population nor the strength. However, without the salt presence, both hydrogen bond population and strength increase. This might imply that the mechanism for PVP inhibition may be different from VC713 inhibition. The hydrogen bond population and hydrogen bond strength are shown in Figure 6.17 and Figure 6.18 respectively.

In conclusion, both VC713 and PVP change the subcooled water solution. The very low concentration of polymer indicates this type of interaction between PVP, VC713 and water is special in the way of the changing the overall water hydrogen bond configuration which is effectively the water structure. It deviates from the favorite structure for hydrate formation to some other configuration.

6.5. THF+H_2O Solutions as Function of Temperature

Since the water OH band is a strong function of temperature, the study of temperature effect on this band with the presence of THF was conducted. Due to the limited temperature range studied, from 0°c to 25°C, there was not a very significant temperature effect on either the position of

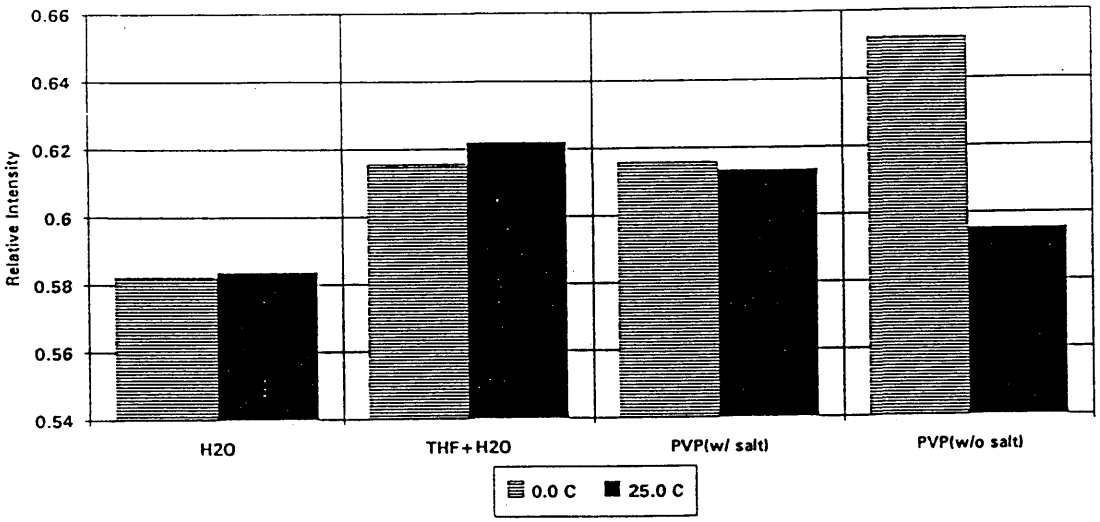

Figure 6.17 Hydrogen bond population for PVP system

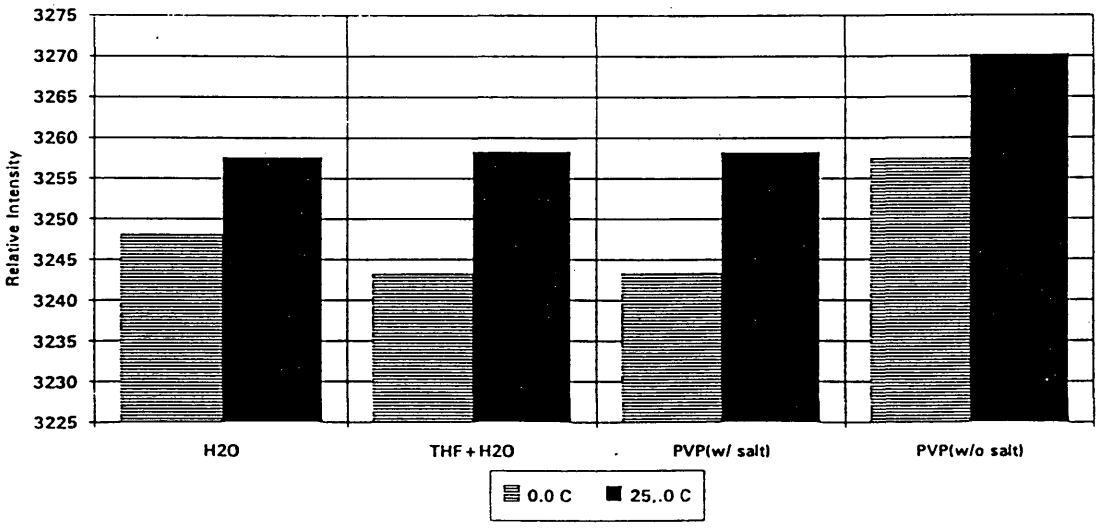

Figure 6.18 Hydrogen bond strength for PVP system

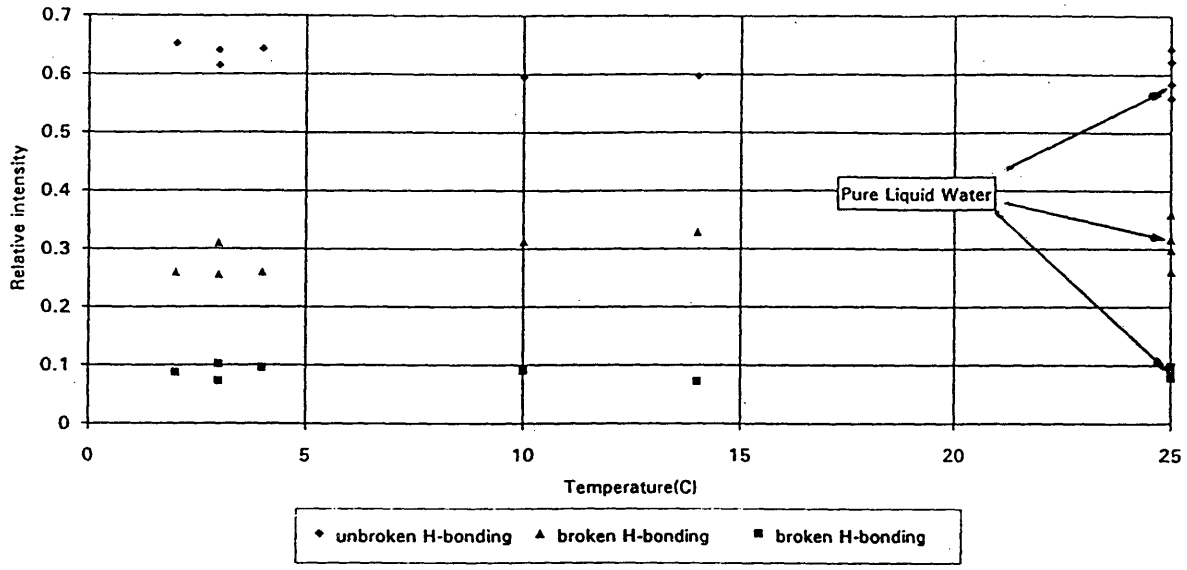

Figure 6.21 Comparison of relative intensity for peak 1 between THF solutions and THF hydrates

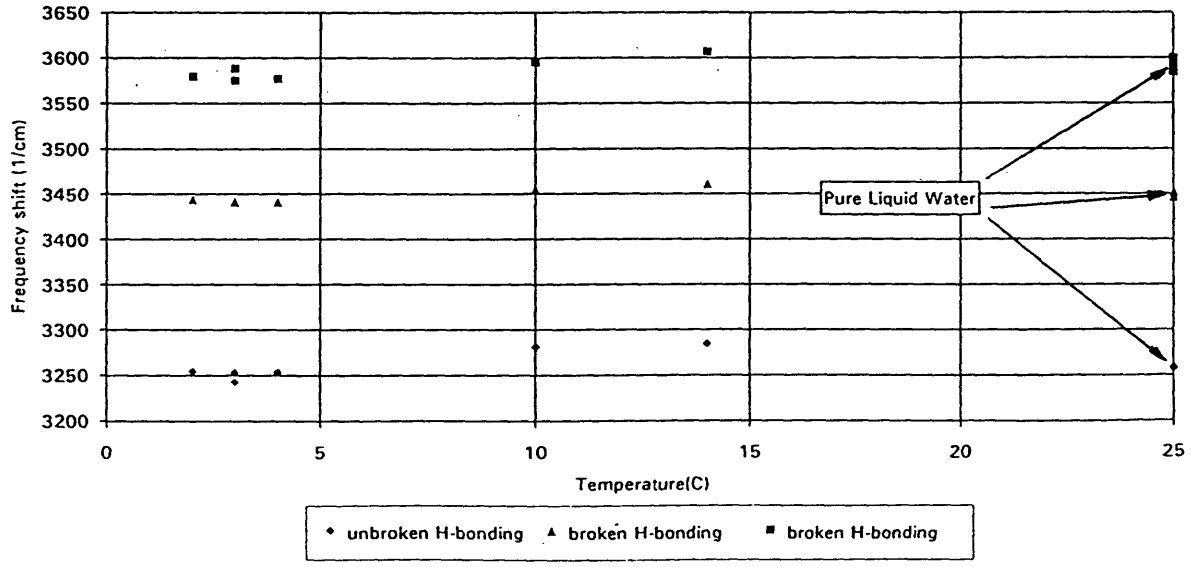

Figure 6.22 Comparison for peak 1 positions between THF solutions and THF hydrates

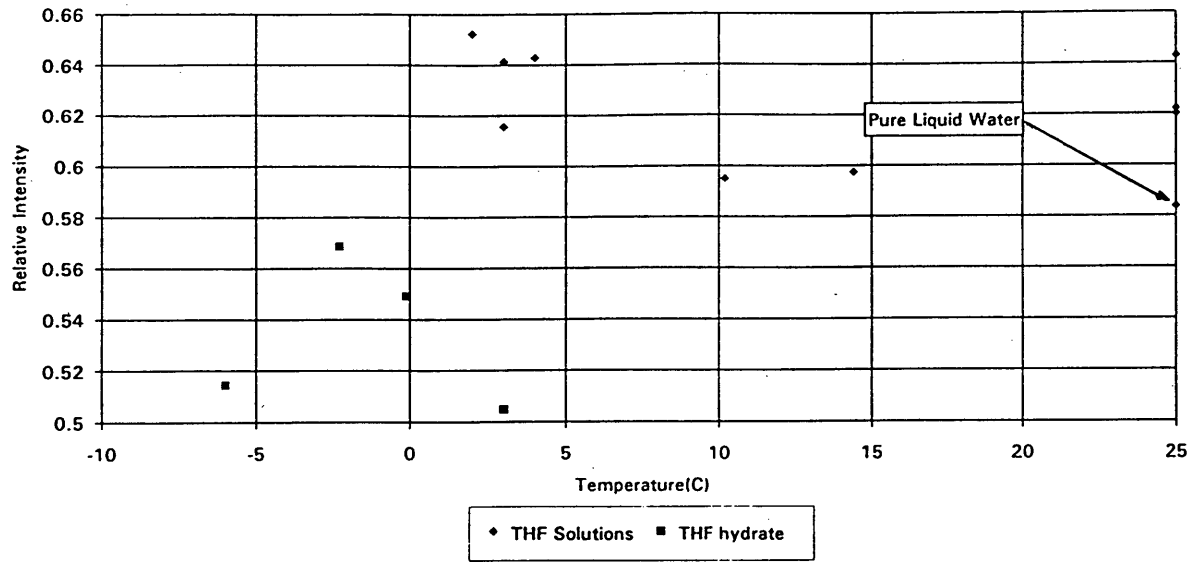

Figure 6.19 Relative intensity vs. temperature for THF+Water solutions

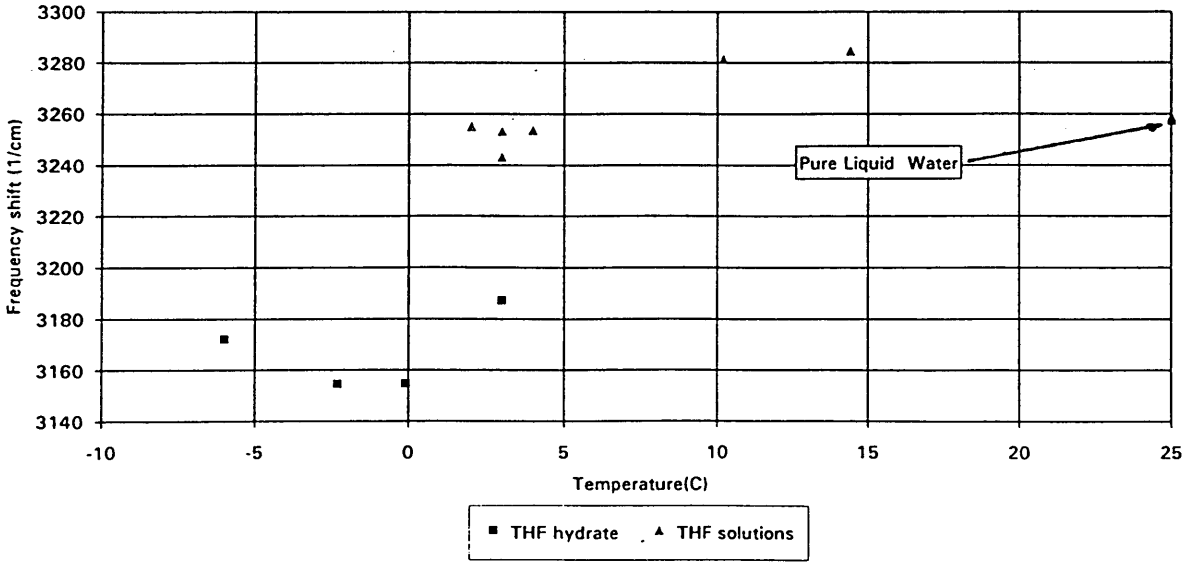

Figure 6.20 Frequency shift vs. temperature for THF+Water solutions

different peaks or the relative intensity of different peaks. The results are shown in Figure 6.19 and Figure 6.20. The frequency shift of three peaks are relatively constant. Pure liquid water data at room temperature are shown in all figures.

The comparison between THF+H_2O solution and THF hydrate are shown in Figures 6.21, and 6.22. As shown in Figure 6.21, when the hydrate forms, the peak 1 position moved to the lower wavenumber by about 80 cm^{-1}. The relative intensity of peak 1 dropped by about 25%. This is against the intuition of most people. The hydrate formation process might be due to a bond breaking process followed by a bond formation process. The decrease in the unbroken hydrogen bonding contribution could be due to the bond breaking process. As the formed hydrate becomes structurally stable, this unbroken hydrogen bonding would become dominant.

CHAPTER VII

CONCLUSIONS

The THF+water system has been studied extensively using Raman spectroscopy. The vibrational frequencies of pure THF and water are consistent with literature values.

Five conclusions can be drawn from this research. First, THF molecules form complexes with solvent molecules such as water, methanol and chloroform due to hydrogen bonding between solvent molecules and solute molecules. In the case of water, the complex has a 2:1 ratio between water and THF molecules as discussed in chapter 5.

Secondly, the intensity of vibrational effects due to the complexing decreases appreciably as the hydrate forms. The interaction between water and THF molecule becomes much less than that in the solution phase after THF molecule is encaged in the hydrate. However, the guest molecule vibrational frequency is still a small function of the hydrate host structure. The isotopic substitution experiments show that the THF C-O-C stretching frequency is shifted by 1 cm^{-1} between H_2O, D_2O, and HDO hydrate phases.

The third conclusion is that the THF molecule rotational relaxation time is faster in the cage than that in the liquid

indicating a faster rotational motion within the cage than in the liquid.

The fourth conclusion is that additives, such as the polymers VC713 and PVP, can change the water structure. VC713 and PVP in THF-water solutions increases both the population and strength of the hydrogen bond. The presence of salt (ASTM sea salt) enhances more and stronger hydrogen bonding interaction in the VC713 solution. However, for PVP-THF-water solution, the population and strength of hydrogen bonding is greater in the absence of salt than it is in the presence of salts.

The fifth conclusion is that the time-dependent spectra can be obtained using diode array detector. The first time-resolved spectra of THF hydrate formation proves that Raman spectroscopy is a valid technique to probe some microscopic interaction during the hydrate nucleation and growth period.

RECOMMENDATIONS

It is very important in the future to investigate gas systems, such as CH_4, C_3H_8, and CO_2, or gas mixtures. More parameters that could have strong effects on the hydrate formation need to be investigated using Raman Spectroscopy. Time-dependent experiments need to be continued.

In studies of kinetic inhibition mechanisms, the effects of polymer concentrations, salinity, pressure and temperatures, etc., should be examined more carefully. It is possible that nonlinear Raman spectroscopy techniques may be useful to examine polymer solutions to obtain more information.

A model needs to be developed to relate the spectroscopic and macroscopic observations.

LIST OF REFERENCES

Albayrak, C. and Zeidler, M.D., **Interactions of Water in Ionic and Nonionic Hydrates**, H. Kleeberg, Ed., Spinger-Verlag Berlin Heidelberg, (1987)

Anderson, A., (Ed.) **The Raman Effect**, Marcel Dekker, Inc., New York(1971)

Bartoli, F.J., and Litovitz, T.A., **J. Chem. Phys.**, 56 404(1972)

Bertie, J.E., and Jacobs, S.M., **Can. J. Chem.**, 55, 1777(1977)

Bertie, J.E., and Jacobs, S.M., **J. Chem. Phys.**, 77, 3230(1982)

Bertie, J.E., and Jacobs, S.M., **Can. J. Chem.**, 78, 6430(1983)

Bonner, O.D. and Choi, Y.S., **J. Phys. Chem.**, 78(17), 1723(1974)

Bryan, J.B. and Curnutte, B., **J. Mol. Spectrosc.**, 41, 512(1972)

Burruss, R.C., Ging, T.G., Eppinger, R.G., and Samson, I.M., **Geochimica et Cosmochimica Acta**, Vol. 56, 2713(1992)

Cates, D.A. and MacPhail, R.A., **J. Phys. Chem.**, 95, 2209(1991)

Curnutte, B. and Bandekar, J., **J. Mol. Spectrosc.**, 41, 500(1972)

LIST OF REFERENCES

(Continued)

Davidson, D.W., "Clathrate Hydrates," in **Water: A Comprehensive Treatise**, Vol. 2, Chapter 3, 115 Plenum, New York, (1973)

Davidson, D.W.,Garg, S.K., Gough, S.R., Hawkins, R.E., And Ripmeester, J.A., **Can. J. Chem.**, 55, 3641(1977)

Davidson, D.W. and Ripmeester, J. A., **in Inclusion Compounds**, Vol. 3, Chapter 3, J.L. Atwood, J.E.D. Davies, and D.D. MacNichol, Ed., Academic Press, (1984)

Devlin, J.P., and Richardson, H.H., **J. Phys. Chem.**, 87, 4185(1983)

Dunning, W.J, "General and Theoretical Introduction" in **Nucleation**, Zettlemoyer, A.C, Ed., Chapter 1, Marcel Dekker, Inc., New York, (1969)

Dyadin, Y., Kuzentzov, P.N., Yokovlov I.I., and Pyinova, A.V., **Dokl. Chem.**, 208(9), (1973)

Eisenberg, D. and Kauzmann, W., **The Structure and Properties of Water**, Oxford University Press, New York, (1969)

Ferguson, L.N., **J. Am. Chem. Soc.**, 77, 5288(1955)

Franks, F., **Water: A Comprehensive Treatise**, Vol. 2, Chapter 1, F.Franks, Ed., Plenum, New York, (1973)

Hanley, H.J.M., Meyers, G.J., White, J.W., and Sloan, E.D.,

LIST OF REFERENCES

(Continued)

Int. J. Thermophysics, Vol. 10(4), 903(1989)

Hills, B.P., **Mol. Phys.**, 53, 731(1984)

Iwata, H.A., **J. Chem. Phys.**, 58, 4184(1973)

Irish, D.E., " Vibrational Spectral Studies of Electrolyte Solutions and Fused Salts" in **Ionic Interactions**, S. Petrucci,Ed., Chapter 9, Academic Press,New York,(1971)

Johari, G.P. and Chew, H.A.M., **Phil. Mag.**, Vol. 49(3), 281(1984)

Johari, G.P. and Chew, H.A.M.,**Nature**, Vol. 330(16), 604(1983)

Kohlrausch, K.W.F., and Reitz, A.W., **Z.physik. Chem.**, B45, 249(1940)

Krishnan, R.S., "Historical Introduction" in **Raman Effect Volume 1: Principles**, A. Anderson, Ed., Marcel Dekker, Inc, New York, (1971)

Kunze, F., **Monatshefte fur chemie**, 78, 362(1948)

Long, D.A., **Raman Spectroscopy**, McGraw-Hill,New York, (1977)

Long, J.P, and Sloan, E.D., **Molecular Simulation**, Vol. 11(24), 145(1993)

Luther, H., Lampe, F., Goudeau, J. and Rodewald, W., **Z.Naturforsch.**, 5, 34(1950)

LIST OF REFERENCES

(Continued)

Makogon, Y.F., **Hydrates of Natural Gas**, Moscow, Nedra, Izadatelstro(1974), Translated from Russian by W.J. Cieslesicz, PennWell Books, Tulsa, Oklahoma,(1981)

Mashimo, Satoru, **J. Chem. Phys.**, Vol. 67(6), 2651(1977)

Montgomery, D., Heston, B.O. and Blankenship, F., **Proc. Okl. Acad. Soc.**, 30, 140(1949)

Nakahara, J., Shigesato, Y, Higashi, A., Hondoh, T. and Langway, C.C., Jr., **Phil. Mag.**, Vol. 57(3), 421(1988)

Palmer, A. and Bissell, E.R., **Spectrochimica Acta**, Vol. 16, 450(1960)

Pinder, K.L., **Can. J. Chem.**, 10, 271(1965)

Rahman, A. and Stillinger, F.H., **J. Am. Chem. Soc.**, 95(24), 7943(1973)

Scherer, J.R., "The Vibrational Spectroscopy of Water", 145(1989)

SchrÖtter, H.W., "Raman Spectroscopy with Laser Excitation" in **Raman Spectrsocopy Theory and Practice**, Szymanski, H.A., Ed., Plenum Press, New York, (1970)

Sloan, E.D., Jr., **Clathrate Hydrates of Natural Gases**, Marcel Dekker, Inc., New York , Chpater 2, 24,(1990)

Sloan, E.D., Jr., Christiansen, R.L., Lederhos,L.P.,J.P.,

LIST OF REFERENCES

(Continued)

Long, X.P.,Long, Pratt, R., Kalbus, J., and Li, Qian, "**Kinetic Inhibition of Natural Gas Hydrates In Offshore Drilling, Production, and Processing Operations**", DEA 62/CEA-20 Annual Report, Sept. 1, 1990 -Dec. 31, 1991

Sloan, E.D., Jr., Christiansen, R.L., Lederhos,L.P., J.P., Long, X.P.,Long, Pratt, R., Kalbus, J., and Li, Qian, **"Kinetic Inhibition of Natural Gas Hydrates In Offshore Drilling, Production, and Processing Operations"**, DEA-62/CEA-20 Annual Report, Jan. 1, 1992 -Dec. 31, 1992

Sloan, E.D., Jr., Christiansen, R.L., Lederhos,L.P., J.P., Long, X.P.,Long, Pratt, R., Kalbus, J., and Li, Qian, **"Kinetic Inhibition of Natural Gas Hydrates In Offshore Drilling, Production, and Processing Operations"**, DEA-62/CEA-20 Annual Report, Jan. 1, 1993 -Dec. 31, 1993, in press.

Szymanski, P.P., (Ed.), **Raman Spectroscopy**, Plenum Press, New York, (1967)

Tschamler, H. and Voetter, H., **Montash. Chem.**, 83, 302(1952)

Tarjus, G. and Bratos, S., **Mol. Phys.**, 51, 793(1984)

Terpstra, P., Combes, D. and Zwick, A., **J. Chem. Phys.**, 92, 65(1990)

LIST OF REFERENCES

(Continued)

von Stackelberg, M. and Meuthen, B., **Zeit. fur Electrochemie**, 62, 130(1958)

Wada, G. and Uneda, S., **Bull. Chem. Soc. Japan**, 35(11), 1797(1962)

Walrafen, G.E., "Raman and Infrared Spectral Investigations of Water Structure," in **Water: A Comprehensice Treatise**, Vol. 1, Chapter 5, 151 (1973)

Walrafen, G.E., Fisher, M.R., Hokmabadi, M.S. and Yang, W.H., **J. Chem. Phys.**, 12, 6970(1985)

Walrafen, G.E., Hokmabadi, M.S. and Yang, W.H., **J. Phys. Chem.**, 92, 2433(1988)

Walrafen, G.E., Hokmabadi, M.S. and Yang, W.H., **J. Chem. Phys.**, 92, 6964(1985)

Walrafen, G.E., Hokmabadi, M.S. and Yang, W.H., **J. Phys. Chem.**, 94, 2237(1990)

Wilson, E.B., Decius, J.C., and Cross, P.C., **Molecular Vibrations**, McGraw-Hill, New York, (1955)

Woodward, L.A., " Vibrational Rules of Selection and Polarizattion: Their Practice Uses and Limitations" in **Raman Spectrsocopy: Theory and Practice,**, Vol. 2, Chapter 1, 16, (1970)